1 Comments from referees/public and author's response

1.1 Response to Referee #1 (J.Severinghaus)

We thank Referee #1 for the interesting comments and detailed explanations on various aspects, and address the questions raised below.

Comment 1: One important improvement can be made in the magnitude of isotopically relevant O2 production, which of course also must match respiratory consumption. 11 Pmol O2/yr seems much too small to me, given that many plants produce O2 without engaging the carbon fixation apparatus, for example during times of stress. The plants are able to produce ATP by absorbing photons and creating O2. Thus my guess is that by scaling O2 production to carbon uptake we have badly underestimated the true O2 production and destruction. Furthermore, even within the carbon fixation framework, I think we have underestimated the amount of photorespiration. Most plant physiology experiments are done under ideal, well- watered, nutrient-replete conditions. In the real world, drought stress is common, and plants often photorespire at these times because of closure of stomata to preclude water loss. In the oligotrophic subtropical surface oceans, nutrient limitation seems to drive picoplankton to produce O2 without fixing carbon and nitrogen, and so O2 production by the marine realm has also been underestimated. Based on the rapidity of the changes we see in the d18Oatm record in ice cores, a total O2 production figure of 40 Pmol per yr seems more likely, with perhaps half of that from the terrestrial biosphere.

It seems that our manuscript was not clear enough that photorespiration is well taken into account in our approach. Actually, we have taken into account dark respiration (soils and plants), Mehler reaction and photo-respiration. As a consequence, oxygen production is not scaled in a simple way to carbon gross primary production but we take into account the photorespiration in addition. Photorespiration is calculated from the proportion of C4 vs C3 plants, temperature and CO2 level (assumed constant in our study) as depicted in the biochemical model of photosynthesis from Farquhar et al. (1980) and already done in the studies of Hoffmann et

al. (2004) and Landais et al. (2007) (FYI see attached Figure R1). Increasing photorespiration modifies 18ϵresp, as photorespiration is associated with a high discrimination, and in turn affects δ18Oterr. With 60 % of photorespiration instead of 30%, the O2 production would amount to 18.7 Pmol/yr. We propose to explain more clearly that photorespiration has been taken into account in the revised version of the manuscript. Second, the reviewer is concerned by the value of 11 Pmol O2/yr for the LGM which seems too small. Present day carbon and oxygen production amount to 10.5 Pmol C/yr and 17.95 PmolO2/yr (taking into account photorespiration) in the ORCHIDEE model, respectively. This is in line with other estimates e.g. Angert et al. (2003) or Welp et al. (2011), estimating 8 to 13 Pmol C/yr and 12.5 to 14.2 Pmol C/yr, respectively. ORCHIDEE carbon production seems to be consistent with observations, and the scaling of O2 production to C uptake leads to a value in agreement with former studies. For LGM and HS, estimates from the ORCHIDEE model are indeed lower than other estimates. It gives land carbon productions of 6.8 and 6.5 Pmol C/yr for LGM and HS, respectively, which translates as 11.8 and 11.4 Pmol O2/yr for LGM and HS, respectively. This is up to a factor of 2 lower than LGM estimates from Joos (2004), Hoffmann (2004) or Bender (1994), ranging from 23 Pmol O2/yr to 16.7 Pmol O2/yr. The carbon production seems to be underestimated in ORCHIDEE model for glacial times, and the low oxygen production is a consequence of it. We will clearly point this out in a revised version. Reviewer #1 also suggests that the scaling factor between carbon and oxygen (Keeling, 1988) of 1.07 used in our study may be underestimated. We can modify the scaling factor to reach literature oxygen production value. For instance, with a scaling of 1.47 (1.87), the O2 production reaches 16.17 (20.56) Pmol/yr without modifying δ18Oterr. The scaling may have been underestimated, but must be strongly (too much) increased to reconcile O2 production with previous studies. Therefore the scaling factor alone probably cannot explain the discrepancy, but we'll acknowledge its potential underestimation in the revised version.

Comment 2:A second improvement can be made in explicitly treating the effect of poor exchange between wet soil air and atmosphere, as described by Angert et al. in several papers, and its connection to water saturation of the soil. Water saturated soils are known to be very poor at transmitting oxygen from the sites of respiration back to the atmosphere. For this rea-

son actual soil respiration in wet soils has a much weaker effect on d18Oatm than would be estimated from the enzymatic fractionation itself. This effect can be understood via the following thought experiment: imagine a liter of air taken from the atmosphere in a flask, then the valve is closed. Then respiratory fractionation consumes all the oxygen in the flask. When the valve is reopened, only nitrogen and argon diffuse back out to the atmosphere. This flask has therefore made no contribution to d18Oatm. In other words, a back flux of isotopically enriched oxygen to the atmosphere, the residual left over after partial respiratory consumption, is necessary to make an effect on d18Oatm. If this back flux does not exist, no effect on the atmosphere occurs. Therefore during strong monsoon intervals, some large fraction of respiratory isotope enrichment goes unrealized as a d18Oatm contributor due to the waterlogged soils in these climates. During a Heinrich event, these zones dry out and the soils become well aerated, greatly increasing the respiratory contribution to d18Oatm. In my opinion the authors have not adequately evaluated this 'Angert' mechanism. I was surprised that the authors found a small effect of opposite sign to this hypothesis, in fact a reduction in the isotopic enrichment during Heinrich events from soil respiration. This is probably wrong and needs to be re-evaluated, since Heinrich events are times when waterlogged soils dry out and start having a stronger impact on d18O.

The authors greatly thank the reviewer for this very clear explanation. It is indeed important to consider the weakening of respired O2 back-diffusion in waterlogged soils. In our model, the soil isotope discrimination is already taken into account. Indeed, we directly used Angert's results on soil water limited diffusion during respiration in using their values of respiration fractionation factors (taking into account limitation by diffusion of oxygen in water) for the different types of soils. We have assigned fractionation factors for each soil using the soil type discrimination proposed by Angert et al. (2003). For this, we relate the Angert's soil types to the type of vegetation cover over the considered soil in ORCHIDEE model, hence indirectly to soil temperature (see Fig. 2 of Angert et al., 2003). As an example, we have assigned tropical soils (fractionation coefficient of -10.1 ‰) to soil covered by dominant PFT Tropical broadleaf evergreen trees and PFT Tropical broadleaf raingreen trees. Tropical soils (-10.1 ‰) discrimi-

nate significantly less than temperate (-17.8 ‰) or boreal soils (-22.4 ‰) following Angert et al. (2003). The global respiratory isotope fractionation for the control run calculates as -15.895 ‰, much weaker than the common value (-18 ‰) used for terrestrial ecosystems. As soil respiration only occurs where vegetation exists, a shift of the latter modifies the spatial distribution of soils where dark respiration takes place. In our model, the change of vegetation cover from LGM to HS leads to a very slight weakening of soil respiration isotope fractionation using fractionation values of Angert et al. (2003), thus considering soil aeration. A figure of the simulated soil respiratory fractionation for LGM is attached (figure R2). In order to further address the role of soil water saturation on respiration δ18O, we perform a sensitivity test by reducing soil respiration in waterlogged soils. To do so, we half the soil respiratory isotope fractionation in the tropics of the rainy hemisphere, NH for LGM, SH for HS. The soil respiratory isotope fractionation calculates to -13.44 ‰, 2.45 ‰weaker than in the LGM_ctrl control run, and close to the value estimated by Angert et al. (2003), -13.8 ‰. The terrestrial fractionation factor, the terrestrial component of the Dole Effect, decreases from 23.41 in the LGM_control run to 22.41 ‰in the modified one. The picture is even amplified for HS_exp run, where soil respiratory isotope fractionation weakens from -15.61 to -12.71 ‰, leading to terrestrial fractionation factor depletion from 23.52 to 22.28 ‰over HS. This sensitivity experiment indicates that in our simulation, soil respiration does not strengthen during a HS, once the climatic system has reached equilibrium. This may be different over a Heinrich Event, involving shorter timescales. Aerated soils in the NH do not compensate the diffusion limitations in water saturated soils of the SH, even with half of the soils shut down in the tropics of the most rainy (and productive) hemisphere. If the reviewer and/or editor feels that this sensitivity test is useful to discuss the robustness of the small effect of soil respiration on the LGM-HS anomaly, we propose to add its discussion in the revised version.

Comment 3: A third area that could be improved is the precipitation isotopic match between data and model. For example, the model produces 1.6‰changes at DO events in Greenland, but the data show 4‰changes. This is not really satisfactory, even though the authors say it is acceptable. While Greenland is not important for O2 production, there are other somewhat

more troubling mismatches between data and model in the low latitudes and the authors seem to wave away these issues. A more candid and realistic discussion of these model shortcomings would boost the effectiveness of the paper.

We agree that the comparison is not very good for Greenland but we also think that it is difficult to quantitatively compare the δ18O change simulated by a freshwater input (the most efficient way to model a Heinrich event) and the δ18O decrease between a Greenland interstadial and a Greenland stadial. Indeed, there are more and more evidence that the δ18O decrease at the end of a Greenland interstadial is not due to the same freshwater discharge than the one associated with a Heinrich event. It can well be due to a threshold in the extent in sea-ice or an atmospheric heat transport. This indeed needs to be explained much more clearly in the new version and discuss potential implication for low latitudes uncertainties in the modeling approach. We thus propose to make a clear case in the new version that the most efficient way to produce an Heinrich event with a model is to throw freshwater in the high latitudes of the Atlantic ocean but results from recent studies (Marcott et al., 2011; Guillevic et al., 2014; Rhodes et al., 2015; Alvares-Solas et al, 2013) suggest that this does not satisfactorily explain the observed sequences of events and especially the decoupling between Greenland and low latitudes. This is also the reason why we only focused on Heinrich Stadials and not D/O events. Regarding low latitude model data mismatches, in addition to the modeling approach potential implications, we will also discuss the low latitude model-data anomalies in more details in the revised version to emphasize the model shortcomings. Specifically, in addition to the orography, another reason can be invoked to explain the poor match between model and data in Northern India (Timta Cave): Figure 9 (lower panel) of Kageyama et al. (2009) depicts precipitation change between HS (LGMc) and LGM (LGMb). Since the largest Indian monsoon signal is simulated over the ocean, and not over land (Kageyama et al., 2009) in the control simulation, no changes in monsoonal activity takes place over India over HS (-0.5 to -2 mm/day is only simulated over the ocean). In Northern India, hence Timta cave site, the model does not simulate any significant rainfall change between the 2 periods. A more intense weakening of the Indian monsoon over land in the HS run, hence less rainfall, would have helped reconciling model and data at Timta

Cave, since precipitation δ18O would have been enriched through the amount effect. It will be clearly stated in the revised version that at Timta Cave and Cave of the Bells, our model fails to capture the calcite δ18O anomaly recorded in speleothems. However, the modelled precipitation δ18O anomaly is quantitatively consistent with observations for most of the compared sites (Table 3 and Figure 4). The 2 sites where model and data completely disagreee (Timta Cave, India and Cave of the Bells, North America) are located in altitude and they do not correspond to the regions where most of the oxygen is produced.

Comment 4:Why aren't the time series of the model output shown, for direct comparison with the ice core d18Oatm data? Just curious. It would strengthen the paper.

We agree that it would be nice to have time series for direct comparison with data. Unfortunately, we think that this would not make sense because the model has been run at equilibrium, i.e. one experiment for the Heinrich and one experiment for the LGM. LGM and HS experiment have been run 1000 and 800 years, respectively, so that we can reach an equilibrium, and we use the averages of years 200-250 yrs and last 100 years, respectively. As a consequence, showing time-series would only show the time needed to reach an equilibrium state without any link to the reality of climatic sequences.

Comment 5: It would be useful to show a zonally-averaged d18O of terrestrial precipitation curve versus latitude from the model, both pre- and post-Heinrich, so the viewer can see how the d18O changes. This d18O zonal average should be a weighted average, weighted by terrestrial photosynthetic production of O2, so that it is most relevant to the question at hand. Of course, the weighting will change as the rainfall changes and the photosynthetic production changes. A second plot should show the latitudinal variation of O2 production, so that the reader can see that it is concentrated in the tropics. On a third plot, the total terrestrial rainfall amount both pre- and post- should also be shown. This way it is clear to the reader that the total rainfall shifts south during a Heinrich event, and at the same time becomes isotopically heavier. It is also an interesting question, whether the total amount of rainfall on land becomes less during

a HS. The total amount of rainfall on both ocean and land is tightly constrained to equal the amount of evaporation, but no such constraint applies to the land fraction. So it is quite possible that more rain fell over the ocean at HS, compared with D/O Stadial conditions.

We thank the reviewer for his suggestion. In our study, we consider a system at equilibrium for 2 periods, LGM and HS. We have 2 sets of monthly resolved data averaged over LGM and HS. We thus provide here 2 figures (one with the full latitudinal profile (R3), the other zooming on the intertropical zone (R4), where most of the production occurs) for the control (LGM_ctrl) and HS (HS_exp) simulations. In addition to the southward shift of the tropical rain belt, they clearly show how rainfall amount and δ18Op are anticorrelated as expected on most of the latitudinal profile. During a HS, δ18Op is enriched in the NH down to 14°S. The figure zooming on the intertropical band reveals a particular pattern between the equator and 14°S, where oxygen production is most enhanced at HS, as precipitation are more abundant but also heavier in δ18O. We'll present the figure zooming on the intertropical band (R4) in the revised version of the manuscript. Total amount of terrestrial rainfall decreases by around 0.02 mm/day during a HS, while total amount of rainfall is similar (1.85 mm/day) between the 2 time periods.

Comment 6:The maps of isotopic composition of rainfall aren't very useful. It would be better if the color scale was adjusted so that the most relevant range of values are more finely graduated. As it stands most of the interesting parts of the tropics are all one color.

The colorscale has been adjusted to better see tropical variations. Note that δ18Op difference between the two periods is also displayed in Fig. 4a (whose colorscale was unfortunately slightly offset, see figure R5). Figure 3 has been modified to follow recommendations of reviewer #2 (see comment 1 and attached figure R6 and R6bis in reply to reviewer #2).

Comment 7:I was surprised to see no reference to the controversial David Battisti hypothesis. This idea is that rainfall amount does not change at cave sites like Hulu Cave, but rather the d18O of precipitation changes without change in rainfall amount. What does your model say

about this hypothesis?

We suppose (please correct if I'm wrong) you refer to the hypothesis described in Pausata et al. (2011)? Battisti is a coauthor and they propose that change in rainfall amount in Indian rather than in South East Asia explains changes observed in calcite d18O in Chinese stalagmites (in South-East Asia). In our model, as shown in Table 3, the modelled increase in δ18Op quantitatively agrees with data δ18Oc increase during Heinrich Stadials in most of the compared sites. - 0.17 and -0.13 mm/day are simulated at Hulu and Songjia Cave during HS. Rainfall amount drops in East-Asia and North-West India, mostly over the ocean (see comment 3) but increases in South-East India, as shown in the attached figure. However, δ18Op is enriched over the whole India (with an abrupt change south of Timta Cave) and South Asia. As in Pausata et al's (2011) study, a freshwater pulse was applied to the control simulation with LGM background climate. The enrichment in δ18Op observed in Chinese caves is reproduced by the model (as in Pausata et al.'s (2011) study) but the latter fails to capture the enrichment in Timta cave, as in Lewis et al. (2012) study, where the freshwater pulse was applied to a present-day simulation. Results of our simulation do not discard a possible role of the Indian monsoon in the oxygen isotopic enrichment of Chinese stalagmites, but local amount effect can at least partly explain the increase in δ18O over South-East Asia.

More detailed comments: Page 2282, line 24 'effusion processes' This is incorrect. Harmon Craig and Michael Bender erroneously used this term long ago and it has unfortunately stuck. Effusion is a different process, having to do with Graham's Law of Effusion, in which a gas is fractionated by passing through orifices smaller than the mean free path length, which is about 1 micron at atmospheric pressure. Because the light isotope has a higher velocity than the heavy isotope, in inverse proportion to the square root of the masses, the light isotope is enriched by a factor of the square root of the ratio of the masses. This process was used, for example, to enrich uranium isotopes during the second world war. Current understanding of the bubble close-off fractionation in glacial firn is that permeation of the gases through the ice lattice surrounding an overpressurized bubble is responsible for the fractionation (Severinghaus and Battle, 2006;

Huber et al., 2006). Instead of transport through orifices of 1 micron, the permeation mostly occurs by breaking of bonds in the ice lattice, for gases like O2 and N2. So it should be called "a permeation process" or just "permeation through the ice lattice", or "ice permeation fractionation".

Thank you once again for a very clear explanation. In Page 2282, line 24 'effusion processes' will be replaced by 'permeation through the ice lattice' as suggested.

Page 2283, line 1. Rather than 'infer..' this should probably read 'have thus been explored as possible constraints on biospheric productivity', since no truly successful inference has been made yet.

Will be replaced by 'have thus been explored as possible constraints on biospheric productivity'

Page 2283, line 13. Should be 'd18Oatm variations actually reflect in large part 'because it is the variability that is dominated by meteoric water. The absolute value of d18Oatm (+24 per mil on the VSMOW scale) is dominated by respiratory fractionation, in contrast.

The reviewer is right, and the sentence will be corrected accordingly: d18Oatm variations actually reflect in large part the isotopic composition of the meteoric water.

Page 2283, line 14. 'latter' not 'later'

Will be corrected.

Page 2284, line 16. 'Millennial-scale climate variability is perhaps best known from the Greenland ice cores, where it is manifested in the stable water isotopes of ice. During the last

glacial period, these cores show 25 Dansgaard-Oeschger (DO) events.'

Thank you for clarifying the writing. The sentence will be replaced.

Page 2284, line 4. This is not really an accurate history, to say that 'the supposed key role of the ocean stems in part from the presence of ice rafted debris'. The original papers on Heinrich events (by Bond, for example) stated very clearly than the Heinrich events came out into an ocean that was already in a cold, stadial state. Subsequent analyses have confirmed this timing relationship. So it was always known, right from the beginning of the discussions on Heinrich events, that Stadials were NOT caused by Heinrich events. Rather, the thinking at that time was that the stadials and DO events were a manifestation of a bistable nonlinear system in which the coupled ocean-atmosphere circulation could jump between two quasi- stable modes (Broecker and Denton, 1989). Today's thinking on this has not changed very much, and such bistability can indeed be found in a wide range of ocean circulation models. [Many IPCC-class coupled ocean-atmosphere general circulation models cannot reproduce this bistability, which is widely seen in simpler models, but this fact is viewed by most workers in the field as a model defect rather than as an indication of how the real ocean circulation operates. The model defect is likely due to the computational limitations inherent in representing the non- geostrophic (frictional) hydraulics of the bottom hugging overflow currents on the Greenland-Scotland ridge. In the real world, these currents allow dense water to sink much deeper (to 3000 m) than they can in the model, and so the model produces a too-shallow AMOC that is also not subject to hysteresis, bifurcation, and bistability]

Once again, we thank the reviewer for this clear explanation. We agree the sentence was not accurate and will remove the part mentioning the supposed key role of the ocean. The new sentence will read as 'The presence of ice rafted debris (IRD, Ruddiman, 1977; Heinrich, 1988) in marine sediments from the North Atlantic region during the largest GS document episodes...'

Page 2285, line 9. "Even if IRD can be recorded" this doesn't make sense. please fix. Perhaps you meant to say something else? "Even though IRD is present in each GS, not all GS contain a Heinrich event."?

This was indeed meant to say what reviewer #1 said: 'Even though IRD is present in each GS, not all GS contain a Heinrich event.' The sentence will be replaced.

Page 2285, line 12 should be Barker, not Baker

We will address this issue in the revised version.

Page 2286, line 4. It is implied here that temperature records follow the Greenland signal, in speleothems. This is not correct, in that speleothems mainly record a rainfall signal, not a temperature signal.

We agree with the reviewer that the sentence was confusing and will be replaced by: 'Abrupt climate variation associated with the Greenland signal is found down to low latitudes in numerous terrestrial and marine archives (e.g. Clement and Peterson, 2008). Its climatic impact is recorded in a large part of the North Atlantic region, both in marine cores (e.g. Bond et al., 1993; Broecker, 2000) and in speleothems (Fleitmann et al., 2009).

Page 2286, line 8. The 'ITCZ' is a term that is reserved by the atmospheric science community for situations over the ocean. Over land, it is advised to NOT use this term, because the dynamics of the rising air motion is quite different. Therefore many of us in the paleo community are now using the term 'tropical rain belts' (e.g. Rhodes et al., Science 2015) for terrestrial air convergence zones with high rainfall. You can also say 'through a shift in the ITCZ and its terrestrial equivalent, the tropical rain belt'.

In the revised version, the term 'tropical rain belt' will be used if it relates to terrestrial precipitation. Therefore the sentence will be corrected as: '...monsoon intensity through a shift in the ITCZ and its terrestrial equivalent, the tropical rain belt...'

Page 2286, line 15. Redundant use of 'onset'

The corrected sentence will read as: '... using Rasmussen et al. (2013) definitions of onset of GS.'

Page 2286, line 17. Spelling - should be 'inflection' not inflexion

Will be corrected accordingly.

Page 2286, line 22. '... should provide added value'

'strong' will be removed from the sentence as suggested by the reviewer #1

Page 2287, line 4. 'repartition' is not widely understood in English - perhaps use '...water, vegetation redistribution, and productivity...'

We will replace repartition by distribution, so the sentence in the revised version will read as: 'We combine climatic parameters (temperature and humidity), isotopic composition of meteoric water, vegetation distribution and productivity simulated by different models with monthly mean temporal resolution.

Page 2287, line 12. Again, please do not use ITCZ. Instead, 'shifts in the tropical rain belt' is more accurate, because d18Oatm is only affected by terrestrial precipitation, not marine precipitation.

The sentence will be corrected according to the reviewer #1 suggestion.

Page 2287, line 14. 'build up of atmospheric oxgen ...' this means to most readers an increase in oxygen concentration. Instead you should say 'The isotopic content of atmospheric oxygen is controlled by numerous processes, so we must consider...'

The sentence will be corrected according to the reviewer #1 suggestion in the revised version.

Page 2287, line 19 spelling - photosynthetically

Spelling mistake is corrected in the revised version.

Page 2287, line 19 to this list you should add a fourth category, soil aeration, be- cause this strongly affects the effective respiratory fractionation - see papers by Alon Angert. In water-logged tropical soils in monsoon regions, the respiratory contribution to d18Oatm is perhaps only half of what it is in temperate soils. The reason is that the backflux of isotopically enriched oxygen to the atmosphere is hampered by the poor diffusivity of oxygen in liquid water. Therefore the effective respiratory fractionation in monsoon regions may be quite reduced, adding to the depleted isotope signature in d18Oatm from the monsoon meteoric water.

We thank reviewer #1 for this comment. Soil aeration is taken into account in our study, as explained in comment 2 of the present review. More than soil aeration alone, we would rather add 'respiratory processes' as soil respiration, but also mitochondrial respiration, photorespiration and Mehler respiration are considered. The corrected sentence will read as: '... is calculated, (iii) the worldwide vegetation cover and Gross Primary Productivity, defining the photosynthetically and respiratory active areas that contribute to 18Oatm, as well as (iv) respiratory processes.

Page 2287, line 22. 'Assuming a steady state, d18Oatm can thus be...'

The sentence will be corrected according to the reviewer #1 suggestion in the revised version.

Page 2288, line 7. '... because the CO2 level remains relatively stable (Bender..)' or other appropriate reference to the strat-trop CO2 isoflux.

The relevant references will be added, i.e. Bender 1994 and Ahn and Brook, 2015. We assume a constant CO2 level between LGM and HS in our study. Ahn and Brook's (2014) study show that variations over HS are small (less than 20 ppm). Effect of isotopic exchange between CO2 and O2 in the statosphere on δ18Oatm is expected to be proportional to CO2 mixing ratio. Following Bender's (1994) calculation, which estimates a δ18Oatm depletion of 0.4 ‰for a CO2 concentration of 353 ppm, we can conclude that 20 ppm difference between LGM and HS can modify δ18Oatm by $\pm$ 0.023 ‰. *Page 2288, line 9. '...influence, in this first approach, for the...'*

The sentence will be corrected according to the reviewer #1 suggestion in the revised version.

Page 2288, line 11. '...variations are largely driven by changes in the..,' [these authors did not propose that precipitation d18O was the sole control]

We agree with reviewer #1 that other controls were proposed by these authors. The sentence will be corrected according to the reviewer #1 suggestion in the revised version.

Page 2288, line 12. '... low-latitude hydrological cycle..'

The sentence will be corrected according to the reviewer #1 suggestion in the revised version.

Page 2288, line 22. '...as the leaf water.'

The sentence will be corrected according to the reviewer #1 suggestion in the revised version.

Page 2289, line 3. '... global production-weighted average isotopic composition of leaf water...'

The sentence will be corrected according to the reviewer #1 suggestion in the revised version.

Page 2289, line 13. '..is the temperature-dependent liquid-vapor equilibrium isotope effect (Majoube, 1971)'

The sentence will be corrected according to the reviewer #1 suggestion in the revised version.

Page 2290, line 3. '..leading 18ekinetic to values as low as 19‰when using the Merlivat...'

The sentence will be corrected according to the reviewer #1 suggestion in the revised version.

Page 2290, line 5. 'because higher values led to too high a global value for d18Oatm.'

The sentence will be corrected according to the reviewer #1 suggestion in the revised version.

Page 2291, line 5. '... qualitatively agrees with paleoarchive reconstructions...'

The sentence will be corrected (paleoarchive for paleoarchives)) according to the reviewer #1 suggestion in the revised version. *Page 2291, line 10. '... followed the Lloyd and Farquhar...'*

The sentence will be corrected according to the reviewer #1 suggestion in the revised version.

Page 2291, line 26 again, repartition is not a word widely recognized in English

'...the d18Op repartition...' will be replaced by '...the d18Op distribution...' in the revised version.

Page 2293, line 3. 'leaf:, not leave

The sentence will be corrected according to the reviewer #1 suggestion in the revised version.

Page 2304, line 12. '... more important than..'

The sentence will be corrected according to the reviewer #1 suggestion in the revised version.

Page 2307, line 8. 'low latitude water cycle...'

The sentence will be corrected according to the reviewer #1 suggestion in the revised version.

Page 2307, line 11. '..Rhodes et al.'s (2015) recent study suggests that ... WAIS Divide ice core...

The sentence will be corrected according to the reviewer #1 suggestion in the revised version.

Page 2307, line 14. 'Guillevic et al.'s (2014) ice core multi-proxy approach...'

The sentence will be corrected according to the reviewer #1 suggestion in the revised version.

Page 2307, line 18. '... is a valuable tool..'

The sentence will be corrected according to the reviewer #1 suggestion in the revised version.

REFERENCES

Ahn, J. and Brook, E. J.: Siple Dome ice reveals two modes of millennial CO2 change during the last ice age, Nature communications, 5, 2014.

Alvarez-Solas, J., Robinson, A., Montoya, M., and Ritz, C.: Iceberg discharges of the last glacial period driven by oceanic circulation changes, Proceedings of the National Academy of Sciences, 110, 16 350-16 354, doi:10.1073/pnas.1306622110, URL http://www.pnas.org/content/110/4 2013.

Angert, A., Barkan, E., Barnett, B., Brugnoli, E., Davidson, E. A., Fessenden, J., Maneepong, S., Panapitukkul, N., Randerson, J. T., Savage, K., Yakir, D., and Luz, B.: Contribution of soil respiration in tropical, temperate, and boreal forests to the 18O enrichment of atmospheric O2, URL http://dx.doi.org/10.1029/2003GB002056, 2003.

Barker, S., Diz, P., Vautravers, M. J., Pike, J., Knorr, G., Hall, I. R., and Broecker, W. S.: Interhemispheric Atlantic seesaw response during the last deglaciation, Nature, 457, 1097-1102, 2009.

Bender, M., Sowers, T., and Labeyrie, L.: The Dole Effect and its variations during the last 130,000 years as measured in the Vostok Ice Core, Global Biogeochemical Cycles, 8, 363-376, doi: 10.1029/94GB00724, URL http://dx.doi.org/10.1029/94GB00724, 1994.

Farquhar, G., von Caemmerer, S. v., and Berry, J.: A biochemical model of photosynthetic CO2 assimilation in leaves of C3 species, Planta, 149, 78-90, 1980.

Guillevic, M., Bazin, L., Landais, A., Stowasser, C., Masson-Delmotte, V., Blunier, T., Eynaud, F., Falourd, S., Michel, E., Minster, B., Popp, T., Prie, F., and Vinther, B. M.: Multi- proxy fingerprint of Heinrich event 4 in Greenland ice core records, Climate of the Past Discussions, 10, 1179-1222, doi:10.5194/cpd-10-1179-2014, URL http://www.clim- past-discuss.net/10/1179/2014 2014.

Hoffmann, G., Cuntz, M., Weber, C., Ciais, P., Friedlingstein, P., Heimann, M., Jouzel, J., Kaduk, J., Maier-Reimer, E., Seibt, U., and Six, K.: A model of the Earth's Dole effect, Global Biogeochemical Cycles, 18, doi:10.1029/2003GB002059, gB1008, 2004.

Joos, F., Gerber, S., Prentice, I. C., Otto-Bliesner, B. L., and Valdes, P. J.: Transient simulations of Holocene atmospheric carbon dioxide and terrestrial carbon since the Last Glacial Maximum, Global Biogeochemical Cycles, 18, doi:10.1029/2003GB002156, URL http://dx.doi.org/10.102 gB2002, 2004.

Kageyama, M., Mignot, J., Swingedouw, D., Marzin, C., Alkama, R., and Marti, O.: Glacial climate sensitivity to different states of the Atlantic Meridional Overturning Circulation: results from the IPSL model, Climate of the Past, 5, 551-570, doi:10.5194/cp-5-551- 2009, URL http://www.clim-past.net/5/551/2009/, 2009.

Keeling, R. F.: Development of an interferometric oxygen analyzer for precise measurement of the atmospheric O2 mole fraction, Ph.D. thesis, Harvard University, 1988.

Landais, A., Lathiere, J., Barkan, E., and Luz, B.: Reconsidering the change in global biosphere productivity between the Last Glacial Maximum and present day from the triple oxygen iso- topic composition of air trapped in ice cores, Global Biogeochemical Cycles, 21, n/a-n/a, doi: 10.1029/2006GB002739, URL http://dx.doi.org/10.1029/2006GB002739, gB1025, 2007.

Lewis, S. C., LeGrande, A. N., Kelley, M., and Schmidt, G. A.: Water vapour source impacts on oxygen isotope variability in tropical precipitation during Heinrich events, Climate of the Past, 6, 325-343, doi:10.5194/cp-6-325-2010, URL http://www.clim- past.net/6/325/2010/, 2010.

Marcott, S. A., Clark, P. U., Padman, L., Klinkhammer, G. P., Springer, S. R., Liu, Z., Otto-Bliesner, B. L., Carlson, A. E., Ungerer, A., Padman, J., He, F., Cheng, J., and Schmittner, A.: Ice-shelf collapse from subsurface warming as a trigger for Heinrich events, Proceedings of the National Academy of Sciences, 108, 13415-13419, doi:10.1073/pnas.1104772108, URL http://www.pnas.org/content/108/33/13415.abstract, 2011.

Pausata, F. S., Battisti, D. S., Nisancioglu, K. H., and Bitz, C. M.: Chinese stalagmite [delta] 18O controlled by changes in the Indian monsoon during a simulated Heinrich event, Nature Geoscience, 4, 474-480, 2011.

Rhodes, R. H., Brook, E. J., Chiang, J. C. H., Blunier, T., Maselli, O. J., McConnell, J. R., Romanini, D., and Severinghaus, J. P.: Enhanced tropical methane production in response to ice-

berg discharge in the North Atlantic, Science, 348, 1016-1019, doi:10.1126/science.1262005, URL http://www.sciencemag.org/content/348/6238/1016.abstract, 2015.

Welp, L. R., Keeling, R. F., Meijer, H. A., Bollenbacher, A. F., Piper, S. C., Yoshimura, K., Francey, R. J., Allison, C. E., and Wahlen, M.: Interannual variability in the oxygen isotopes of atmospheric CO2 driven by El Nino, Nature, 477, 579-582, 2011.

1.2 Response to Referee #2

We thank Referee #2 for the interesting comments and address the questions raised below.

Comment 1: The conclusion of the paper is that d18Oatm increases during H events because of hydrological changes, which in turn affect the vegetation. Given the results of Figure 4a I would have expected a decrease in d18Op over vegetated areas, contrarily to what is shown in figure 8b. It seems that the only region with positive d18Op and vegetation cover is over China and Southeast Asia. There is a large positive d18Op region between 0-20N in Africa, but it is associated with bare soil, so should not impact the GPP-O2 weighted d18Op. These changes would then overcompensate for the simulated negative d18Op in the Southern Hem. and over Europe. The zonal mean GPP-O2 weighted d18Op is shown in figure 9, but it looks surprising to see such a small effect in the latitudinal band 0-30S. Maybe a GPP-O2 weighted d18Op anomaly map might help. In addition, simulated precipitation anomalies between HS and LGM should be shown, as it would considerably help understand the processes at play. Why is d18Op increasing over South East Asia? Moreover, in its present state figure 3b is not informative and d18Op anomalies between HS and LGM as shown in Figure 4 is much better. Figures 3 and 4 should thus be reorganized to reflect these changes. If the drier (?) conditions over Southeast Asia are the main driver of d18Oatm, then the Southeast Asian Monsoon changes should play a significant role. The processes and robustness of this result should be briefly discussed. At the moment, there are some apparently contradictory statements in the text: P11, L. 7-9: 'However, the model does not simulate an Antarctic warming or weakened East Asian Monsoon (noted EASM hereafter) (Kageyama et al.,2009).' P17, L11-13: it is stated that the model reproduces

the weak Asian monsoon.

We thank reviewer #2 for this detailed comment. There was indeed an unfortunate issue with the colorscale of Figure 4a that was slightly offset towards negative values. The figure in the revised version (R5) is corrected and precipitation in the latitudinal band 0-30S does not appear as depleted in 18O. Indeed, most of the GPP is located in 3 main regions, namely Amazonia, southern Africa and Asia. In the O-30S zonal band, South East Asia and Africa global δ18Op slight increase compensate for the South America δ18Op decrease. In order to clarify this point, an additional figure will depict the HS-LGM difference of soil water δ18O, that is the water used by the plants to produce O2. As explained in the paper, the amount weighted δ18Op annual mean is affected to every month of the year for each gridcell (if monthly values would be kept, gppO2 weighted δ18Op would be more enriched by O.4 ‰, and would transfer it to δ18Oterr). Once again, it is important to keep in mind that a few areas concentrate most of the O2 production, and thus account for most of the δ18Op variations. Rainfall amount anomalies between LGM and HS will be displayed in the revised version of the manuscript. As answered to the comment 7 of review #1, rainfall amount generally drops in South East Asia, consistent with the observed increase of speleothem's d18Oc. In the Indian monsoon region, the positive anomaly is centered over the Bay of Bengal, with almost no change over land (Kageyama et al., 2009), and our simulation does not suggest a direct link between Indian Monsoon (North West India rainfall amount is lower over HS) and calcite d18O depletion of Chinese Cave's speleothems. In summary, Figure 3 of the revised version will display amount weighted δ18Op for LGM (control run) (R6) and maybe for HS (R6bis), soil water d18Op HS- LGM anomaly (R7) and rainfall amount HS-LGM anomaly (R8). The statement Page 17, line 11-13 about the model reproducing the weak Asian monsoon is removed as it indeed confuses the readers.

Comment 2: It is shown in equation 2 that the gross O2 fluxes from terrestrial and oceanic origin should have a similar impact on d18Oatm. Section 4.1. briefly discusses the possible changes in d18Omar and rules out pretty quickly an oceanic origin. I understand the current explanation for changes in d18Oatm involves changes in low latitude terrestrial processes. While

the authors and this hypothesis is most likely correct, it is quiteworthwhile to discuss the potential impact of changes in marine export. In order for section 4.1. to be very useful, a bit more caution should be used. There are still quite some uncertainties associated with the global change in oceanic export production, with some large regions (i.e. EEP), where the net change is quite unknown. A more robust approach would be to examine the impact on d18Oatm of -10 to +10% change in export. If a +10% change in export production has no significant impact on d18Oatm, then oceanic processes could be ruled out with confidence. If not then it should be acknowledge that there is room for uncertainties.

We agree with reviewer #2 to use more caution with the marine hypothesis. We simulated a change in the marine production to assess its impact on δ18Oatm signal. With a change of 10 % in marine export, δ18Oatm varies by 0.05 ‰. However this result has to be taken with caution for 2 main reasons. 1. The fraction of land versus ocean production is strongly affecting δ18Oatm if the isotope fractionation factors associated with the terrestrial and marine production are not similar. Pioneer studies in the Dole effect often invoked marine to terrestrial production ratio to explain the observed variations. Recent studies suggest their magnitude to be very close, which is not the case in our model, with δ18Omar 1.8 ‰higher than δ18Oterr. So the change in δ18Oatm is likely to be smaller in the real world. 2. As explained in the paper, recent studies (eg. Mariotti et al., 2012) rather suggest a decrease in marine export after a Heinrich event. This would lead to a decrease of δ18Oatm signal that is opposing the observations as mentioned in the discussion section. We will clearly state in the revised version that change in marine export can contribute to millennial timescale variations of δ18Oatm.

Comment 3: Additional information about the models and uncertainties associated with experiment design. Model IPSL-CM4 resolution should be in degrees or km. Since it is a central part of the paper, more information is needed about LMDZ4. Design of isotopic experiments: SST and sea ice fields during HS-exp are used to force the oxygen isotope enabled atmospheric model. SST and sea ice anomalies will impact air temperature, precipitation and evaporation. These 3 effects will be recorded in d18Oprecip. However, two potentially important factors are

neglected: if HS are driven by meltwater input from an icesheet, then 18O depleted water was added to the North-Atlantic, thus lowering North Atlantic surface d18O. In addition, climatic changes occurring during HS will impact surface ocean d18O everywhere. Thus the d18O signature of the source water during evaporation would have changed as well. This effect should lower d18Op in the Atlantic region sites, where few proxies exist. One sentence or two about the associated uncertainty could be added.

The resolution is now expressed in degrees. More information will be given on LMDZ4 in the revised version. We agree with the reviewer that other effects may have the potential to modify δ18Op. Monthly mean outputs of the IPSL are imposed to the LMDZ4 model, so there is no coupling between ocean and atmosphere, and nonlinear sub-monthly scale processes are thus not taken into account. The potential alteration of mean ocean water by the freshwater input and of depleted source regions during HS will be acknowledged based on LeGrande and Schmidt (2008) study of the 8.2k event in the revised version.

Comment 4: P17, L15: It is stated Greenland ice cores suggest a 4 ‰d18O decrease, whereas a 1.6 ‰decrease is simulated. I don't know if the term 'consistent with available data' is appropriate here. This discrepancy is most likely due to the weak cooling simulated over Greenland in the IPSL and should simply be acknowledged.

The reviewer #1 did a similar comment. We agree with both and will clearly state the model data discrepancy in the revised version. Please refer to comment 3 of reviewer #1 for details.

Comment 5: Please note that legend of figure 4 might be wrong: 'comparison of d18O precipitation anomaly'

The legend "(a) Model-data comparison of precipitation anomaly during HS compared to LGM. Data represent speleothem's calcite δ18O from various locations (see Table 3 for details)." is changed to '(a) Model-data comparison of δ18O precipitation anomaly during HS

compared to LGM. Data represent speleothem's calcite δ18O anomalies from various locations (see Table 3 for details).'

Minor comments: Typos:
Figure 1: L 4 'by using' P21, L. 26. Unnecessary d18Olw?
P26, L. 12: 'IPSL'
Figure 8: 2 a) iof a) and b)

Thanks for catching those errors. Typos and wrong figure numbers will be corrected in the revised version.

REFERENCES

Kageyama, M., Mignot, J., Swingedouw, D., Marzin, C., Alkama, R., and Marti, O.: Glacial climate sensitivity to different states of the Atlantic Meridional Overturning Circulation: results from the IPSL model, Climate of the Past, 5, 551-570, doi:10.5194/cp-5-551- 2009, URL http://www.clim-past.net/5/551/2009/, 2009.

LeGrande, A. N. and Schmidt, G. A.: Ensemble, water isotope-enabled, coupled general circulation modeling insights into the 8.2 ka event, Paleoceanography, 23, n/a-n/a, doi:10.1029/2008PA00 URL http://dx.doi.org/10.1029/2008PA001610, pA3207, 2008.

Mariotti, V., Bopp, L., Tagliabue, A., Kageyama, M., and Swingedouw, D.: Marine productivity response to Heinrich events: a model-data comparison, Climate of the Past, 8, 1581-1598, doi: 10.5194/cp-8-1581-2012, URL http://www.clim- past.net/8/1581/2012/, 2012.

2 Author's changes in manuscript

[1]C.Reutenauer [2]A.Landais [1]T.Blunier [2]C.Bréant [2]M.Kageyama [2,a]M-N.Woillez [3]C.Risi [2]V.Mariotti [2]P.Braconnot
Manuscript prepared for Clim. Past Discuss.
with version 4.1 of the LaTeX class copernicus_discussions.cls.
Date: 1 October 2015

Quantifying molecular oxygen isotope variations during a Heinrich Stadial

Centre for Ice and Climate, Niels Bohr Institute, University of Copenhagen, Copenhagen, Denmark

Institut Pierre Simon Laplace (IPSL), Laboratoire des Sciences de Climat et de l'Environnement (LSCE), UMR8212 (CEA-CNRS-UVSQ), CE Saclay, Orme des Merisiers, Bat. 701, 91191 Gif-sur-Yvette Cedex, France

Laboratoire de Météorologie Dynamique UMR8539, IPSL/CNRS/UPMC, 4, place Jussieu, 75252 Paris Cedex 05, France

now at: IFPEN, 14 avenue de Bois Préau, 92852 Rueil-Malmaison Cedex, France

Correspondence to: C. Reutenauer (creuten@nbi.dk)

Abstract

$\delta^{18}O$ of atmospheric oxygen ($\delta^{18}O_{atm}$) undergoes millennial scale variations during the last glacial period, and systematically increases during Heinrich Stadials (HS). Changes in $\delta^{18}O_{atm}$ combine variations in biospheric and water cycle processes. The identification of the main driver of the millennial variability of $\delta^{18}O_{atm}$ is thus not straightforward. Here, we quantify the response of $\delta^{18}O_{atm}$ to such millennial events using a freshwater hosing simulation ~~(HS_exp)~~ performed under glacial boundary conditions. Our global approach takes into account the latest estimates of isotope fractionation factor for respiratory and photosynthetic processes and make use of atmospheric water isotopes and vegetations changes. Our modeling approach allows to reproduce the main observed features of a HS in terms of climatic conditions, vegetation distribution and $\delta^{18}O$ of precipitation. We use it to decipher the relative importance of the different processes behind the observed changes in $\delta^{18}O_{atm}$. The results highlight the dominant role of hydrology on $\delta^{18}O_{atm}$ and confirm that $\delta^{18}O_{atm}$ can be seen as a global integrator of hydrological changes over vegetated areas.

3 Introduction

Oxygen is one of the most abundant species in atmospheric air. As oxygen is produced by photosynthesis and consumed by respiration, a record of oxygen concentration in the past should help us to constrain these two major biospheric fluxes on Earth and potentially provide information on their link with the carbon cycle.

Changes in the O_2/N_2 ratio can be measured in air trapped in ice core back to 800 kyr (Bender, 2002; Kawamura et al., 2007; Landais et al., 2012; Bazin et al., 2014). Unfortunately the O_2/N_2 ratio in ice cores does not provide a direct information on the true atmospheric variations because it is affected by ~~effusion process~~ permeation through the ice lattice during bubble formation at pore close-off, roughly 100 m below the ice-sheet surface, and by gas loss during ice core storage. These effects have less impact on the isotopic composition of oxygen. These

isotopic compositions have thus been ~~used to infer information on past~~ explored as possible constraints on biospheric productivity (Luz et al., 1999).

When dealing with isotopes, it is standard to use the isotope ratio, R, defined as the fraction of the abundance of the rare isotope over the dominant one in a substance. Since changes in isotope ratios through natural processes are very small, they are expressed in relation to a standard (recent air and Vienna Standard Mean Ocean Water (VSMOW) being used for O_2 and H_2O respectively) using the δ notation,

$$\delta^{18}\mathrm{O} = \frac{{}^{18}R_{\mathrm{sample}}}{{}^{18}R_{\mathrm{standard}}} - 1, \tag{1}$$

$\delta^{18}\mathrm{O}$ and $\delta^{17}\mathrm{O}$ of atmospheric oxygen have been measured ~~over the~~ for the period of the past 800 kyr with a mean resolution of about 1500 yrs (e.g. Landais et al., 2010, and references therein; Blunier et al., 2012). As shown by Bender et al. (1994), $\delta^{18}\mathrm{O}$ of atmospheric oxygen, noted $\delta^{18}\mathrm{O_{atm}}$ hereafter, cannot easily be related to biospheric productivity through photosynthesis and respiration fluxes. $\delta^{18}\mathrm{O_{atm}}$ variations actually reflects for a large part the isotopic composition of the meteoric water. The ~~later~~ latter is transmitted to the plant through its roots and stems to the leaves where photosynthesis produces oxygen with an isotopic composition close to the isotopic composition in leafwater. Respiration modifies the isotopic composition of atmospheric oxygen in a complex way. While the processes consuming oxygen enrich atmospheric oxygen through a preferential consumption of the lightest molecules, individual biological pathways are associated with a wide range of oxygen fractionations (Helman et al., 2005).

Based on fractionation factors available at the time, Bender et al. (1994) established that the relative proportion of oceanic vs. terrestrial biospheric productivities together with the difference in isotope fractionation over land and ocean were driving the $\delta^{18}\mathrm{O_{atm}}$ budget. Several studies built on this idea and interpret the $\delta^{18}\mathrm{O_{atm}}$ variations mainly as variations of the oceanic vs. terrestrial biospheric productivities (Hoffmann et al., 2004; Ciais et al., 2012). However, recent measurements have revealed that over all fractionation associated with oceanic productivity is very similar to its terrestrial counterpart (Hendricks et al., 2004; Eisenstadt et al., 2010),

questioning the interpretation of $\delta^{18}O_{atm}$ as an indicator of the relative proportion of oceanic vs. terrestrial biosphere productivity (Luz and Barkan, 2011b).

Despite the complex interpretation of $\delta^{18}O_{atm}$, several robust features have already been observed highlighting the potential of these measurements. At the orbital scale, $\delta^{18}O_{atm}$ is showing clear variations at a 23 kyr periodicity (Dreyfus et al., 2007). This strong link with precession is probably related to the variations of the hydrological cycle at low latitudes (Bender et al., 1994). Indeed, variations related to the monsoon regime strongly imprint the isotopic composition of meteoric water as observed in speleothem records (e.g. Wang et al., 2008). They are easily transmitted to the isotopic composition of atmospheric oxygen because the major part of the biospheric productivity, hence photosynthesis, is occurring in the tropics and subtropics.

At the millennial scale, it has recently been shown that $\delta^{18}O_{atm}$ is responding to the abrupt climate changes of the last glacial period (Landais et al., 2007a; Severinghaus et al., 2009). ~~The references for the millennial scale variability are the~~ Millennial-scale climate variability is perhaps best known from the Greenland ice cores, where it is manifested in the stable water isotopes ~~from Greenland icecores record exhibiting~~ of ice. During the last glacial period, these cores show 25 Dansgaard-Oeschger (DO) events ~~during the last glacial period~~ (NGRIP members et al., 2004). A DO event typically exhibits a sawtooth pattern: (i) a cold phase (Greenland Stadial, noted GS hereafter) lasting from centuries to millennia, followed by a warm phase (Greenland Interstadial, GI) starting with (ii) a rapid transition (a few decades) with an amplitude of up to $16 \pm 2.5\,^{\circ}C$ (Landais et al., 2004; Huber et al., 2006; Kindler et al., 2014) and ending with (iii) a gradual cooling before an abrupt ~~jump towards glacial~~ decrease towards cold, stadial values.

During the last decade, mechanisms of glacial abrupt events have been investigated using coupled ocean–atmosphere models of varying complexity (e.g. ~~Kageyama et al., 2013; Stouffer et al., 200~~ Recent hypotheses often invoke internal variability (Kleppin et al., 2015; Dokken et al., 2013), involving sea-ice atmosphere interactions (e.g. Li et al., 2005, 2010), through ice-albedo feedback and the impact of sea ice cover on regional temperatures by preventing heat exchange between ocean and atmosphere. ~~However there~~ There remains robust evidence from multiple lines of paleoceanographic information and modeling that millennial scale variability is linked

to changes in the AMOC intensity (e.g. Mc Manus et al., 1998), potentially initiated by large freshwater input in the North Atlantic (e.g. Broecker et al., 1990). The ~~supposed key role of the ocean stems in part from the~~ presence of ice rafted debris (IRD, Ruddiman, 1977; Heinrich, 1988) in marine sediments from the North Atlantic region during the largest GS ~~. Such layers~~ document episodes of massive iceberg discharge in the North Atlantic (Heinrich Events) mainly from the Laurentide (H2, H4, H5) and Fennoscandian (H3, H6) ice sheets (Grousset et al., 1993; Guillevic et al., 2014 and references therein). Even ~~if IRD can be recorded for each GS in some northern marine cores of the Atlantic~~ though IRD is present in each GS (Elliot et al., 2002), not all GS ~~are associated with~~ contain a Heinrich event. Heinrich Stadials (noted HS hereafter) are GS associated with a Heinrich event ~~(Baker et al., 2009; Sanchez Goni and Harrison, 2010)~~(Barker et a

Several aspects of the observed patterns during DO events can be captured through the response of the Earth system to imposed freshwater perturbations in the North Atlantic (Liu et al., 2009; Otto-Bliesner and Brady, 2010; Kageyama et al., 2010; Roche et al., 2010), mimicking Heinrich events. Depending on the background state of the climate (glacial or interglacial, orbital context), of the AMOC, and ~~of~~ on the magnitude of the freshwater forcing, these models produce a complete shutdown of the AMOC (HS-like state) or a reduction of the strength of the AMOC (GS-like state) (e.g. Menviel et al., 2014). The injection of freshwater produces in all models a significant cooling of the North Atlantic region. The amplitude of the associated temperature change is probably affected by the simulated change in sea-ice extent and feedbacks between sea-ice and temperature that vary in the different models (Kageyama et al., 2013). These hosing experiments also produce an inter-hemispheric seesaw temperature pattern~~and associated impacts on the position~~ , associated with a southward shift of the ITCZ (e.g. Dahl et al., 2005; Broccoli et al., 2006; Krebs and Timmermann, 2007; Swingedouw et al., 2009; Cvijanovic and Chiang, 2013)~~through a modification of the upper part of the thermohaline circulation~~. Abrupt climate variation associated with the Greenland signal is found down to low latitudes in numerous terrestrial and marine archives (e.g. Clement and Peterson, 2008). ~~In a large part~~ Its climatic impact is recorded in large parts of the North Atlantic region, ~~the temperature records follow the Greenland signal but with a smaller amplitude~~ both in marine cores (e.g. Bond et al., 1993; Broecker, 2000) and in speleothems (Fleitmann et al., 2009).

Concomitant methane excursions and variations in the isotopic composition of the calcite of speleothems in East Asia (e.g. Wang et al., 2001; Cheng et al., 2012) strongly support the fact that these DO events are associated with major reorganization of the tropical water cycle and hence monsoon intensity through a shift ~~of the ITCZ~~ in the ITCZ and its terrestrial equivalent, the tropical rain belt (Chappellaz et al., 2013; Wang et al., 2008; Pausata et al., 2011).

~~Over this~~ For this period of millennial scale variability, high-resolution measurements of $\delta^{18}O_{atm}$ have been obtained in Greenland and Antarctic ice cores (e.g. Guillevic et al., 2014; Landais et al., 2007a, 2010; Severinghaus et al., 2009). We present in Fig. 1 a synthesis of $\delta^{18}O_{atm}$ evolution from the Siple Dome ice core over HSs displayed on Greenland Ice Core Chronology 2005 (GICC05) timescale, using Rasmussen et al.'s (2013) definitions of onset of ~~Rasmussen et al. (2013) for onsets of~~ GS. The $\delta^{18}O_{atm}$ records show a systematic increase in a few kyrs following the onset of a HS (Fig. 2) by around 0.13 ‰, from +0.08 ‰ (HS1) to +0.18 ‰ (HS5). The difference in the slope ~~inflexion~~ inflection at the onset of HS4 and HS5, more pronounced that for HS1, HS2 and HS3, may be due to the long-term trend observed in $\delta^{18}O_{atm}$. Indeed, from 35 to 15 kyr, $\delta^{18}O_{atm}$ exhibits a constant increase, consistent with the build-up of polar ice-sheet, hence enrichment of ocean water in ^{18}O, but remains relatively stable over MIS3 (Fig. 1).

Because of its global character, $\delta^{18}O_{atm}$ should provide ~~a strong~~ added value compared to the different local records of hydrological cycle variations in different continental and marine archives. However, until now, no quantitative, robust interpretation of past variations in $\delta^{18}O_{atm}$ has been established, which limits the use of $\delta^{18}O_{atm}$ as a quantitative indicator for past biospheric production or variations of the hydrological cycle. The aim of this modeling study is thus to provide a quantitative interpretation for the systematic increase in $\delta^{18}O_{atm}$ over HSs. To reach this objective, we propose a global approach incorporating outputs from a general circulation model implemented with water isotopes and focus on the millennial variability of the last glacial period. We follow a modeling approach already developed by Hoffmann et al. (2004). We combine climatic parameters (temperature and humidity), isotopic composition of meteoric water~~and vegetation repartition~~ , vegetation distribution and productivity simulated by different models with monthly mean temporal resolution.

In a first section, we describe the general method used to simulate a global $\delta^{18}O_{atm}$ signal. A second part is dedicated to model validation and the third part proposes to quantify the different contributions (hydrology, vegetation, climatic conditions) to the $\delta^{18}O_{atm}$ signal over a HS equivalent.

4 Method

According to Landais et al. (2007a, 2010) and Severinghaus et al. (2009), the millennial variations of $\delta^{18}O_{atm}$ during the last glacial period are driven by shifts in ~~ITCZ~~ the tropical rain belt modifying the relative humidity distribution and the isotopic composition of meteoric water consumed by terrestrial biosphere. The ~~build-up~~ isotopic content of atmospheric oxygen ~~involves numerous processesso that we need to~~ is controlled by numerous processes, so we must consider (i) the worldwide meteoric water isotopic composition, from which ground water is derived, (ii) the worldwide temperature and humidity, from which evaporative enrichment of leaf water $\delta^{18}O$ is calculated, ~~as well as~~ (iii) the worldwide vegetation cover and Gross Primary Productivity, defining the ~~photosyntetically~~ photosynthetically and respiratory active areas that contribute to $\delta^{18}O_{atm}$, as well as (iv) respiratory processes.

4.1 Oxygen isotopes mass balance model

Oxygen is exchanged with the terrestrial and marine biospheres as well as with the stratosphere. Assuming a steady state, $\delta^{18}O_{atm}$ can thus be expressed as follows:

$$\delta^{18}O_{atm} = \frac{(F_{terr} \cdot \delta^{18}O_{terr} + F_{mar} \cdot \delta^{18}O_{mar})}{(F_{terr} + F_{mar})} - {}^{18}\epsilon_{strat}, \quad (2)$$

where ${}^{18}\epsilon_{strat}$ represents the stratospheric isotope fractionation caused by photochemical reaction in the stratosphere involving O_2, O_3 and CO_2. F_{terr} and F_{mar} denote O_2 fluxes of gross terrestrial and oceanic productivity, respectively. $\delta^{18}O_{terr}$ and $\delta^{18}O_{mar}$ are the isotopic composition arising from the terrestrial and oceanic realms, respectively. ${}^{18}\epsilon_{strat}$ is a small term,

~~0.3~~0.4 ‰ against ~ 23.8 ‰ for $\delta^{18}O_{atm}$ with reference to V-SMOW (Luz et al., 2014) and is not assumed to change significantly over a HS because CO_2 level remains relatively stable. We assume a constant CO_2 level between LGM and HS in our study. Ahn and Brook's (2014) study show that variations over HS are small (increase of less than 20 ppm). Effect of isotopic exchange between CO_2 and O_2 in the statosphere on $\delta^{18}O_{atm}$ is expected to be proportional to CO_2 mixing ratio. Following Bender et al.'s (1994) calculation, which estimates a $\delta^{18}O_{atm}$ depletion of 0.4 ‰ for a CO_2 concentration of 353 ppm, we can estimate that a 20 ppm increase between LGM and HS can modify $\delta^{18}O_{atm}$ by -0.023 ‰. The sign of this change is actually opposite to the sign of the observed $\delta^{18}O_{atm}$ signal. We focus mainly on the millennial scale variations of the terrestrial contribution to $\delta^{18}O_{atm}$ signal, i.e. $F_{terr} \cdot \delta^{18}O_{terr}/(F_{terr} + F_{mar})$.

We do not consider the marine influence~~in a first approach~~, in this first approach, for the following reasons. First, our aim is to test the hypothesis of Landais et al. (2007b) and Severinghaus et al. (2009) that $\delta^{18}O_{atm}$ millennial scale variations are ~~driven by variations~~ largely driven by changes in the low ~~latitudes~~ latitude hydrological cycle through changes in the $\delta^{18}O$ of precipitation. Second, Hendricks et al. (2004) and Luz and Barkan (2011a) have shown that the difference between $\delta^{18}O_{terr}$ and $\delta^{18}O_{mar}$ is not significant. Finally, the spatial and temporal variations of water $\delta^{18}O$ and respiration pathways in the ocean are expected to be relatively small compared to the variations on land, which ~~render~~ renders their integration for $\delta^{18}O_{atm}$ ~~modelling~~ modeling less crucial as illustrated in the study of Hoffmann et al. (2004).

4.2 Calculation of $\delta^{18}O_{terr}$

The major source of atmospheric oxygen from the terrestrial biosphere is the oxygen produced during photosynthesis. The fractionation associated with photosynthesis is small (Guy et al., 1993; Eisenstadt et al., 2010). The oxygen produced by this process has thus almost the same isotopic composition ~~than~~ as the leaf water. Consumption of oxygen is also associated with biosphere productivity through different pathways (dark respiration, photorespiration, Mehler reaction). $\delta^{18}O_{terr}$ thus results from isotope fractionation associated with photosynthesis and oxygen uptake. Following Bender et al. (1994); Blunier et al. (2002); Hoffmann et al. (2004); Landais et al. (2007b), we assume a steady-state, where photosynthesis equals respiration. $\delta^{18}O_{terr}$ cal-

culates as:

$$\delta^{18}\mathrm{O}_{\mathrm{terr}} = \frac{(\delta^{18}\mathrm{O}_{\mathrm{lw}} + 1)}{{}^{18}\alpha_{\mathrm{resp}}} - 1, \tag{3}$$

where $\delta^{18}\mathrm{O}_{\mathrm{lw}}$ is the global production-weighted average isotopic composition of leaf water and ${}^{18}\alpha_{\mathrm{resp}}$ is the global apparent respiratory isotope fractionation factor associated with global oxygen uptake, i.e. oxygen consumption weighted average of fractionation factors associated with specific respiratory pathways.

4.3 Photosynthetic oxygen

As classically done, we estimate the value of $\delta^{18}\mathrm{O}$ of leaf water, hereafter $\delta^{18}\mathrm{O}_{\mathrm{lw}}$, based on Craig and Gordon (1965) equation (C&G) of evaporation applied to leaf transpiration (Dongmann, 1974; Flanagan et al., 1991b). It is thus calculated in the following way:

$$\delta^{18}\mathrm{O}_{\mathrm{lw}} = h \cdot (\delta^{18}\mathrm{O}_{\mathrm{vap}} + {}^{18}\epsilon_{\mathrm{eq}}) + (1-h) \cdot (\delta^{18}\mathrm{O}_{\mathrm{gw}} + {}^{18}\epsilon_{\mathrm{eq}} + {}^{18}\epsilon_{\mathrm{kin}}), \tag{4}$$

where h is the relative humidity at the site of photosynthesis, ${}^{18}\epsilon_{\mathrm{eq}}$ is the ~~liquid vapor~~ temperature-depen liquid-vapor equilibrium isotope effect ~~dependent of temperature~~ (Majoube, 1971), ${}^{18}\epsilon_{\mathrm{kin}}$ is the kinetic isotope effect occurring when humidity is below saturation, $\delta^{18}\mathrm{O}_{\mathrm{gw}}$ is the isotopic composition of soil water and $\delta^{18}\mathrm{O}_{\mathrm{vap}}$ is the water vapor $\delta^{18}\mathrm{O}$ near the surface. ${}^{18}\epsilon_{\mathrm{kin}}$ is deduced from the ratio of the diffusion coefficient associated with $\mathrm{H_2^{16}O}$ (D) and $\mathrm{H_2^{18}O}$ (D*). Several values for the ratio D/D^* can be found in the literature (Merlivat, 1978; Cappa et al., 2003; Luz et al., 2009), varying from 1.028 to 1.032. For leaf water evaporation, many studies have reported lower enrichment in $\delta^{18}\mathrm{O}_{\mathrm{lw}}$ than that predicted by Eq. (4) with ${}^{18}\epsilon_{\mathrm{kin}} = D/D^* - 1$ as classically assumed (e.g. Allison et al., 1985; Bariac et al., 1989; Walker et al., 1989; Walker and Brunel, 1990; Yakir et al., 1990; Flanagan et al., 1991b,a, 1993, 1994). Farquhar et al. (1989) suggested that ${}^{18}\epsilon_{\mathrm{kin}}$ depends on the importance of either stomatal or boundary layer resistances. In moist conditions, stomata resistance is low and boundary layer resistance high, leading ${}^{18}\epsilon_{\mathrm{kin}}$ to ~~value~~ values as low as 19 ‰ when using the Merlivat (1978) value for D/D^*.

In this study, we have imposed a mean value for $^{18}\epsilon_{kin}$ of 20 ‰ ~~, higher values leading~~ because higher values led to too high ~~global values~~ a global value for $\delta^{18}O_{atm}$.

The calculation of $\delta^{18}O_{lw}$ using Eq. (4) requires spatial and temporal variations of temperature and relative humidity as well as the variations of the isotopic composition of water vapor and meteoric water, from which $\delta^{18}O_{gw}$ will be deduced (Sect. 4.3.2). These variables are obtained from outputs of modeling experiments.

4.3.1 Simulated climatic variations over an abrupt cooling

~~For inferring temperature~~ Temperature and relative humidity variations over a HS ~~, we have used~~ are inferred from simulations with the atmosphere–ocean general circulation model (AOGCM) IPSL_CM4 (Marti et al., 2010) with a horizontal resolution for the atmosphere grid of ~~$96 \times 72 \times 19$ in longitude $\times$~~ $3.75° \times 2.5°$ (latitude $\times$ ~~altitude. As stated above, to model~~ longitude) and with a 19 vertical layer atmosphere. To model the $\delta^{18}O_{atm}$ variations over a HS, we have used ~~the simulation of a HS achieved from a~~ a glacial simulation perturbed by a freshwater hosing experiment~~run in glacial conditions in a coupled general circulation model~~. We will ~~thus~~ compare in the following the outputs of two simulations: one for the Last Glacial Maximum (LGM_ctrl) and one for the Heinrich Stadial (HS_exp).

The ~~glacial~~ LGM_ctrl boundary conditions are as follows (see Kageyama et al., 2009 for a detailed presentation of the climate setup): orbital parameters for 21 ky BP, CO_2, CH_4 and N_2O levels set to 185 ppm, 350 and 200 ppb respectively (Monnin et al., 2001; Dällenbach et al., 2000; Flückiger et al., 1999), ICE-5G ice-sheet reconstruction and land-sea mask (Peltier, 2004).

The first experiment is an equilibrated glacial run (LGM_ctrl) used as reference run (see LGMb in Kageyama et al., 2009). The second experiment (HS_exp) is a water hosing experiment, where an additional freshwater flux of 0.1 Sv ($1\,Sv = 10^6\,m^3s^{-1}$) is imposed instantaneously in the Atlantic North of 40° N and the Arctic (see LGMc in Kageyama et al., 2009) from year 150 ~~of the reference run until year 550 of the reference run~~for 400 yrs. The input of freshwater in HS_exp, mimicking a Heinrich event, leads to an AMOC collapse in 250 years (see Fig. ~~1a in Woillez et al., 2013).~~ 1 in Kageyama et al., 2009). We selected this HS_exp

experiment since the most efficient way to simulate the climate state during an Heinrich event with a model is to add freshwater in the high latitudes of the Atlantic ocean, eventhough results from recent studies (Marcott et al., 2011; Guillevic et al., 2014; Rhodes et al., 2015; Alvarez-Solas et al. that this does not satisfactorily explain the observed sequences of events (freshwater discharges from ice sheets might not be the initial trigger of Heinrich events) and especially the decoupling between Greenland and low latitudes. We therefore center our study on the mean state of 2 contrasted periods rather than investigate the dynamics of the transition from LGM to HS. It also explains why we only focus on Heinrich Stadials and not DO events.

The climate response to the AMOC collapse in the HS_exp is of global extent and qualitatively agrees with ~~paleoarchives~~ paleoarchive reconstructions for the North-Atlantic cooling, southwards Atlantic ITCZ migration and weakening of Indian and African monsoons (Kageyama et al., 2009, 2013). However, the model does not simulate an Antarctic warming or weakened East Asian Monsoon ~~(noted EASM hereafter)~~ (Kageyama et al., 2009). In the following we used the monthly-averaged spatial fields of temperature (Tm) and humidity calculated on the ~~coupled model~~ first layer of the atmosphere grid. From these data we followed the Lloyd and Farquhar (1994) approach to link leaf temperature during photosynthesis, Tp, to ~~monthly temperature in the first layer of the model,~~ Tm, through $\mathrm{Tp} = 1.05 \cdot (\mathrm{Tm} + 2.5)$. $2.5\,^{\circ}\mathrm{C}$ are added to Tm to account for the daytime increase in air temperature at the time of photosynthesis. The $5\,\%$ increase allows for net canopy to air heat fluxes (Farquhar and Lloyd, 1993). The relative humidity from the first layer is not modified (Farquhar et al., 2007).

4.3.2 Modeling of δ^{18}O of meteoric water and groundwater

For our estimate, we also need the distribution of the oxygen isotopic composition of meteoric water. We extract it from the isotopic version of the atmospheric general circulation model developed at the Laboratoire de Météorologie Dynamique (LMDZ4) (Risi et al., 2010). LMDZ is the atmospheric component of the IPSL-CM4 model used above. The physical package is described in detail by Hourdin et al. (2006). It includes in particular the Emanuel convective parameterization (Emanuel, 1991; Grandpeix et al., 2004) coupled to the Bony and Emanuel's (2001) cloud scheme. Each grid cell is divided into four subsurfaces: ocean, land, ice sheet and

sea ice (Risi et al., 2010). The monthly sea surface temperature and sea ice fields obtained from the two aforementioned experiments at equilibrium (LGM_ctrl and HS_exp) have been used as surface boundary conditions for the isotopic simulations.

We present on Fig. 3 the mean annual Monthly mean outputs of the IPSL-CM4 are imposed to the LMDZ4 model, so there is no coupling between ocean and atmosphere, and nonlinear sub-monthly scale processes are thus not taken into account here. This choice should not alter our results. Indeed, LeGrande and Schmidt (2008) analyze changes in water isotopes following the 8.2 ka event's meltwater pulse (meltwater $\delta^{18}O$: -30 ‰) in a fully coupled AOGCM (Goddard Institute for Space Studies ModelE-R) and show that the effect of the freshwater impulse on $\delta^{18}O$ of precipitation, noted $\delta^{18}O_p$ hereafter, can be neglected, because the signal is very short-lived, only a few decades, before the climatic component dominates. Furthermore, the main changes are constrained to the northern North-Atlantic and its surrounding regions (Fig. 6 of LeGrande and Schmidt, 2008). Those regions only have a limited contribution to the $\delta^{18}O_{atm}$ signal, as most of the terrestrial photosynthesis occurs in the tropics. Fig. 7 of LeGrande and Schmidt (2 that 2 decades after a meltwater pulse, the ensemble mean (5 simulations) anomaly of $\delta^{18}O_p$ calculates to -0.01 ‰, confirming the small impact of $\delta^{18}O$ depleted meltwater.

Fig. 3 shows the mean annual $\delta^{18}O_p$, simulated for the LGM_ctrl and the HS_exp experiments. The $\delta^{18}O_p$ repartition distribution for the LGM_ctrl experiment has already been confronted to data for validation in Risi et al. (2010).In HS_exp, we observe a general decrease of $\delta^{18}O_p$ compared to the $\delta^{18}O_p$ in the LGM_ctrl experimentobservations of water isotopes in vapor and precipitation (Risi et al., 2010) and seasonal patterns are well captured. For validation purpose, $\delta^{18}O_p$ changes from LGM to HS are compared with changes in (i) calcite $\delta^{18}O$ in speleothems, noted $\delta^{18}O_c$ hereafter, and in (ii) ice $\delta^{18}O$ in Greenland ice cores over Heinrich events (Sect. 5.1.2, see Fig. 4a for $\delta^{18}O_p$ anomaly).

Finally Eq. (4) also requires an estimate of $\delta^{18}O_{gw}$. Groundwater pumped through the plant's roots represents a mixture of stored water and incoming precipitation water (McGuire et al., 2002). Indeed, during spring/summer when maximal productivity occurs the groundwater is composed of significant amounts of fall/winter precipitation. In order to take the mixing into account we use amount-weighted annual-mean $\delta^{18}O$ of precipitation. This approach has been

shown to be realistic in a field experiment in Kenya (Wang et al., 2012) and has been implemented in global coupled climate model of intermediate complexity (Caley et al., 2014). Doing so, we neglect the fractionation effects that can significantly affect the soil water isotopic composition, especially in dry regions (Kanner et al., 2014).

4.4 Oxygen uptake in respiratory processes

4.4.1 Global oxygen production

The geographical distribution of respiratory O_2 fluxes (noted GPP_O_2 hereafter from the hypothesis of equilibrium between oxygen production and consumption) is computed from the vegetation cover and Gross Primary Productivity (GPP) distribution provided by the ORCHIDEE model which simulates the vegetation distribution of 10 natural plant functional types (PFT) and bare soil (Krinner et al., 2005). ORCHIDEE is the land surface component of the IPSL-CM4 model. It is used here with the same spatial resolution as the aforementioned models (latitude $\times$ longitude $3.75^\circ \times 2.5^\circ$) and is run in offline mode, forced by the high-frequency outputs from IPSL-CM4 ~~_v1~~ for the two experiments LGM_ctrl and_HS_exp. The prescribed forcing has a 6 h time-step temporal resolution, and thus takes into account daily variability and diurnal cycle simulated by the IPSL model (Woillez, 2012). Each grid cell simulates the vegetation cover by splitting the cell into fractions of 10 Plant Functional Types (PFT, see Table 1 for names) and provides GPP fluxes ($\mathrm{g\,C\,m^{-2}\,yr^{-1}}$) for each PFT. Validation of the vegetation cover can be found in Woillez et al. (2011) for LGM_ctrl and Woillez et al. (2013) for HS_exp over Western Europe. Here we extend this work and compare LGM and HS simulation with worldwide vegetation reconstructions selected from marine (coastal) and terrestrial paleoarchives with high temporal resolution (Sect. 5.1.3).

In this study, following Hoffmann et al. (2004), we calculate the terrestrial biosphere's O_2 fluxes in 3 steps. First, the outputs from ORCHIDEE provide the GPP expressed in $\mathrm{g\,C\,m^{-2}\,yr^{-1}}$ for each of the 10 PFT's on each model grid point. Second, simulated carbon molar fluxes for each PFTs are converted to oxygen molar fluxes, based on the biochemical model of photosynthesis from Farquhar et al. (1980). The model accounts for fraction of photorespiration and the

photosynthetic quotient (PQ) -measured by Keeling (1988) and Severinghaus (1995) as ~ 1.1. Third, GPP_O_2 for each PFT is expressed in terms of dark respiration (mitochondrial), Mehler respiration and photorespiration, each of these respiratory uptake processes being associated with a specific fractionation (refer to Table 2 for values):

$$\begin{aligned} \text{GPP\_O}_2 &= \text{GPP\_O}_2\text{\_Mehler} + \text{GPP\_O}_2\text{\_dark} + \text{GPP\_O}_2\text{\_photo} \\ &= \frac{\text{GPP} \cdot \text{PQ} \cdot (1 + f_{\text{photo}})}{1 - f_{\text{Mehler}}}, \end{aligned} \tag{5a}$$

With,

$$\text{GPP\_O}_2\text{\_Mehler} = f_{\text{Mehler}} \cdot \text{GPP\_O}_2, \tag{5b}$$

$$\text{GPP\_O}_2\text{\_dark} = (1 - f_{\text{Mehler}}) \cdot \text{PQ} \cdot \text{GPP}, \tag{5c}$$

$$\begin{aligned} \text{GPP\_O}_2\text{\_photo} &= (1 - f_{\text{Mehler}}) \cdot (\text{GPP\_O}_2 - \text{PQ} \cdot \text{GPP}) \\ &= (1 - f_{\text{Mehler}}) \cdot \text{PQ} \cdot \text{GPP} \cdot f_{\text{photo}}, \end{aligned} \tag{5d}$$

where f_{Mehler} denotes the fraction of Mehler reaction, and accounts for 10 % of the total respiration (Badger et al., 2000) and f_{photo} represents the fraction of photorespiration.

4.4.2 Photorespiration

All types of C3 plants photorespire, but in different proportions. In contrast, C4 plants do not photorespire, because of a ~~C~~CO_2 concentration mechanism allowing them to operate at high chloroplast CO_2 partial pressures and thereby to inhibit the oxygenation reaction during photosynthesis (Von Caemmerer, 2000). The proportion of photorespiration is calculated from the proportion of C4 vs C3 plants, ~~f_{photo}, depends thus on the type of plants (10 PFT's in this study), on the atmospheric concentration of~~ temperature and CO_2 ~~(taken constant in this study) and on temperature.~~ level (assumed constant in our study) as depicted in the biochemical model of photosynthesis from Farquhar et al. (1980) and already done in the studies of Hoffmann et al. (2004) and Landais et al. (2007a). Increasing photorespiration modifies $^{18}\epsilon_{\text{resp}}$, as photorespiration is associated

with a high discrimination, and in turn affects $\delta^{18}O_{terr}$. Details on equations used in our offline model for $\delta^{18}O_{terr}$ calculation can be found in Hoffmann et al. (2004).

4.4.3 Soil respiration

We have assigned fractionation factors for each soil using the soil type discrimination proposed by Angert et al. (2003), taking into account the weakening of respired O_2 back-diffusion in waterlogged soils . For this, we relate the Angert's soil types to the type of vegetation cover over the considered soil in ORCHIDEE model. As an example, we have assigned tropical soils (fractionation coefficient of -10.1 ‰) to soil covered by dominant PFT Tropical broadleaf evergreen trees and PFT Tropical broadleaf raingreen trees. Tropical soils (-10.1 ‰) discriminate significantly less than temperate (-17.8 ‰) or boreal soils (-22.4 ‰) following Angert et al. (2003). The global respiratory isotope fractionation for the control run calculates as -15.895 ‰, much weaker than the common value (-18 ‰) used for terrestrial ecosystems. As soil respiration only occurs where vegetation exists, a shift of the latter modifies the spatial distribution of soils where dark respiration takes place. In our model, the change of vegetation cover from LGM to HS leads to a very slight weakening of soil respiration isotope fractionation using fractionation values of Angert et al. (2003), thus considering soil aeration.

4.4.4 Global terrestrial fractionation factor

Uptake of oxygen by respiration discriminates against heavy isotopes, leaving the substrate oxygen, atmospheric O_2, enriched in ^{18}O. Each of the oxygen uptake processes is affected by a specific, spatially and temporally constant fractionation (Table 2) and the global terrestrial isotope fractionation factor $^{18}\alpha_{resp}$ is expressed as follows:

$$^{18}\alpha_{resp} = {}^{18}\alpha_{photo} \cdot f_{photo} + {}^{18}\alpha_{Mehler} \cdot f_{Mehler} + {}^{18}\alpha_{dark\_soil} \cdot f_{dark\_soil} + {}^{18}\alpha_{dark\_leaves} \cdot f_{dark\_leaves}, \quad (6)$$

The latest estimations of $^{18}\alpha_{Mehler}$, $^{18}\alpha_{photo}$ and $^{18}\alpha_{dark\_leaves}$ can be found in Table 2. A significant proportion of terrestrial respiration (30 to 40 %) occurs below the surface (Raich and

Potter, 1995) with varying fractionation values. Respiration below surface (~~$^{18}\alpha_{\text{dark\_leaves}}$~~ $^{18}\alpha_{\text{dark\_soil}}$) thereby needs to be considered for the different types of soils (boreal, temperate, tropical), as each soil type is associated with a specific fractionation factor because of different diffusion pathways (Angert et al., 2003). The Mehler fraction, f_{Mehler}, represents 10 % of global respiration (Badger et al., 2000) and f_{photo} is calculated from the outputs of the ORCHIDEE and IPSL-CM4 models. ~~Dark~~ The dark respiration fraction is composed of ~~leave~~ leaf (38 %) and soil (62 %) respiration, following Landais et al. (2007b).

5 Results

5.1 Simulation of regional climate, vegetation and isotopic pattern during a HS

We propose here a model–data comparison on a regional scale to evaluate the model performances, as the climatic and water cycle responses during a HS are not spatially homogeneous. ~~While the climatic~~ Climatic outputs of the HS experiments are already discussed in Kageyama et al. (2009) and Woillez et al. (2013)~~, we discuss the~~ . We thus mainly discuss in the following the simulated change in relative humidity (Sect. 5.1.1) since the latter has an important influence on the $\delta^{18}O_{lw}$ and hence $\delta^{18}O_{terr}$. Then, we further compare the modeled change in $\delta^{18}O$ of precipitation over a HS with changes in speleothems calcite $\delta^{18}O$ (Sect. 5.1.2) and modeled fraction of vegetation with vegetation reconstructions (Sect. 5.1.3).

5.1.1 Simulated humidity validation

According to climate reconstructions, during HS, wet periods in northeastern Brazil are synchronous with periods of weak East Asian summer monsoons (Wang et al., 2001) and with cold periods in Greenland (Grootes and Stuiver, 1997) and Europe (Genty et al., 2003). Reorganization in tropical rainfall patterns leads to wetter conditions in southwestern North America (Asmerom et al., 2010) and southern South America (Kanner et al., 2012), and to dryer conditions in the Australian-Indonesian monsoon region (Mohtadi et al., 2011), wide parts of Asia

(Wang et al., 2008), ~~Northern~~ northern South America (Peterson and Haug, 2006), Mediterranean region (Fleitmann et al., 2009), and equatorial western Africa (e.g. Weldeab, 2012).

During HS, the model simulates similar humidity patterns as reconstructed ones, with dryer conditions over Europe, the Mediterranean region, ~~Northern and Equatorial Africa, South and East~~ northern and equatorial Africa, southern and eastern Asia, Middle East, India, southern Australia and parts of Indonesia. In South America, a region of particular interest, where major simulated changes in vegetation and oxygen production occur, the model captures well the observed contrast with increased moisture in ~~Northeastern~~ northeastern Brazil, and drying in ~~Northern~~ northern South America and Central America.

These rapid comparisons show that there is a good general agreement between modeled changes in humidity over an HS and climatic reconstructions over the different regions.

5.1.2 Simulated amount-weighted $\delta^{18}O_p$ validation

Tropics

Comparisons of modeled hosing-driven amount-weighted $\Delta\delta^{18}O_p$ anomalies with reconstructed $\Delta\delta^{18}O$ of speleothem's calcite during HSs are presented in Table 3 and Fig. 4. Thirteen Heinrich $\Delta\delta^{18}O_p$ proxy-reconstructions arise from Lewis et al. (2010) ($n = 11$) and Pausata et al. (2011) ($n = 4$)~~,~~. They are located in the Eastern Mediterrannean~~(EM),~~, and in the regions of the South American Monsoon~~(SASM), EASM and~~ , East Asian Monsoon, Indian Summer Monsoon~~(ISM)~~, North American Monsoon ~~(NAM)~~ and the Australian-Indonesian Monsoon~~(AIM) regions~~. Those regions represent the most productive ones and therefore carry a substantial part of $\delta^{18}O_{terr}$ signal. Although reconstructed $\Delta\delta^{18}O_p$ from Lewis et al. (2010) and Pausata et al. (2011) studies were estimated differently, they are consistent and common reconstructed $\Delta\delta^{18}O_p$ estimates (for Hulu and Songjia cave) are similar in both studies (Table 3, this study; method section of Pausata et al., 2011).

The dominant hydrological controls on reconstructed $\delta^{18}O_p$ are site specific and are described by Lewis et al. (2010). Figure 4 demonstrates the ability of the AGCM LMDZ-iso to reproduce the observed $\Delta\delta^{18}O_p$ spatial pattern for most of the sites, particularly in regions

strongly affected by ITCZ (and its land extension) variations and hence by changes in the water cycle, regardless of the processes at play. There are two regions where the model does not properly reproduce the observed signal over HS. The first one occurs in the ~~ISM~~ Indian Summer Monsoon domain (Timta Cave). Model and observation would reconcile 2 gridcells south of Timta cave, as it is located just at the transition between a positive and negative simulated $\delta^{18}O_p$ anomaly. This disagreement can be due to a model bias~~in a region where the coarse model resolution does not allow to properly represent the role of orography. Indeed, model and observation would reconcile~~ . The IPSL model indeed does not simulate the monsoonal signal at the right place, with an Indian monsoon located too far south even for modern climate (Marti et al., 2010). In the LGM simulation also, the IPSL model predicts that it mostly takes place over the ocean (-0.5 to -2 $\mathrm{mm\,day^{-1}}$ is only simulated over the ocean, see Figure 9 (lower panel) of Kageyama et al., 2009) while there is evidence for a monsoonal signal over land. In Northern India, hence Timta cave site, the model does not simulate any significant rainfall change between the 2 ~~gridcells south of Timta cave, as it is located just at the transition between a positive and negative simulated~~ periods. A more intense weakening of the Indian monsoon over land in the HS run, hence less rainfall, would have helped reconciling model and data at Timta Cave, since $\delta^{18}O_p$ ~~anomaly.~~ would have been enriched through the amount effect. Pausata et al. (2011) recently suggested that change in rainfall amount associated with Indian monsoon rather than in the South East Asia explains changes observed in calcite $\delta^{18}O$ in Chinese stalagmites (in South-East Asia). As in Pausata et al. (2011), a freshwater is was applied to the control simulation with LGM background climate. Rainfall amount drops in East-Asia and North-West India, mostly over the ocean but increases in South-East India, as shown in Fig. 3d. Values of -0.17 and $-0.13\,\mathrm{mm\,day^{-1}}$ are simulated at Hulu and Songjia Cave during HS, respectively. The enrichment in $\delta^{18}O_p$ observed in Chinese caves is reproduced by the model but the latter fails to capture the enrichment in Timta cave. Overall, $\delta^{18}O_p$ is enriched over the whole India (with an abrupt change south of Timta cave) and South Asia. The possible role of the Indian monsoon in the oxygen isotopic enrichment of Chinese stalagmites is limited in our simulation, probably because the monsoonal signal is located too far south in the IPSL model. The increase in $\delta^{18}O$ over South-East Asia is consistent with local amount effect.

Another mismatch occurs in the ~~NAM~~ North-American Monsoon domain (Cave of the Bells), where the observed $\Delta\delta^{18}O_p$ ($-0.8‰$) and the modeled $\Delta\delta^{18}O_p$ ($0.9‰$) are of opposite sign. Elevation of the site (1700 m a.s.l.) might explain the disagreement between model and data , in a region where the coarse model resolution does not allow to properly represent the role of orography.

As shown in Table 3, the modeled increase in $\delta^{18}O_p$ quantitatively agrees with data $\delta^{18}O_c$ increase during HS in most of the compared sites (Figure 4). In conclusion, the key features of HS precipitation inferred from speleothem's $\delta^{18}O_c$, i.e. a low latitude inter-hemispheric see-saw pattern (Cheng et al., 2012), ~~with a weakened Asian Monsoon and increased SASM as prominent feature,~~ are generally well captured by the LMDZ model.

High latitudes

In Greenland, HS can hardly be distinguished from the GS or from the mean LGM state. The only clear $\delta^{18}O_{ice}$ signal is observed from GI to GS (or HS) with an approximately $4‰$ decrease in central Greenland sites (GRIP, GISP2, NGRIP). The depletion simulated in Greenland, with a $1.6‰$ decrease at GRIP site, by the model for a HS compared to a glacial background state ~~is thus consistent~~ does not compare well with available data. However, it is difficult to compare the $\delta^{18}O$ change simulated by a freshwater input (the most efficient way to model a Heinrich event, as mentioned in Sect. 4.3.1) and the $\delta^{18}O$ depletion between a GI and a GS. Indeed, there are more and more evidence that the $\delta^{18}O_p$ depletion at the end of a GI is not due to the same freshwater discharge than the one associated with a Heinrich event. It can well be due to a threshold in the extent in sea-ice or an atmospheric heat transport. Therefore our choice of modeling approach may potentially explain some of the discrepancies observed in the low latitudes, but our approach is the best we can afford today.

5.1.3 Validation of simulated vegetation

In order to compare ~~easily~~ model and data easily, simulated PFT's are gathered into 5 mega-biomes (boreal, temperate and tropical trees, C3 and C4 grasses) as well as bare soil. We dis-

tinguish among C3 and C4 plants as their partitioning has a strong impact on photorespiration fraction. The simulated dominant vegetation fraction is shown for LGM_ctrl (Fig. 5) and HS_exp (Fig. 6), together with pollen-based reconstructed mega-biomes. Given its domination, we display bare soil fraction only if it covers more than 80 percent of a gridcell.

Global oxygen production

Present day carbon and oxygen productions amount to 10.5 Pmol $C\,yr^{-1}$ and 17.95 Pmol $O_2\,yr^{-1}$ (taking into account photorespiration) in the ORCHIDEE model, respectively. This is in line with other estimates e.g. Angert et al. (2003) or Welp et al. (2011), estimating 8 to 13 Pmol $C\,yr^{-1}$ and 12.5 to 14.2 Pmol $O_2\,yr^{-1}$, respectively. For LGM and HS, land carbon production estimates from the ORCHIDEE model are rather low, 6.8 and 6.5 Pmol $C\,yr^{-1}$, which translates as 11.8 and 11.4 Pmol $O_2\,yr^{-1}$ for LGM and HS, respectively. This is up to a factor of 2 lower than model based LGM estimates from Joos et al. (2004); Hoffmann et al. (2004) or Bender et al. (1994), ranging from 23 Pmol $O_2\,yr^{-1}$ to 16.7 Pmol $O_2\,yr^{-1}$.

The ORCHIDEE model is known to underestimate LGM productivity both at low latitudes (too low productivity in tropical forests, especially Amazonia) and at high latitudes (too low productivity in the absence of permafrost modeling).

Photorespiration fraction (see Sect. 4.4.2) may also be invoked to explain part of the model-data discrepancy for LGM and HS. Underestimation of photorespiration may arise from uncertainties related to the time of photosynthesis. In the real-world, plants must reduce their CO_2 uptake under water stress, as stomata close to preclude water loss. This leads to higher proportion of photorespiration, not necessarily considered during experiments performed under ideal hydric conditions, whose results are used in the classical Farquhar parametrization (Farquhar et al., 1980).

The classical scaling factor between carbon uptake and oxygen production (Keeling, 1988) of 1.07 used in our study may also have been underestimated. Indeed, plants can produce oxygen without involving carbon uptake during times of stress, which is not considered in experiments run under ideal conditions. The oxygen production calculated here from the ORCHIDEE model seems to be biased toward too low values for the LGM. The same bias is true for HS. Still, it

should be noted that the $\delta^{18}O_{terr}$ calculations of our study and hence the final results do not depend on the absolute value of oxygen production at LGM and HS.

LGM_ctrl vegetation

The main features of the glacial vegetation are correctly reproduced by ORCHIDEE model, as briefly presented by Woillez et al. (2011): reduced fractions of tropical forest, particularly in Amazonia, and high grass fractions in Siberia, Alaska, western North-America. Main biases are an overestimation of the tree fractions over Western Europe, eastern Eurasia and eastern North America, as well as an overestimation in bare soil fractions over India, southern Africa, Siberia and South-America (Woillez et al., 2011), leading to an underestimation of the global carbon production, as mentioned in previous section.

The model simulates temperate trees in southern East Asia (Vietnam, Southern China, Cambodia), tropical trees and grasses over the western pacific warm pool (Malaysia, Thailand, Indonesia) and over southern Africa, in agreement with BIOME6000 reconstructions (Prentice et al., 2000). The model underestimates temperate trees in Asia and overestimates bare soil in South Africa.

A more detailed comparison shows that the important (boreal) tree fraction over southern Western Europe differs from palynological reconstructions depicting an important grass fraction, but this bias mainly comes from the overestimation of ~~BoBS~~Boreal broadleaf summergreen trees, which is a common feature in the version of ORCHIDEE used here, also found in present-day vegetation simulations. The bias might also be the sign that the LGM climate simulated by IPSL-CM4 over western Europe is too warm and wet (Woillez et al., 2011). In a few regions, ORCHIDEE correctly simulates the presence of forest, but the dominant type of tree disagrees with pollen reconstructions: tropical trees over Papua-New-Guinea and western Indonesia, while reconstructions reveal the presence of temperate trees over these regions. Simulated forests over southern Australia (a thin coastal band in the South-East) are composed of temperate and tropical trees, while reconstructions rather indicate the presence of a few tropical trees. The model simulates mixed vegetation composed of grasses, boreal and temperate trees in eastern North-America, consistent with pollen data, but the spatial distribution is incorrect.

It is important to keep in mind that model data comparison of vegetation can only remain qualitative given the coarse resolution of the vegetation model, related to the model resolution of the climatic forcing fields. Besides, pollen records represent the surrounding vegetation distribution at different altitudes, while ORCHIDEE model does not account for elevation changes within a grid cell (Woillez et al., 2013).

HS_exp vegetation

To validate the simulated HS vegetation, we compare the millennial-scale changes in selected high resolution (< 800 yr, mean resolution is 400 yr) pollen records of 48 sites described for HS1-GS2 ($n = 16$) in South-America and southern Africa (Hessler et al., 2010; Handiani et al., 2012), and for HS4-GS9 ($n = 31$) in Europe (Fletcher et al., 2010), North-America (Jimenez-Moreno et al., 2010), Japan (Takahara et al., 2010) and Australasia (Harrison and Goni, 2010). Figure 7 displays the location of paleo records discussed in this study. Table 4 summarizes the model–data comparison at a gridcell level and provides additional information revealed by palynological reconstructions. The sampling resolution for the analysed period (MIS2 for HS1, MIS3 for HS4), the other biomes represented for a given site and the potential occurrences of similar reconstructed vegetation changes over other HS's are presented.

The model–data comparison has been performed as follows: the 2 dominant reconstructed biomes are compared with the 2 dominant simulated biomes over the gridcell covering the site where the proxy originates. Among the 48 sites with pollen reconstructions, 12 of them were discarded because of absence of vegetation on the considered gridcell. Among the remaining 36 terrestrial and coastal sites, 11 disagree (30 %) and 25 (70 %) of them display a moderate to good agreement (Table 4). A good agreement ($n = 13$) is obtained when reconstructed and simulated dominant biomes are alike, a fair agreement ($n = 9$) when a subdominant biome agrees with a dominant one, and a moderate agreement ($n = 3$) when subdominant biomes only are similar.

Simulated vegetation in regions associated with high oxygen productivity agrees well with pollen reconstruction. This is the case for South America, where a strong increase of tropical forest at the expense of bare soil is simulated in Eastern Brazil, ~~or~~ and in the West Pacific Warm Pool region, where tropical forest represents the dominant biome. The slight southward shift of

the southern border of desert areas in Equatorial Africa is also well captured by ORCHIDEE. In the ~~ISM~~ Indian summer monsoon region, the simulated weakened monsoon (Kageyama et al., 2009) leads to the appearance of desert areas south and east of India, consistent with a dryer climate revealed by a core from the Indus region (Deplazes et al., 2014).

From this analysis it appears that sites showing a disagreement between model and data are either coastal sites and/or have a very high bare soil fraction. Coastal sites do not necessarily only represent the vegetation in the coastal region, but they offer numerous records and allow high-resolution analysis thanks to their high sedimentation rate, so it is crucial to include them for millennial scale analysis. 5 (50 %) of the sites showing no agreement present a very high simulated bare soil fractions ($> 90\,\%$). Woillez et al. (2013) already pointed out the overestimation of the bare soil fractions by the ORCHIDEE model. We argue that this bias might partly explain the observed discrepancy between model and data. Besides, the other sites showing a disagreement, over Europe and Australia, underestimate grass fraction. For Europe, the bias is already present in the LGM simulation and is probably partly due to the systematic overestimation of forest by ORCHIDEE in this region (Woillez et al., 2011). Given the scarcity of data offering a time resolution high enough to catch millennial-scale vegetation variability, further testing of the simulated vegetation remains challenging. In conclusion, HS_exp vegetation agrees reasonably well with available pollen based vegetation reconstruction.

Finally, based on the reasonable agreement of the simulated changes in vegetation, humidity and precipitation with observations depicted in this section, we can rely on the validity of the model to simulate $\delta^{18}O_{terr}$ over a HS.

5.2 Global increase of $\delta^{18}O_{terr}$ during a HS

The model calculates $\delta^{18}O_{terr}$ for LGM_ctrl and HS_exp as 23.41 and 23.52 ‰, respectively (Table 2). This average $\delta^{18}O_{terr}$ value is coherent with the $\delta^{18}O_{atm}$ value of 23.8 ‰ with respect to V-SMOW and the finding that terrestrial and marine contribution to $\delta^{18}O_{atm}$ are similar (Luz et al., 2014). Moreover, the global increase in $\delta^{18}O_{terr}$ of 0.11 ‰, (Fig. 8) can quantitatively explain most of the 0.1 ‰ $\delta^{18}O_{atm}$ increase over HS (Severinghaus et al., 2009; Guillevic

et al., 2014) (Fig. 1). In the following, we use the different model outputs to decipher the main influences on $\delta^{18}O_{terr}$ and hence on $\delta^{18}O_{atm}$.

By construction (Eq. 3), $\delta^{18}O_{terr}$ is linearly dependent on both $\delta^{18}O_{lw}$ and $^{18}\epsilon_{resp}$, so that we discuss these two effects below. Figure 8 (upper panel) details the different contributions to $\delta^{18}O_{terr}$ change over a HS and demonstrates the dominant role of $\delta^{18}O_{lw}$ (Sect. 5.2.1) compared to $^{18}\epsilon_{resp}$ (Sect. 5.2.2). Indeed, the 0.11 ‰ increase in $\delta^{18}O_{terr}$ exclusively stems from $\delta^{18}O_{lw}$ increase (+0.14 ‰ over HS_exp), while respiratory fractionation leads to a negative anomaly (−0.03 ‰) over HS_exp. We explore in more details below the origin of the relative changes in $^{18}\epsilon_{resp}$ and $\delta^{18}O_{lw}$ as calculated by our ~~modelling~~ modeling approach. In particular, we look at the different regional contributions to the global $^{18}\epsilon_{resp}$ and $\delta^{18}O_{lw}$ signals since low latitude regions are associated with the largest GPP_O_2 (Fig. 9a for the whole latitudinal range and Fig. 10a for a zoom on the tropics) and hence have the strongest influence on the global $\delta^{18}O_{terr}$ signal (Fig. 9c).

5.2.1 Leafwater

We find global $\delta^{18}O_{lw}$ values of 5.16 and 5.30 ‰ for LGM_ctrl and HS_exp, respectively. The 0.14 ‰ difference is similar to the $\delta^{18}O$ increase observed in ice cores during HS (Fig. 2). The increase of $\delta^{18}O_{lw}$ is clearly visible in the low latitude regions~~and explained by the combined effects of~~ . It corresponds to an increase in $\delta^{18}O_p$ and a ~~-~~decrease in GPP_O_2 weighted relative humidity, both effects leading to a global $\delta^{18}O_{lw}$ increase (Fig. 9b). ~~δ.~~

Still, when looking at the ~~global budget~~whole latitudinal range, the GPP_O_2 weighted relative humidity is not significantly different in HS and in LGM state. This is due to the decrease in relative humidity during HS in the extra-tropical regions (Fig. 9b). The net effect of relative humidity on $\delta^{18}O_{lw}$ is thus nil. As a consequence, the main driver of $\delta^{18}O_{lw}$ (and hence on $\delta^{18}O_{terr}$) increase is the increase in GPP_O_2 weighted $\delta^{18}O_p$ (Fig. 9b) by 0.18 ‰ (Fig. 8). This increase is linked to the southward shift of the tropical belt occurring during HS, as suggested from the speleothem data compilation (see Sect. 5.1.2).

Fig. 10 clearly shows how rainfall amount and $\delta^{18}O_p$ are anticorrelated as expected on most of the intertropical band. During a HS, $\delta^{18}O_p$ is enriched in the NH down to 14 °S. A particular

pattern occurs between the equator and 14 °S, where oxygen production is most enhanced at HS, as precipitation are more abundant but also heavier in $\delta^{18}O_p$.

5.2.2 Respiration

Respiratory processes lead to a 0.03 ‰ decrease of $\delta^{18}O_{terr}$ in HS_exp compared to $\delta^{18}O_{terr}$ in LGM_ctrl (Fig. 8a)~~,~~. This variation is too small to challenge $\delta^{18}O_{terr}$ enrichment caused by hydrological processes. Here we explain the stability of ${}^{18}\epsilon_{resp}$ on millennial timescales by a compensatory mechanism taking place between the main respiratory pathways.

${}^{18}\epsilon_{resp}$ is classically separated into 4 contributions as given in Eq. (6): soil respiration, leaf respiration, photorespiration and Mehler reaction.

Soil respiration with associated fractionation factor ${}^{18}\alpha_{dark\_soil}$ represents 63 % of dark respiration (Schlesinger and Andrews, 2000). It represents 39 % of global terrestrial respiration in our simulation, in agreement with estimates from Raich and Potter (1995) of 30 to 40 %. ${}^{18}\alpha_{dark\_soil}$ is temperature dependent (Angert et al., 2003), with higher fractionation associated with colder soils, causing a high zonal contrast. This temperature effect leads to a change of ${}^{18}\alpha_{dark\_soil}$ by 0.28 ‰ over HS, increasing ${}^{18}\epsilon_{resp}$ by 0.12 ‰ and in turn depleting $\delta^{18}O_{terr}$.

Photorespiration fraction, strongly discriminative against ${}^{18}O$ (${}^{18}\alpha_{photo} = -21.4$ ‰), represents 28.56 % of the global terrestrial oxygen uptake in LGM_ctrl. The proportion of photorespiration is mainly linked to the change in the C3 vs. C4 plant proportions and in temperature during photosynthesis (Von Caemmerer, 2000; Hoffmann et al., 2004). During HS_exp, photorespiration fraction increases by 1 % (29.52 %), driven by a slight decrease in C4 grass (1.3 %) and a slight photosynthesis temperature increase (0.3 °C). As a result, ${}^{18}\epsilon_{resp}$ decreases by ~~0.04~~0.03 ‰ in HS_exp, thus causing $\delta^{18}O_{terr}$ enrichment.

Summarizing, in high latitudes, cold temperatures lead to a weak photorespiration but strong soil isotope fractionation. In low latitudes, high temperatures and variable C4 fraction lead to a weak soil isotope fractionation and a highly variable photorespiration. This compensatory mechanism between photorespiration and soil respiration fractionations explains thus the minor role of respiration in $\delta^{18}O_{terr}$ anomaly during HS.

6 Discussion

Our results suggest a strong control of tropical hydrology on $\delta^{18}O_{terr}$ through changes in $\delta^{18}O_p$. It suggests that $\delta^{18}O_{atm}$ is very strongly related to tropical hydrology and may be a good tracer for global monsoon signal. The aim of the following discussion is to evaluate these results by (i) providing some insights on $\delta^{18}O_{mar}$ estimate and (ii) testing the robustness of our conclusion on the driver of $\delta^{18}O_{terr}$ changes through 3 sensitivity experiments separating the different parameters (hydrology, climate and vegetation).

6.1 Estimate of $\delta^{18}O_{mar}$ over a Heinrich Stadial

$\delta^{18}O_{mar}$ has been recently estimated as 24.3 ± 2.0 ‰ for present day (Luz et al., 2014). In order to estimate $\delta^{18}O_{mar}$ for LGM and HS, we assumed that fractionation during oxygen uptake by marine biosphere remained constant between LGM/HS and present-day and used a mean ocean $\delta^{18}O$ enriched by 1 ‰ at LGM (Waelbroeck et al., 2002). This results in a value of $\delta^{18}O_{mar}$ of 25.3 ± 2.0 ‰ for LGM and HS. It is important to note that a rise in sea level during a HS would lead to a depleted mean ocean $\delta^{18}O$, as polar ice sheet accumulate ^{16}O, and can therefore not explain the increased $\delta^{18}O_{atm}$ observed during stadials.

Because of the spatial limitation of paleo-records to provide a global picture of marine primary productivity, we have estimated the marine productivity for LGM and HS by the Pelagic Interaction Scheme for Carbon and Ecosystem Studies (PISCES) model. The PISCES model is a biogeochemical model of the global ocean including a simple representation of marine ecosystem and forced offline by the AOGCM IPSL-CM4 (Aumont and Bopp, 2006; Mariotti et al., 2012). The model PISCES has already been compared under glacial conditions with observations (Mariotti et al., 2012; Tagliabue et al., 2009; Bopp et al., 2003) and reproduces roughly the paleoproductivity reconstruction of Kohfeld et al. (2005). Using the same forcings as for our simulations, Mariotti et al. (2012) simulate a global decrease of oceanic primary productivity of 16 % during a Heinrich event, in agreement with independent modeling studies (Schmittner, 2005; Menviel et al., 2008; Schmittner and Galbraith, 2008) and more important ~~that~~ than the one in terrestrial GPP (3.5 %). Because $\delta^{18}O_{mar}$ is larger than $\delta^{18}O_{terr}$, this decrease in marine

productivity would lead to a decrease in global $\delta^{18}O_{atm}$ during the HS, opposite to the observation. We simulated a change in the marine production to assess its impact on $\delta^{18}O_{atm}$ signal. With a change of 10 % in marine export, $\delta^{18}O_{atm}$ varies by 0.05 ‰. However this result has to be taken with caution for 2 main reasons: (i) The fraction of land versus ocean production is strongly affecting $\delta^{18}O_{atm}$ if the isotope fractionation factors associated with the terrestrial and marine production are not similar. Pioneer studies in the Dole effect often invoked marine to terrestrial production ratio to explain the observed variations. Though it is not the case in our model, recent studies suggest their magnitude to be very close, with $\delta^{18}O_{mar}$ 1.8 ‰ higher than $\delta^{18}O_{terr}$. The change in $\delta^{18}O_{atm}$ is thus likely to be smaller in the real world. (ii) Recent studies (eg. Mariotti et al., 2012) rather suggest a decrease in marine export after a Heinrich event. This would lead to a decrease of $\delta^{18}O_{atm}$ signal that is opposing the observations as mentioned in the discussion section. We conclude that marine productivity is not the driver for $\delta^{18}O_{atm}$ increase during HS.

6.2 Disentangling the influences of climate, hydrology and vegetation on $\delta^{18}O_{atm}$: sensitivity experiments.

In order to assess the robustness of our conclusion stating that low latitude hydrological cycle is the driver of $\delta^{18}O_{atm}$ changes, we have run 3 different experiments:

- In HSclim we test the impact of the climatic conditions. This simulation is similar to LGM-ctrl, except that the temperature and relative humidity from HS_exp are prescribed as boundary conditions.
- In HShydro we test the impact of the hydrological cycle. This simulation is similar to LGM-ctrl, except that $\delta^{18}O_p$ and $\delta^{18}O_{vap}$ from HS_exp are prescribed as boundary conditions.
- In HSveget we test the impact of the vegetation. This simulation is similar to LGM-ctrl, except that the vegetation production and distribution from HS_exp are prescribed as boundary conditions.

Figure 11 summarises the results of the sensitivity analysis in terms of temperature, humidity, oxygen isotopic composition of $\delta^{18}O_p$, $\delta^{18}O_{lw}$ ~~, δ~~and $\delta^{18}O_{terr}$. The sensitivity tests show that the implementation of one parameter from HS_exp (HSclim, HShydro and HSveget) leads to a simulated $\delta^{18}O_{terr}$ anomaly similar or higher than in the full HS_exp.

In HSclim, $\delta^{18}O_{terr}$ enrichment is mostly caused by the 0.3 % decrease in relative humidity over the LGM vegetated areas after the AMOC collapse, since $\delta^{18}O_p$ and $\delta^{18}O_{lw}$ are not modified by definition. This global decrease in GPP_O_2 weighted relative humidity is not visible in the global HS_exp (Fig. 8) and hence does not explain the $\delta^{18}O_{terr}$ increase in HS_exp. In HSveget, the southward shift of HS_exp vegetation leads to a global GPP_O_2 weighted relative humidity decrease by 0.5 %. As in ~~Hsclim~~HSclim, this leads to a high $\delta^{18}O_{terr}$ positive anomaly. The effect of relative humidity on $\delta^{18}O_{terr}$ is minimized in HS_exp, as the southward shift in vegetation counterbalances the change in climatic conditions. This compensation explains why the final GPP_O_2 weighted relative humidity does not vary.

In HShydro, the $\delta^{18}O_p$ increase explains the whole $\delta^{18}O_{terr}$ increase. This increase in GPP_O_2 weighted $\delta^{18}O_p$ is similar in Hshydro and HS_exp which confirms that the $\delta^{18}O_{terr}$ simulated by the model in the full experiment HS_exp is arising from a change intrinsic to the hydrological cycle, only slightly affected by vegetation distribution.

In addition, note that a weakening of $\delta^{18}O_{lw}$ only occurs with HS vegetation (HS_exp, HSveget), regardless of the climatic conditions. Besides, HSclim depicts a stronger $\delta^{18}O_{lw}$, caused by a higher temperature increase over HS, leading to an enhanced photorespiration fraction among C3 plants. However, the temperature effect on $\delta^{18}O_{lw}$ remains minor.

The global impact of $^{18}\epsilon_{resp}$ is negligible in all experiments, with variations one order of magnitude lower than $\delta^{18}O_p$.

Finally, ~~sensitivity~~ these tests confirm the strong control of hydrological processes on $\delta^{18}O_{terr}$, and highlight the role of the vegetation distribution in defining $\delta^{18}O_p$ and climatic conditions recorded by $\delta^{18}O_{terr}$.

7 Conclusions and perspective

Our study first aimed at testing quantitatively the driving of $\delta^{18}O_{atm}$ by tropical hydrology as suggested by the strong correlation between local records of $\delta^{18}O_c$ and global record of $\delta^{18}O_{atm}$ on the millennial scale. For this we used a HS-type simulation under LGM background conditions with an oxygen isotope mass balance model using spatial and temporal fields of (i) temperature and relative humidity from the AOGCM ~~IPSl-CM4~~IPSL-CM4, (ii) PFT distribution and GPP provided by the DVGM ORCHIDEE, (iii) oxygen isotope composition of water vapor and precipitation from the AGCM LMDZ-iso, as well as (iv) the latest isotope fractionation factor measurements involved in respiratory and photosynthetic processes.

Validation of AOGCM outputs feeding the oxygen isotope mass balance model was performed through a model–data comparison of the main drivers of $\delta^{18}O_{terr}$: (i) simulated $\delta^{18}O_p$ was compared to speleothem's calcite $\delta^{18}O$ anomalies, and showed in most sites an excellent agreement despite the complexity of the $\delta^{18}O_c$ signal, (ii) simulated HS humidity to the reconstructed ones, broadly agreeing with paleo-data and (iii) simulated vegetation during LGM and HS, qualitatively consistent with palynological reconstructions.

The model simulates a terrestrial enrichment of $\delta^{18}O_{terr}$ of 0.11 ‰, which mostly arises from $\delta^{18}O_p$ signal. On a global scale, respiration fractionation only plays a minor role in the anomaly observed during HS, and slightly decreases $\delta^{18}O_{terr}$ in our simulation, driven by a weaker isotope fractionation of soil respiration during HS that masks the effect of increased photorespiration. Results thus confirm the strong control of $\delta^{18}O_p$ on $\delta^{18}O_{terr}$ at millennial timescale.

The strong control of the low latitude hydrological cycle on simulated $\delta^{18}O_{atm}$ on millennial timescales suggests that $\delta^{18}O_{atm}$ records at first order changes in monsoonal activity on millennial timescales, in agreement with CH_4 mixing ratio variations. Indeed, rapid CH_4 variations during the last glacial period are generally attributed to changes in the low ~~latitudes~~ latitude water cycle (Baumgartner et al., 2014; Brook et al., 2000; Chappellaz et al., 1993) driven by latitudinal shifts of the ITCZ and the monsoon systems (e.g. Chiang, 2009). Such signal can also be used for exploring the low latitude hydrological cycle characteristic of Heinrich events. Indeed, Rhodes et al.'s (2015) recent study suggests that observed CH_4 spikes in Wais Divide

ice core during the cold phases of HSs represent the hydrological signature of Heinrich Events, through activation of SH wetlands. ~~Guillevic et al. (2014)~~ Guillevic et al.'s (2014) multi ice-core proxies approach over GS9-HS4 also suggests a decoupling between changes in Greenland temperatures and low latitude hydrology identified in both CH_4 and $\delta^{18}O_{atm}$, and demonstrates the need for high-resolution data with common precise chronology to explore sub millennial variations.

$\delta^{18}O_{atm}$ is a ~~valuated~~ valuable tool to assess the validity of earth system model simulations, as it integrates a combination of hydrological, climatic and biological processes. Besides, $\delta^{18}O_{atm}$ is a global signal, which mostly arises from the tropics and integrates all vegetated areas. Therefore, the ability of a model to catch $\delta^{18}O_{atm}$ millennial scale variations implies a correct spatial representation of an ensemble of processes. The confrontation of Earth System Models outputs with global proxies such as $\delta^{18}O_{atm}$, involving the main components of the climatic system, is crucial to gain confidence in their ability to represent the real world. Our approach is mainly restricted to terrestrial contribution but future modeling exercises should also include the oceanic $\delta^{18}O_{atm}$ signal.

Acknowledgements. Thanks goes to the Marie Curie Initial Training Network INTRAMIF (FP7), which has funded C. Reutenauer's PhD at CIC; to the CIC, for their full support, and to the ANR EL PASO ~~,~~ (no. 2010 BLANC 608 01). The climate model simulations were run on CEA supercomputers and we thank GENCI and TECC for computer time and storage. We are also very grateful for the detailed and constructive comments of Jeff Severinghaus and an anonymous reviewer that greatly helped improving the manuscript.

References

Ahn, J. and Brook, E. J.: Siple Dome ice reveals two modes of millennial CO_2 change during the last ice age, Nat. comm., 5, 3723, doi:http://dx.doi.org/doi:10.1038/ncomms4723doi:10.1038/ncomms4723, 2014.

Ahn, J., Brook, E. J., Schmittner, A., and Kreutz, K.: Abrupt change in atmospheric CO_2 during the last ice age, Geophys. Res. Lett., 39, 18, doi:http://dx.doi.org/10.1029/2012GL05301810.1029/2012GL053018, 2012.

Allison, G., Gat, J., and Leaney, F.: The relationship between deuterium and oxygen-18 delta values in leaf water, Chem. Geol., 58, 145–156, doi:http://dx.doi.org/10.1016/0168-9622(85)90035-110.1016/0168-9622(85)90035-1, 1985.

Alvarez-Solas, J., Robinson, A., Montoya, M, and Ritz, C: Iceberg discharges of the last glacial period driven by oceanic circulation changes, PNAS, 110, 16350–16354, doi:http://dx.doi.org/10.1073/pnas.130662211010.1073/pnas.1306622110, 2013.

Angert, A., Barkan, E., Barnett, B., Brugnoli, E., Davidson, E. A., Fessenden, J., Maneepong, S., Panapitukkul, N., Randerson, J. T., Savage, K., Yakir, D., and Luz, B.: Contribution of soil respiration in tropical, temperate, and boreal forests to the ^{18}O enrichment of atmospheric O_2, Global Biogeochem. Cy., 17, 3, doi:http://dx.doi.org/10.1029/2003GB00205610.1029/2003GB002056, 2003.

Asmerom, Y., Polyak, V. J., and Burns, S. J.: Variable winter moisture in the southwestern United States linked to rapid glacial climate shifts, Nat. Geosci., 3, 114–117, doi:http://dx.doi.org/10.1038/NGEO75410.1038/NGEO754, 2010.

Aumont, O. and Bopp, L.: Globalizing results from ocean in situ iron fertilization studies, Global Biogeochem. Cy., 20, 2, doi:http://dx.doi.org/10.1029/2005GB00259110.1029/2005GB002591, 2006.

Badger, M. R., von Caemmerer, S., Ruuska, S., and Nakano, H.: Electron flow to oxygen in higher plants and algae: rates and control of direct photoreduction (Mehler reaction) and rubisco oxygenase, Philos. T. Roy. Soc. B, 355, 1433–1446, doi:http://dx.doi.org/10.1098/rstb.2000.070410.1098/rstb.2000.0704, 2000.

~~Baker, P., Fritz, S., Burns, S., Ekdahl, E., and Rigsby, C.: The nature and origin of decadal to millennial scale climate variability in the southern tropics of South America: the holocene record of Lago Umayo, Peru, in: Past Climate Variability in South America and Surrounding Regions, edited by: Vimeux, F., Sylvestre, F., and Khodri, M., vol. 14 of Developments in Paleoenvironmental Research, 301–322, Springer, the Netherlands, doi:http://dx.doi.org/10.1007/978-90-481-2672-9_1310.1007/978-90-481-2672-9_13 , 2009.~~

Bariac, T., Rambal, S., Jusserand, C., and Berger, A.: Evaluating water fluxes of field-grown alfalfa from diurnal observations of natural isotope concentrations, energy budget and ecophysiological parameters, Agr. Forest Meteorol., 48, 263–283, doi:http://dx.doi.org/10.1016/0168-1923(89)90073-710.1016/0168-1923(89)90073-7, 1989.

Baumgartner, M., Kindler, P., Eicher, O., Floch, G., Schilt, A., Schwander, J., Spahni, R., Capron, E., Chappellaz, J., Leuenberger, M., Fischer, H., and Stocker, T. F.: NGRIP CH_4 concentration from 120 to 10 kyr before present and its relation to a $\delta^{15}N$ temperature reconstruction from the same

ice core, Clim. Past, 10, 903–920, doi:http://dx.doi.org/10.5194/cp-10-903-201410.5194/cp-10-903-2014, 2014.

Barker, S., Diz, P., Vautravers, M. J., Pike, J., Knorr, G., Hall, I. R., and Broecker, W. S.: Interhemispheric Atlantic seesaw response during the last deglaciation, Nat., 457, 1097–1102, doi:http://dx.doi.org/10.1038/nature07770,10.1038/nature07770, 2009.

Bazin, L., Lemieux-Dudon, B., Landais, A., Guillevic, M., Kindler, P., Parrenin, F., and Martinerie, P.: Optimisation of glaciological parameters for ice core chronology by implementing counted layers between identified depth levels, Clim. Past Discuss., 10, 3585–3616, doi:http://dx.doi.org/10.5194/cpd-10-3585-201410.5194/cpd-10-3585-2014, 2014.

Bender, M. L.: Orbital tuning chronology for the Vostok climate record supported by trapped gas composition, Earth Planet. Sc. Lett., 204, 275–289, doi:http://dx.doi.org/10.1016/S0012-821X(02)00980-910.1016/S0012-821X(02)00980-9, 2002.

Bender, M. L.,Sowers, T., and Labeyrie, L.: The Dole Effect and its variations during the last 130,000 years as measured in the Vostok Ice Core, Global Biogeochem. Cy., 8, 363–376, doi:http://dx.doi.org/10.1029/94GB0072410.1029/94GB00724, 1994.

Blunier, T., Barnett, B., Bender, M. L., and Hendricks, M. B.: Biological oxygen productivity during the last 60,000 years from triple oxygen isotope measurements, Global Biogeochem. Cy.,16, 3-1–3-13, doi:http://dx.doi.org/10.1029/2001GB00146010.1029/2001GB001460, 2002.

Blunier, T., Bender, M. L., Barnett, B., and von Fischer, J. C.: Planetary fertility during the past 400 ka based on the triple isotope composition of O_2 in trapped gases from the Vostok ice core, Clim. Past, 8, 1509–1526, doi:http://dx.doi.org/10.5194/cp-8-1509-201210.5194/cp-8-1509-2012, 2012.

Bond, G., Broecker, W., Johnsen, S., McManus, J., Labeyrie, L., Jouzel, J., Bonani, G.: Correlations between climate records from North Atlantic sediments and Greenland ice, Nature, 365, 143–147, 1993.

Bony, S., and Emanuel, K. A.: A Parameterization of the Cloudiness Associated with Cumulus Convection; Evaluation Using TOGA COARE Data., J. Atm. Sci., 58, 3158–3183, doi:http://dx.doi.org/10.1175/1520-0469(2001)058¡3158:APOTCA¿2.0.CO;210.1175/1520-0469(2001)058¡3158:APOTCA¿2.0.CO;2, 2001.

Bopp, L., Kohfeld, K. E., Le Quere, C., and Aumont, O.: Dust impact on marine biota and atmospheric CO_2 during glacial periods, Paleoceanography, 18, 2, doi:http://dx.doi.org/10.1029/2002PA00081010.1029/2002PA000810, 2003.

Broccoli, A. J., Dahl, K. A., and Stouffer, R. J.: Response of the ITCZ to Northern Hemisphere cooling, Geophys. Res. Lett., 33, 1, doi:http://dx.doi.org/10.1029/2005GL02454610.1029/2005GL024546, 2006.

Broecker, W. S.: Abrupt climate change: causal constraints provided by the paleoclimate record, Earth-Sci. Rev., 51, 137–154, 2000.

Broecker, W. S., Bond, G., Klas, M., Bonani, G., and Wolfli, W.: A salt oscillator in the glacial Atlantic? 1. The concept, Paleoceanography, 5, 469–477, doi:http://dx.doi.org/10.1029/PA005i004p0046910.1029/PA005i004p00469, 1990.

Brook, E. J., Harder, S., Severinghaus, J., Steig, E. J., and Sucher, C. M.: On the origin and timing of rapid changes in atmospheric methane during the Last Glacial Period, Global Biogeochem. Cy., 14, 559–572, doi:http://dx.doi.org/10.1029/1999GB00118210.1029/1999GB001182, 2000.

Brook, E. J., White, J. W., Schilla, A. S., Bender, M. L., Barnett, B., Severinghaus, J. P., Taylor, K. C., Alley, R. B., and Steig, E. J.: Timing of millennial-scale climate change at Siple Dome, West Antarctica, during the last glacial period, Quaternary Sci. Rev., 24, 1333–1343, doi:http://dx.doi.org/10.1016/j.quascirev.2005.02.00210.1016/j.quascirev.2005.02.002, 2005.

Caley, T., Roche, D. M., Waelbroeck, C., and Michel, E.: Oxygen stable isotopes during the Last Glacial Maximum climate: perspectives from data–model (*i*LOVECLIM) comparison, Clim. Past, 10, 1939–1955, doi:http://dx.doi.org/10.5194/cp-10-1939-201410.5194/cp-10-1939-2014, 2014.

Cappa, C. D., Hendricks, M. B., DePaolo, D. J., and Cohen, R. C.: Isotopic fractionation of water during evaporation, J. Geophys. Res.-Atmos., 108, D16, doi:http://dx.doi.org/10.1029/2003JD00359710.1029/2003JD003597, 2003.

Chappellaz, J., Blunier, T., Raynaud, D., Barnola, J., Schwander, J., and Stauffer, B.: Synchronous changes in atmospheric CH_4 and Greenland Climate between 40-kyr and 8-kyr BP, Nature, 366, 443–445, doi:http://dx.doi.org/10.1038/366443a010.1038/366443a0, 1993.

Chappellaz, J., Stowasser, C., Blunier, T., Baslev-Clausen, D., Brook, E. J., Dallmayr, R., Faïn, X., Lee, J. E., Mitchell, L. E., Pascual, O., Romanini, D., Rosen, J., and Schüpbach, S.: High-resolution glacial and deglacial record of atmospheric methane by continuous-flow and laser spectrometer analysis along the NEEM ice core, Clim. Past, 9, 2579–2593, doi:http://dx.doi.org/10.5194/cp-9-2579-201310.5194/cp-9-2579-2013, 2013.

Cheng, H., Sinha, A., Wang, X., Cruz, F., and Edwards, R.: The global paleomonsoon as seen through speleothem records from Asia and the Americas, Clim. Dynam., 39, 1045–1062, doi:http://dx.doi.org/10.1007/s00382-012-1363-710.1007/s00382-012-1363-7, 2012.

Chiang, J. C.: The tropics in paleoclimate, Annu. Rev. Earth Pl. Sc., 37, 263–297, doi:http://dx.doi.org/10.1146/annurev.earth.031208.10021710.1146/annurev.earth.031208.100217, 2009.

Ciais, P., Tagliabue, A., Cuntz, M., Bopp, L., Scholze, M., Hoffmann, G., Lourantou, A., Harrison, S., Prentice, I., Kelley, D., Koven, C. and Piao, S. L.: Large inert carbon pool in the terrestrial biosphere during the Last Glacial Maximum, Nat. Geosci., 5, 74–79, doi:http://dx.doi.org/10.1038/ngeo132410.1038/ngeo1324, 2012.

Clement, A. C. and Peterson, L. C.: Mechanisms of abrupt climate change of the last glacial period, Rev. Geophys., 46, 4, doi:http://dx.doi.org/10.1029/2006RG00020410.1029/2006RG000204, 2008.

Craig, H. and Gordon, L.: Deuterium and oxygen 18 variations in the ocean and the marine atmosphere, in: Stable Isotopes in Oceanographic Studies and Paleotemperatures, edited by: Tongiorgi, E., 26–30 July 1965, Spoleto, Italy, 1965.

Cvijanovic, I. and Chiang, J.: Global energy budget changes to high latitude North Atlantic cooling and the tropical ITCZ response, Clim. Dynam., 40, 1435–1452, doi:http://dx.doi.org/10.1007/s00382-012-1482-110.1007/s00382-012-1482-1, 2013.

Dahl, K., Broccoli, A., and Stouffer, R.: Assessing the role of North Atlantic freshwater forcing in millennial scale climate variability: a tropical Atlantic perspective, Clim. Dynam., 24, 325–346, doi:http://dx.doi.org/10.1007/s00382-004-0499-510.1007/s00382-004-0499-5, 2005.

Dällenbach, A., Blunier, T., Flückiger, J., Stauffer, B., Chappellaz, J., and Raynaud, D.: Changes in the atmospheric CH_4 gradient between Greenland and Antarctica during the last glacial and the transition to the Holocene, Geophys. Res. Lett., 27, 1005–1008, doi:http://dx.doi.org/10.1029/1999GL01087310.1029/1999GL010873, 2000.

Deplazes, G., Lückge, A., Stuut, J.-B. W., Pätzold, J., Kuhlmann, H., Husson, D., Fant, M., and Haug, G. H.: Weakening and strengthening of the Indian monsoon during Heinrich events and Dansgaard-Oeschger oscillations, Paleoceanography, 29, 99–114, doi:http://dx.doi.org/10.1002/2013PA00250910.1002/2013PA002509, 2014.

Dokken, T. M., Nisancioglu, K. H., Li, C., Battisti, D. S., and Kissel, C.: Dansgaard–Oeschger cycles: interactions between ocean and sea ice intrinsic to the Nordic seas, Paleoceanography, 28, 491–502, doi:http://dx.doi.org/10.1002/palo.2004210.1002/palo.20042, 2013.

Dongmann, G.: The contribution of land photosynthesis to the stationary enrichment of ^{18}O in the atmosphere, Radiat. Environ. Bioph., 11, 219–225, doi:http://dx.doi.org/10.1007/BF0132319110.1007/BF01323191, 1974.

Dreyfus, G. B., Parrenin, F., Lemieux-Dudon, B., Durand, G., Masson-Delmotte, V., Jouzel, J., Barnola, J.-M., Panno, L., Spahni, R., Tisserand, A., Siegenthaler, U., and Leuenberger, M.: Anomalous flow below 2700 m in the EPICA Dome C ice core detected using $\delta^{18}O$ of atmospheric oxygen measurements, Clim. Past, 3, 341–353, doi:http://dx.doi.org/10.5194/cp-3-341-200710.5194/cp-3-341-2007, 2007.

Eisenstadt, D., Barkan, E., Luz, B., and Kaplan, A.: Enrichment of oxygen heavy isotopes during photosynthesis in phytoplankton, Photosynth. Res., 103, 97–103, doi:http://dx.doi.org/10.1007/s11120-009-9518-z10.1007/s11120-009-9518-z, 2010.

Elliot, M., Labeyrie, L., and Duplessy, J.-C.: Changes in North Atlantic deep-water formation associated with the Dansgaard-Oeschger temperature oscillations (60–10 ka), Quaternary Sci. Rev., 21, 1153–1165, doi:http://dx.doi.org/10.1016/S0277-3791(01)00137-810.1016/S0277-3791(01)00137-8, 2002.

Emanuel, K. A.: A scheme for representing cumulus convection in large-scale models, J. Atm. Sci., 48, 2313–2329, doi:http://dx.doi.org/10.1175/1520-0469(1991)048¡2313:ASFRCC¿2.0.CO;210.1175/1520-0469(1991)048¡2313:ASFRCC¿2.0.CO;2, 1991.

Farquhar, G. D. and Lloyd, J.: 5 – Carbon and oxygen isotope effects in the exchange of carbon dioxide between terrestrial plants and the atmosphere, in: Stable Isotopes and Plant Carbon-Water Relations, edited by: Farquhar, G. D., Ehleringer, J. R., Hall, A. E., Academic Press, San Diego, 47–70, doi:http://dx.doi.org/10.1016/B978-0-08-091801-3.50011-810.1016/B978-0-08-091801-3.50011-8, 1993.

Farquhar, G. D., von Caemmerer, S., and Berry, J.: A biochemical model of photosynthetic CO_2 assimilation in leaves of C3 species, Planta, 149, 78–90, 1980.

Farquhar, G. D., Hubick, K., Condon, A., and Richards, R.: Carbon isotope fractionation and plant water-use efficiency, in: Stable Isotopes in Ecological Research, Springer, 21–40, 1989.

Farquhar, G. D., Cernusak, L. A., and Barnes, B.: Heavy water fractionation during transpiration, Plant Physiol., 143, 11–18, 2007.

Flanagan, L. B., Bain, J. F., and Ehleringer, J. R.: Stable oxygen and hydrogen isotope composition of leaf water in C3 and C4 plant species under field conditions, Oecologia, 88, 394–400, 1991a.

Flanagan, L. B., Comstock, J. P., and Ehleringer, J. R.: Comparison of modeled and observed environmental influences on the stable oxygen and hydrogen isotope composition of leaf water in Phaseolus vulgaris L., Plant Physiol., 96, 588–596, 1991b.

Flanagan, L. B., Marshall, J. D., and Ehleringer, J. R.: Photosynthetic gas exchange and the stable isotope composition of leaf water: comparison of a xylem-tapping mistletoe and its host, Plant Cell

Environ., 16, 623–631, doi:http://dx.doi.org/10.1111/j.1365-3040.1993.tb00480.x10.1111/j.1365-3040.1993.tb00480.x, 1993.

Flanagan, L. B., Phillips, S. L., Ehleringer, J. R., Lloyd, J., and Farquhar, G. D.: Effect of changes in leaf water oxygen isotopic composition on discrimination against $C^{18}O^{16}O$ during photosynthetic gas exchange, Funct. Plant Biol., 21, 221–234, 1994.

Fleitmann, D., Cheng, H., Badertscher, S., Edwards, R. L., Mudelsee, M., Gktürk, O. M., Fankhauser, A., Pickering, R., Raible, C. C., Matter, A., Kramers, J., and Tüysüz, O.: Timing and climatic impact of Greenland interstadials recorded in stalagmites from northern Turkey, Geophys. Res. Lett., 36, 19, doi:http://dx.doi.org/10.1029/2009GL04005010.1029/2009GL040050, 2009.

Fletcher, W. J., Goni, M. F. S., Allen, J. R., Cheddadi, R., Combourieu-Nebout, N., Huntley, B., Lawson, I., Londeix, L., Magri, D., Margari, V., Müller, U. C., Naughton, F., Novenko, E., Roucoux, K., and Tzedakis, P.: Millennial-scale variability during the last glacial in vegetation records from Europe, Quaternary Sci. Rev., 29, 2839–2864, doi:http://dx.doi.org/10.1016/j.quascirev.2009.11.01510.1016/j.quascirev.2009.11.015, 2010.

Flückiger, J., Dällenbach, A., Blunier, T., Stauffer, B., Stocker, T. F., Raynaud, D., and Barnola, J.-M.: Variations in atmospheric N_2O concentration during abrupt climatic changes, Science, 285, 227–230, doi:http://dx.doi.org/10.1126/science.285.5425.22710.1126/science.285.5425.227, 1999.

Genty, D., Blamart, D., Ouahdi, R., Gilmour, M., Baker, A., Jouzel, J., and Van-Exter, S.: Precise dating of Dansgaard–Oeschger climate oscillations in western Europe from stalagmite data, Nature, 421, 833–837, 2003.

Gillon, J. and Yakir, D.: Influence of carbonic anhydrase activity in terrestrial vegetation on the ^{18}O content of atmospheric CO_2, Science, 291, 2584–2587, doi:http://dx.doi.org/10.1126/science.105637410.1126/science.1056374, 2001.

Grandpeix, J.-Y., Phillips, V., and Tailleux, R..: Improved mixing representation in Emanuel's convection scheme, Quarterly Journal of the Royal Meteorological Society, 130, 3207–3222, doi:http://dx.doi.org/10.1256/qj.03.14410.1256/qj.03.144, 2004.

Grootes, P. M. and Stuiver, M.: Oxygen 18/16 variability in Greenland snow and ice with 10^3 to 10^5 year time resolution, J. Geophys. Res.-Oceans, 102, 26455–26470, doi:http://dx.doi.org/10.1029/97JC0088010.1029/97JC00880, 1997.

Grousset, F., Labeyrie, L., Sinko, J., Cremer, M., Bond, G., Duprat, J., Cortijo, E., and Huon, S.: Patterns of ice-rafted detritus in the glacial North Atlantic (40–55 N), Paleoceanography, 8, 175–192, 1993.

Guillevic, M.: Characterisation of rapid climate changes through isotope analyses of ice and entrapped air in the NEEM ice core, PhD thesis, Versailles-St Quentin en Yvelines, 2013.

Guillevic, M., Bazin, L., Landais, A., Stowasser, C., Masson-Delmotte, V., Blunier, T., Eynaud, F., Falourd, S., Michel, E., Minster, B., Popp, T., Prié, F., and Vinther, B. M.: Evidence for a three-phase sequence during Heinrich Stadial 4 using a multiproxy approach based on Greenland ice core records, Clim. Past, 10, 2115–2133, doi:http://dx.doi.org/10.5194/cp-10-2115-201410.5194/cp-10-2115-2014, 2014.

Guy, R. D., Fogel, M. L., and Berry, J. A.: Photosynthetic Fractionation of the Stable Isotopes of Oxygen and Carbon, Plant Physiol., 101, 37–47, doi:http://dx.doi.org/10.1104/pp.101.1.3710.1104/pp.101.1.37, 1993.

Handiani, D., Paul, A., and Dupont, L.: Tropical climate and vegetation changes during Heinrich Event 1: a model–data comparison, Clim. Past, 8, 37–57, doi:http://dx.doi.org/10.5194/cp-8-37-201210.5194/cp-8-37-2012, 2012.

Harrison, S. and Goni, M. S.: Global patterns of vegetation response to millennial-scale variability and rapid climate change during the last glacial period, Quaternary Sci. Rev., 29, 2957–2980, doi:http://dx.doi.org/10.1016/j.quascirev.2010.07.01610.1016/j.quascirev.2010.07.016, 2010.

Heinrich, H.: Origin and consequences of cyclic ice rafting in the northeast Atlantic Ocean during the past 130,000 years, Quaternary Res., 29, 142–152, 1988.

Helman, Y., Barkan, E., Eisenstadt, D., Luz, B., and Kaplan, A.: Fractionation of the three stable oxygen isotopes by oxygen-producing and oxygen-consuming reactions in photosynthetic organisms, Plant Physiol., 138, 2292–2298, doi:http://dx.doi.org/10.1104/pp.105.06376810.1104/pp.105.063768, 2005.

Hendricks, M. B., Bender, M. L., and Barnett, B. A.: Net and gross O_2 production in the southern ocean from measurements of biological O_2 saturation and its triple isotope composition, Deep-Sea Res. Pt. I, 51, 1541–1561, doi:http://dx.doi.org/10.1016/j.dsr.2004.06.00610.1016/j.dsr.2004.06.006, 2004.

Hessler, I., Dupont, L., Bonnefille, R., Behling, H., Gonzalez, C., Helmens, K. F., Hooghiemstra, H., Lebamba, J., Ledru, M.-P., Lezine, A.-M., Maley, J., Marret, F., and Vincens, A.: Millennial-scale changes in vegetation records from tropical Africa and South America during the last glacial, Quaternary Sci. Rev., 29, 2882–2899, doi:http://dx.doi.org/10.1016/j.quascirev.2009.11.02910.1016/j.quascirev.2009.11.029, 2010.

Hoffmann, G., Cuntz, M., Weber, C., Ciais, P., Friedlingstein, P., Heimann, M., Jouzel, J., Kaduk, J., Maier-Reimer, E., Seibt, U., and Six, K.: A model of the Earth's Dole effect, Global Biogeochem. Cy., 18, 1, doi:http://dx.doi.org/10.1029/2003GB00205910.1029/2003GB002059, 2004.

Hourdin, F., Musat, I., Bony, S., Braconnot, P., Codron, F., Dufresne, J.-L., Fairhead, L., Filiberti, M.-A., Friedlingstein, P., Grandpeix, J.-Y., Krinner, G., LeVan, P., Li, Z.-X., and Lott, F.: The LMDZ4

general circulation model: climate performance and sensitivity to parametrized physics with emphasis on tropical convection, Clim. Dynam., 27, 787–813, doi:http://dx.doi.org/10.1007/s00382-006-0158-010.1007/s00382-006-0158-0, 2006.

Huber, C., Leuenberger, M., Spahni, R., Flückiger, J., Schwander, J., Stocker, T., Johnsen, S., Landais, A., and Jouzel, J.: Isotope calibrated Greenland temperature record over marine isotope stage 3 and its relation to CH_4, Earth Planet. Sc. Lett., 243, 504–519, 2006.

Jimenez-Moreno, G., Anderson, R. S., Desprat, S., Grigg, L. D., Grimm, E. C., Heusser, L. E., Jacobs, B. F., Lopez-Martinez, C., Whitlock, C. L., and Willard, D. A.: Millennial-scale variability during the last glacial in vegetation records from North America, Quaternary Sci. Rev., 29, 2865–2881, doi:http://dx.doi.org/10.1016/j.quascirev.2009.12.01310.1016/j.quascirev.2009.12.013, 2010.

author = Joos, Fortunat and Gerber, Stefan and Prentice, I. C. and Otto-Bliesner, Bette L. and Valdes, Paul J.,

Joos, F., Gerber, S., Prentice, I. C., Otto-Bliesner, B. L., and Valdes, P. J.: Transient simulations of Holocene atmospheric carbon dioxide and terrestrial carbon since the Last Glacial Maximum, Global Biogeochem. Cy., 18, 2, doi:http://dx.doi.org/10.1029/2003GB00215610.1029/2003GB002156, 2004.

Kageyama, M., Mignot, J., Swingedouw, D., Marzin, C., Alkama, R., and Marti, O.: Glacial climate sensitivity to different states of the Atlantic meridional overturning circulation: results from the IPSL model, Clim. Past, 5, 551–570, doi:http://dx.doi.org/10.5194/cp-5-551-200910.5194/cp-5-551-2009, 2009.

Kageyama, M., Paul, A., Roche, D. M., and Meerbeeck, C. J. V.: Modelling glacial climatic millennial-scale variability related to changes in the Atlantic meridional overturning circulation: a review, Quaternary Sci. Rev., 29, 2931–2956, doi:http://dx.doi.org/10.1016/j.quascirev.2010.05.02910.1016/j.quascirev.2010.05.029, 2010.

Kageyama, M., Merkel, U., Otto-Bliesner, B., Prange, M., Abe-Ouchi, A., Lohmann, G., Ohgaito, R., Roche, D. M., Singarayer, J., Swingedouw, D., and X Zhang: Climatic impacts of fresh water hosing under Last Glacial Maximum conditions: a multi-model study, Clim. Past, 9, 935–953, doi:http://dx.doi.org/10.5194/cp-9-935-201310.5194/cp-9-935-2013, 2013.

Kanner, L. C., Burns, S. J., Cheng, H., and Edwards, R. L.: High-latitude forcing of the South American summer monsoon during the last glacial, Science, 335, 570–573, doi:http://dx.doi.org/10.1126/science.121339710.1126/science.1213397, 2012.

Kanner, L. C., Buenning, N. H., Stott, L. D., Timmermann, A., and Noone, D.: The role of soil processes in ^{18}O terrestrial climate proxies, Global Biogeochem. Cy., 28, 239–252, doi:http://dx.doi.org/10.1002/2013GB00474210.1002/2013GB004742, 2014.

Kawamura, K., Parrenin, F., Lisiecki, L., Uemura, R., Vimeux, F., Severinghaus, J. P., Hutterli, M. A., Nakazawa, T., Aoki, S., Jouzel, J., Raymo, M. E., Matsumoto, K., Nakata, H., Motoyama, H., Fujita, S., Goto-Azuma, K., Fujii, Y., and Watanabe, O.: Northern hemisphere forcing of climatic cycles in Antarctica over the past 360,000 years, Nature, 448, 912–U4, doi:http://dx.doi.org/10.1038/nature0601510.1038/nature06015, 2007.

Keeling, R. F.: Development of an interferometric oxygen analyzer for precise measurement of the atmospheric O_2 mole fraction, PhD thesis, Harvard University, 1988.

Kindler, P., Guillevic, M., Baumgartner, M., Schwander, J., Landais, A., and Leuenberger, M.: Temperature reconstruction from 10 to 120 kyr b2k from the NGRIP ice core, Clim. Past, 10, 887–902, doi:http://dx.doi.org/10.5194/cp-10-887-201410.5194/cp-10-887-2014, 2014.

Kleppin, H., Jochum, M., Otto-Bliesner, B., Shields, C. A., and Yeager, S.: Stochastic atmospheric forcing as trigger for sudden Greenland warmings, J. Climate, ~~in review,~~ 28, 19, doi:http://dx.doi.org/10.1175/JCLI-D-14-00728.110.1175/JCLI-D-14-00728.1, 2015.

Kohfeld, K. E., Quere, C. L., Harrison, S. P., and Anderson, R. F.: Role of marine biology in glacial-interglacial CO_2 cycles, Science, 308, 74–78, doi:http://dx.doi.org/10.1126/science.110537510.1126/science.1105375, 2005.

Krebs, U. and Timmermann, A.: Tropical air-sea interactions accelerate the recovery of the Atlantic meridional overturning circulation after a major shutdown, J. Climate, 20, 4940–4956, 2007.

Krinner, G., Viovy, N., de Noblet-Ducoudre, N., Ogee, J., Polcher, J., Friedlingstein, P., Ciais, P., Sitch, S., and Prentice, I. C.: A dynamic global vegetation model for studies of the coupled atmosphere-biosphere system, Global Biogeochem. Cy., 19, 1, doi:http://dx.doi.org/10.1029/2003GB00219910.1029/2003GB002199, 2005.

Landais, A., Barnola, J. M., Masson-Delmotte, V., Jouzel, J., Chappellaz, J., Caillon, N., Huber, C., Leuenberger, M., and Johnsen, S. J.: A continuous record of temperature evolution over a sequence of Dansgaard-Oeschger events during Marine Isotopic Stage 4 (76 to 62 kyr BP), Geophys. Res. Lett., 31, 22 doi:http://dx.doi.org/10.1029/2004GL02119310.1029/2004GL021193, 2004.

Landais, A., Lathiere, J., Barkan, E., and Luz, B.: Reconsidering the change in global biosphere productivity between the Last Glacial Maximum and present day from the triple oxygen isotopic composition of air trapped in ice cores, Global Biogeochem. Cy., 21, 1, doi:http://dx.doi.org/10.1029/2006GB00273910.1029/2006GB002739, 2007a.

Landais, A., Masson-Delmotte, V., Nebout, N. C., Jouzel, J., Blunier, T., Leuenberger, M., Dahl-Jensen, D., and Johnsen, S.: Millenial scale variations of the isotopic composition of atmospheric oxygen over marine isotopic stage 4, Earth Planet. Sc. Lett., 258, 101–113, doi:http://dx.doi.org/10.1016/j.epsl.2007.03.02710.1016/j.epsl.2007.03.027, 2007b.

Landais, A., Dreyfus, G., Capron, E., Masson-Delmotte, V., Sanchez-Goñi, M. F., Desprat, S., Hoffmann, G., Jouzel, J., Leuenberger, M., and Johnsen, S.: What drives the millennial and orbital variations of $\delta^{18}O_{atm}$?, Quaternary Sci. Rev., 29, 235–246, doi:http://dx.doi.org/10.1016/j.quascirev.2009.07.00510.1016/j.quascirev.2009.07.005, 2010.

Landais, A., Dreyfus, G., Capron, E., Pol, K., Loutre, M. F., Raynaud, D., Lipenkov, V. Y., Arnaud, L., Masson-Delmotte, V., Paillard, D., Jouzel, J., and Leuenberger, M.: Towards orbital dating of the EPICA Dome C ice core using $\delta O_2/N_2$, Clim. Past, 8, 191–203, doi:http://dx.doi.org/10.5194/cp-8-191-201210.5194/cp-8-191-2012, 2012.

LeGrande, A. N. and Schmidt, G. A.: Ensemble, water isotope-enabled, coupled general circulation modeling insights into the 8.2 ka event, Paleoceanography, 23, 3, doi:http://dx.doi.org/10.1029/2008PA00161010.1029/2008PA001610, 2008.

Lewis, S. C., LeGrande, A. N., Kelley, M., and Schmidt, G. A.: Water vapour source impacts on oxygen isotope variability in tropical precipitation during Heinrich events, Clim. Past, 6, 325–343, doi:http://dx.doi.org/10.5194/cp-6-325-201010.5194/cp-6-325-2010, 2010.

Li, C., Battisti, D. S., Schrag, D. P., and Tziperman, E.: Abrupt climate shifts in Greenland due to displacements of the sea ice edge, Geophys. Res. Lett., 32, L19702, 19, http://dx.doi.org/10.1029/2005GL02349210.1029/2005GL023492, 2005.

Li, C., Battisti, D. S., and Bitz, C. M.: Can North Atlantic sea ice anomalies account for Dansgaard–Oeschger climate signals?, J. Climate, 23, 5457-5475,http://dx.doi.org/10.1175/2010JCLI3409.110.1175/2010JCLI3409.1, 2010.

Liu, Z., Otto-Bliesner, B. L., He, F., Brady, E. C., Tomas, R., Clark, P. U., Carlson, A. E., Lynch-Stieglitz, J., Curry, W., Brook, E., Erickson, D., Jacob, R., Kutzbach, J., and Cheng, J.: Transient Simulation of Last Deglaciation with a New Mechanism for Bølling-Allerød Warming, Science, 325, 310–314, doi:http://dx.doi.org/10.1126/science.117104110.1126/science.1171041, 2009.

Lloyd, J. and Farquhar, G.: ^{13}C discrimination during CO_2 assimilation by the terrestrial biosphere, Oecologia, 99, 201–215, doi:http://dx.doi.org/10.1007/BF0062773210.1007/BF00627732, 1994.

Luz, B. and Barkan, E.: Proper estimation of marine gross O_2 production with $^{17}O/^{16}O$ and $^{18}O/^{16}O$ ratios of dissolved O_2, Geophys. Res. Lett., 38, 19, http://dx.doi.org/10.1029/2011GL04913810.1029/2011GL049138, 2011a.

Luz, B. and Barkan, E.: The isotopic composition of atmospheric oxygen, Global Biogeochem. Cy., 25, 3, doi:http://dx.doi.org/10.1029/2010GB00388310.1029/2010GB003883, 2011b.

Luz, B., Barkan, E., Bender, M., Thiemens, M., and Boering, K.: Triple-isotope composition of atmospheric oxygen as a tracer of biosphere productivity, Nature, 400, 547–550, doi:http://dx.doi.org/10.1038/2298710.1038/22987, 1999.

Luz, B., Barkan, E., Yam, R., and Shemesh, A.: Fractionation of oxygen and hydrogen isotopes in evaporating water, Geochim. Cosmochim. Ac., 73, 6697–6703, doi:http://dx.doi.org/10.1016/j.gca.2009.08.00810.1016/j.gca.2009.08.008, 2009.

Luz, B., Barkan, E., and Severinghaus, J.: 5.14 – The stable isotopic composition of atmospheric O_2, in: Treatise on Geochemistry, edited by: Holland, H. D. and Turekian, K. K., Elsevier, Oxford, 2nd edn., 363–383, doi:http://dx.doi.org/10.1016/B978-0-08-095975-7.00419-810.1016/B978-0-08-095975-7.00419-8, 2014.

Marcott, S. A., Clark, P., U., Padman, L., Klinkhammer, G. P., Springer, S. R., Liu, Z., Otto-Bliesner, B. L., Carlson, A. E., Ungerer, A., Padman, J., He, F., Cheng, J., and Schmittner, A.: Ice-shelf collapse from subsurface warming as a trigger for Heinrich events, PNAS, 108, 13415–13419, doi:http://dx.doi.org/10.1073/pnas.1104772108, 2011.

Majoube, M.: Fractionnement en oxygene-18 et en deuterium entre l'eau et sa vapeur, J. Chim. Phys, 68, 1423–1436, 1971.

Mariotti, V., Bopp, L., Tagliabue, A., Kageyama, M., and Swingedouw, D.: Marine productivity response to Heinrich events: a model–data comparison, Clim. Past, 8, 1581–1598, doi:http://dx.doi.org/10.5194/cp-8-1581-201210.5194/cp-8-1581-2012, 2012.

Marti, O., Braconnot, P., Dufresne, J.-L., Bellier, J., Benshila, R., Bony, S., Brockmann, P., Cadule, P., Caubel, A., Codron, F., de Noblet, N., Denvil, S., Fairhead, L., Fichefet, T., Foujols, M.-A., Friedlingstein, P., Goosse, H., Grandpeix, J.-Y., Guilyardi, E., Hourdin, F., Idelkadi, A., Kageyama, M., Krinner, G., Lžvy, C, Madec, G., Mignot, J., Musat, I., Swingedouw, D. and Talandier, C.: Key features of the IPSL ocean atmosphere model and its sensitivity to atmospheric resolution, Clim. Dynam., 34, 1–26, 2010.

McGuire, K., DeWalle, D., and Gburek, W.: Evaluation of mean residence time in subsurface waters using oxygen-18 fluctuations during drought conditions in the mid-Appalachians, J. Hydrol., 261, 132–149, doi:http://dx.doi.org/10.1016/S0022-1694(02)00006-910.1016/S0022-1694(02)00006-9, 2002.

Menviel, L., Timmermann, A., Mouchet, A., and Timm, O.: Meridional reorganizations of marine and terrestrial productivity during Heinrich events, Paleoceanography, 23, 1, doi:http://dx.doi.org/10.1029/2007PA00144510.1029/2007PA001445, 2008.

Menviel, L., Timmermann, A., Friedrich, T., and England, M. H.: Hindcasting the continuum of Dansgaard–Oeschger variability: mechanisms, patterns and timing, Clim. Past, 10, 63–77, doi:http://dx.doi.org/10.5194/cp-10-63-201410.5194/cp-10-63-2014, 2014.

Merlivat, L.: Molecular diffusivities of $H_2^{16}O$,$HD^{16}O$, and $H_2^{18}O$ in gases, J. Chem. Phys., 69, 2864–2871, doi:http://dx.doi.org/10.1063/1.43688410.1063/1.436884, 1978.

Mohtadi, M., Oppo, D. W., Steinke, S., Stuut, J.-B. W., De Pol-Holz, R., Hebbeln, D., and Lückge, A.: Glacial to Holocene swings of the Australian-Indonesian monsoon, Nat. Geosci., 4, 540–544, 2011.

Monnin, E., Indermühle, A., Dällenbach, A., Flückiger, J., Stauffer, B., Stocker, T. F., Raynaud, D., and Barnola, J.-M.: Atmospheric CO_2 Concentrations over the Last Glacial Termination, Science, 291, 112–114, doi:http://dx.doi.org/10.1126/science.291.5501.11210.1126/science.291.5501.112, 2001.

NGRIP members, Andersen, K., Azuma, N., Barnola, J., Bigler, M., Biscaye, P., Caillon, N., Chappellaz, J., Clausen, H., DahlJensen, D., Fischer, H., Fluckiger, J., Fritzsche, D., Fujii, Y., Goto-Azuma, K., Gronvold, K., Gundestrup, N., Hansson, M., Huber, C., Hvidberg, C., Johnsen, S., Jonsell, U., Jouzel, J., Kipfstuhl, S., Landais, A., Leuenberger, M., Lorrain, R., Masson-Delmotte, V., Miller, H., Motoyama, H., Narita, H., Popp, T., Rasmussen, S., Raynaud, D., Rothlisberger, R., Ruth, U., Samyn, D., Schwander, J., Shoji, H., Siggard-Andersen, M., Steffensen, J., Stocker, T., Sveinbjornsdottir, A., Svensson, A., Takata, M., Tison, J., Thorsteinsson, T., Watanabe, O., Wilhelms, F., White, J. W. C.: High-resolution record of Northern Hemisphere climate extending into the last interglacial period, Nature, 431, 147–151, doi:http://dx.doi.org/10.1038/nature0280510.1038/nature02805, 2004.

Otto-Bliesner, B. L. and Brady, E. C.: The sensitivity of the climate response to the magnitude and location of freshwater forcing: last glacial maximum experiments, Quaternary Sci. Rev., 29, 56–73, doi:http://dx.doi.org/10.1016/j.quascirev.2009.07.00410.1016/j.quascirev.2009.07.004, 2010.

Pausata, F. S., Battisti, D. S., Nisancioglu, K. H., and Bitz, C. M.: Chinese stalagmite [delta] ^{18}O controlled by changes in the Indian monsoon during a simulated Heinrich event, Nat. Geosci., 4, 474–480, 2011.

Peltier, W.: Global glacial isostasy and the surface of the ice-age Earth: the ICE-5G (VM2) model and GRACE, Annu. Rev. Earth Pl. Sc., 32, 111–149, 2004.

Peterson, L. C. and Haug, G. H.: Variability in the mean latitude of the Atlantic intertropical convergence zone as recorded by riverine input of sediments to the Cariaco Basin (Venezuela), Palaeogeogr. Palaeocl., 234, 97–113, doi:http://dx.doi.org/10.1016/j.palaeo.2005.10.02110.1016/j.palaeo.2005.10.021, 2006.

Prentice, I. C., Jolly, D., and Afanaseva, N. B., Ager, T. A., Anderson, K., Anderson, P. M., Andrieu, V., Andreev, A. A., Ballouche, A., Bartlein, P. J., de Beaulieu, J. L., Bengo, M., Berezina, N. A., Bezusko, L. G., Bezusko, T. V., Bigelow, N. H., Blyakharchuk, T. A., Bolikhovskaya, N. S., Bonnefille, R., Bottema, S., Bržnac, P., Brubaker, L. B., Buchet, G., Burney, D., Bykova, G. V., Cheddadi, R., Chen, X., Chernavskaya, M. M., Chernova, G. M., Cwynar, L. C., Dorofeyuk, N. I., Dirksen, V. G., Edorh, T., Edwards, M. E., Eisner, W. R., Elenga, H., Elina, G. A., Elmoutaki, S., Filimonova, L. V., Glebov, F. Z., Guiot, J., Gunova, V. S., Hamilton, A. C., Han, H., Harrison, S. P., Hu, F.-S., Huang, C., Huntley, B., Jolly, D., Jonson, H., Ke, M., Khomutova, V. I., Kong Z., Kvavadze, E. V., Laarif, F., Lamb, H. E., Lžzine, A.-M., Li, S., Li, W., Liew, P., Liu, G., Liu, J., Liu, Q., Liu, K.-B., Lozhkin, A. V., Maley, J., Marchant, R., Mbenza, M., MacDonald, G. M., Miyoshi, N., Mock, C. J., Morita, Y., Newby, P.,Ni, J., Osipova, I. R., Panova, N. K., Perez-Obiol, R., Peyron, O., Prentice, I. C., Qiu, W., Reille, M., Ren, G., Reynaud-Farrera, I., Richard, P. J. H., Riollet, G., Ritchie, J. C., Roche, E., Saarse, L., Scott, L., Sevastyanov, D. V., Sher, A. V., Song, C., Spear, R. W., Ssemmanda, I., Straka, H., Sugita, S., Sun, X., Takahara, H., Tang, L., Tarasov, P. E., Taylor, D., Thompson, R. S., Uchiyama, T., Van Campo, E., Vilimumbalo, S., Vincens, A., Volkova, V. S., Waller, M., Webb, T., Williams, J. W., Xia, Y., Xu, Q., Yan, S., Yang, X., Yu, G., Zernitskaya, V. P., Zhao, J., Zheng, Z.: Mid-Holocene and glacial-maximum vegetation geography of the northern continents and Africa, J. Biogeogr., 27, 507–519, 2000.

Raich, J. W. and Potter, C. S.: Global patterns of carbon dioxide emissions from soils, Global Biogeochem. Cy., 9, 23–36, doi:http://dx.doi.org/10.1029/94GB0272310.1029/94GB02723, 1995.

Rasmussen, S. O., Abbott, P. M., Blunier, T., Bourne, A. J., Brook, E., Buchardt, S. L., Buizert, C., Chappellaz, J., Clausen, H. B., Cook, E., Dahl-Jensen, D., Davies, S. M., Guillevic, M., Kipfstuhl, S., Laepple, T., Seierstad, I. K., Severinghaus, J. P., Steffensen, J. P., Stowasser, C., Svensson, A., Vallelonga, P., Vinther, B. M., Wilhelms, F., and Winstrup, M.: A first chronology for the North Greenland Eemian Ice Drilling (NEEM) ice core, Clim. Past, 9, 2713–2730, doi:http://dx.doi.org/10.5194/cp-9-2713-201310.5194/cp-9-2713-2013, 2013.

Rhodes, R. H., Brook, E. J., Chiang, J. C. H., Blunier, T., Maselli, O. J., McConnell, J. R., Romanini, D., and Severinghaus, J. P.: Enhanced tropical methane production in response to iceberg discharge in the North Atlantic, Science, 348, 1016–1019, doi:http://dx.doi.org/10.1126/science.126200510.1126/science.1262005, 2015.

Risi, C., Bony, S., Vimeux, F., and Jouzel, J.: Water-stable isotopes in the LMDZ4 general circulation model: model evaluation for present-day and past climates and applications

to climatic interpretations of tropical isotopic records, J. Geophys. Res.-Atmos., 115, D12, doi:http://dx.doi.org/10.1029/2009JD01325510.1029/2009JD013255, 2010.

Roche, D., Wiersma, A., and Renssen, H.: A systematic study of the impact of freshwater pulses with respect to different geographical locations, Clim. Dynam., 34, 997–1013, doi:http://dx.doi.org/10.1007/s00382-009-0578-810.1007/s00382-009-0578-8, 2010.

Ruddiman, W. F.: Late Quaternary deposition of ice-rafted sand in the subpolar North Atlantic (lat 40 to 65 N), Geol. Soc. Am. Bull., 88, 1813–1827, 1977.

Sanchez Goni, M. F. and Harrison, S. P.: Millennial-scale climate variability and vegetation changes during the last glacial: concepts and terminology, Quaternary Sci. Rev., 29, 2823–2827, doi:http://dx.doi.org/10.1016/j.quascirev.2009.11.01410.1016/j.quascirev.2009.11.014, 2010.

Schlesinger, W. and Andrews, J.: Soil respiration and the global carbon cycle, Biogeochemistry, 48, 7–20, doi:http://dx.doi.org/10.1023/A:100624762387710.1023/A:1006247623877, 2000.

Schmittner, A.: Decline of the marine ecosystem caused by a reduction in the Atlantic overturning circulation, Nature, 434, 628–633, doi:http://dx.doi.org/10.1038/nature0347610.1038/nature03476, 2005.

Schmittner, A. and Galbraith, E. D.: Glacial greenhouse-gas fluctuations controlled by ocean circulation changes, Nature, 456, 373–376, 2008.

Severinghaus, J. P.: Studies of the terrestrial O_2 and carbon cycles in sand dune gases and in biosphere 2, Tech. rep., Oak Ridge Associated Universities, Inc., TN, 1995.

Severinghaus, J. P., Beaudette, R., Headly, M. A., Taylor, K., and Brook, E. J.: Oxygen-18 of O_2 records the impact of abrupt climate change on the terrestrial biosphere, Science, 324, 1431–1434, doi:http://dx.doi.org/10.1126/science.116947310.1126/science.1169473, 2009.

Stouffer, R. J., Yin, J., Gregory, J., Dixon, K., Spelman, M., Hurlin, W., Weaver, A., Eby, M., Flato, G., Hasumi, H., Hu, A., Jungclaus, J. H., Kamenkovich, I. V., Levermann, A., Montoya, M., Murakami, S., Nawrath, S., Oka, A., Peltier, W. R., Robitaille, D. Y. , Sokolov, A., Vettoretti, G. and Weber, S. L.: Investigating the causes of the response of the thermohaline circulation to past and future climate changes, J. Climate, 19, 1365–1387, http://dx.doi.org/10.1175/JCLI3689.110.1175/JCLI3689.1, 2006.

Swingedouw, D., Mignot, J., Braconnot, P., Mosquet, E., Kageyama, M., and Alkama, R.: Impact of freshwater release in the North Atlantic under different climate conditions in an OAGCM, J. Climate, 22, 6377–6403, 2009.

Tagliabue, A., Bopp, L., and Aumont, O.: Evaluating the importance of atmospheric and sedimentary iron sources to Southern Ocean biogeochemistry, Geophys. Res. Lett., 36, 13, doi:http://dx.doi.org/10.1029/2009GL03891410.1029/2009GL038914, 2009.

Takahara, H., Igarashi, Y., Hayashi, R., Kumon, F., Liew, P.-M., Yamamoto, M., Kawai, S., Oba, T., and Irino, T.: Millennial-scale variability in vegetation records from the East Asian islands: Taiwan, Japan and Sakhalin, Quaternary Sci. Rev., 29, 2900–2917, doi:http://dx.doi.org/10.1016/j.quascirev.2009.11.02610.1016/j.quascirev.2009.11.026, 2010.

Von Caemmerer, S.: Biochemical Models of Leaf Photosynthesis, 2, Csiro publishing, 2000.

Waelbroeck, C., Labeyrie, L., Michel, E., Duplessy, J., McManus, J., Lambeck, K., Balbon, E., and Labracherie, M.: Sea-level and deep water temperature changes derived from benthic foraminifera isotopic records, Quaternary Sci. Rev., 21, 295–305, doi:http://dx.doi.org/10.1016/S0277-3791(01)00101-910.1016/S0277-3791(01)00101-9, 2002.

Walker, C. D. and Brunel, J.-P.: Examining evapotranspiration in a semi-arid region using stable isotopes of hydrogen and oxygen, J. Hydrol., 118, 55–75, doi:http://dx.doi.org/10.1016/0022-1694(90)90250-210.1016/0022-1694(90)90250-2, 1990.

Walker, C. D., Leaney, F. W., Dighton, J. C., and Allison, G. B.: The influence of transpiration on the equilibration of leaf water with atmospheric water vapour, Plant Cell Environ., 12, 221–234, doi:http://dx.doi.org/10.1111/j.1365-3040.1989.tb01937.x10.1111/j.1365-3040.1989.tb01937.x, 1989.

Wang, L., Good, S. P., Caylor, K. K., and Cernusak, L. A.: Direct quantification of leaf transpiration isotopic composition, Agr. Forest Meteorol., 154–155, 127–135, doi:http://dx.doi.org/10.1016/j.agrformet.2011.10.01810.1016/j.agrformet.2011.10.018, 2012.

Wang, Y. J., Cheng, H., Edwards, R. L., He, Y., Kong, X., An, Z., Wu, J., Kelly, M. J., Dykoski, C. A., and Li, X.: The holocene asian monsoon: links to solar changes and North Atlantic climate, Science, 308, 854–857, doi:http://dx.doi.org/10.1126/science.110629610.1126/science.1106296, 2005.

Wang, Y. J., Cheng, H., Edwards, R. L., Kong, X., Shao, X., Chen, S., Wu, J., Jiang, X., Wang, X., and An, Z.: Millennial- and orbital-scale changes in the East Asian monsoon over the past 224,000 years, Nature, 451, 1090–1093, doi:http://dx.doi.org/10.1038/nature0669210.1038/nature06692, 2008.

Wang, Y. J., Cheng, H., Edwards, R. L., An, Z. S., Wu, J. Y., Shen, C.-C., and Dorale, J. A.: A high-resolution absolute-dated late pleistocene monsoon record from Hulu Cave, China, Science, 294, 2345–2348, doi:http://dx.doi.org/10.1126/science.106461810.1126/science.1064618, 2001.

Weldeab, S.: Bipolar modulation of millennial-scale West African monsoon variability during the last glacial (75,000–25,000 years ago), Quaternary Sci. Rev., 40, 21–29, doi:http://dx.doi.org/10.1016/j.quascirev.2012.02.01410.1016/j.quascirev.2012.02.014, 2012.

Welp, L. R., Keeling, R. F., Meijer, H., Bollenbacher, A., F., Piper, S. C., Yoshimura, K., Francey, R. J., Allison, C. E., and Wahlen, M.: Interannual variability in the

oxygen isotopes of atmospheric CO_2 driven by El Nino, Nature, 477, 579–582, doi:http://dx.doi.org/10.1038/nature1042110.1038/nature10421, 2011.

Woillez, M.-N.: Modellisation des variations rapides du systeme atmospherere-ocean-vegetation-cryosphere en climats glaciaires, PhD thesis, Paris Versailles St-Quentin, 2012.

Woillez, M.-N., Kageyama, M., Krinner, G., de Noblet-Ducoudré, N., Viovy, N., and Mancip, M.: Impact of CO_2 and climate on the Last Glacial Maximum vegetation: results from the ORCHIDEE/IPSL models, Clim. Past, 7, 557–577, doi:http://dx.doi.org/10.5194/cp-7-557-201110.5194/cp-7-557-2011, 2011.

Woillez, M.-N., Kageyama, M., Combourieu-Nebout, N., and Krinner, G.: Simulating the vegetation response in western Europe to abrupt climate changes under glacial background conditions, Biogeosciences, 10, 1561–1582, doi:http://dx.doi.org/10.5194/bg-10-1561-201310.5194/bg-10-1561-2013, 2013.

Yakir, D., D., DeNiro, M. J., and Gat, J. R.: Natural deuterium and oxygen-18 enrichment in leaf water of cotton plants grown under wet and dry conditions: evidence for water compartmentation and its dynamics, Plant Cell Environ., 13, 49–56, doi:http://dx.doi.org/10.1111/j.1365-3040.1990.tb01298.x10.1111/j.1365-3040.1990.tb01298.x, 1990.

Table 1. Plant functional types (PFT) in ORCHIDEE, acronyms used and mega-biome assignment in this study.

PFT	Acronym	Mega-biome
Bare soil	Bare soil	Bare soil
Tropical broadleaf evergreen trees	TrBE	Tropical trees
Tropical broadleaf raingreen trees	TrBR	Tropical trees
Temperate needleleaf evergreen trees	TempNE	Temperate trees
Temperate broadleaf evergreen trees	TempBE	Temperate trees
Temperate broadleaf summergreen trees	TempBS	Temperate trees
Boreal needleleaf evergreen trees	BoNE	Boreal trees
Boreal broadleaf summergreen trees	BoBS	Boreal trees
Boreal needleleaf summergreen trees	BoNS	Boreal trees
C3 grass	C3 grass	C3 grass
C4 grass	C4 grass	C4 grass

Table 2. Parameters involved in the calculation of $\delta^{18}O_{atm}$. Uncertainties are given for most of the parameters except for those derived from the ORCHIDEE model.

Parameter	Unit	Definition	LGM_ctrl	HS_exp
$[CO_2]$	ppm	carbon dioxide mixing ratio in the troposphere	190	190
t	°C	temperature at the site of photosynthesis	21.08	21.41
h	%	relative humidity at the site of photosynthesis	66.09	66.12
GPP_C	Pmol C yr^{-1}	gross photosynthetic molar carbon flux from the terrestrial biosphere	6.758	6.450
GPP_O_2	Pmol O_2 yr^{-1}	gross Photosynthetic molar oxygen flux from the terrestrial biosphere	11.768	11.410
f_{C4}	%	C4 fraction (in terms of GPP_C)	36.92	35.59
f_{photo}	%	fraction of photorespiration	28.55	29.52
f_{soil_dark}	%	soil fraction of dark respiration	62[a]	62[a]
f_{dark_soil}	%	fraction of soil respiration	38.10	37.50
f_{dark_leaves}	%	fraction of leaf respiration	23.35	22.98
f_{Mehler}	%	fraction of Mehler respiration	10[b]	10[b]
${}^{18}\epsilon_{dark\_soil}$	‰	global isotopic fractionation associated with dark soil respiration	15.895 ± 0.5[c]	15.610 ± 0.5[c]
${}^{18}\epsilon_{dark\_leaves}$	‰	mitochondrial (AOX + COX) isotopic fractionation in leaves	19 ± 1[c]	19 ± 1[c]
${}^{18}\epsilon_{Mehler}$	‰	global Mehler respiration isotopic fractionation	10.8 ± 0.2[d]	10.8 ± 0.2[d]
${}^{18}\epsilon_{photo}$	‰	global photorespiration isotopic fractionation	21.4 ± 1[d]	21.4 ± 1[d]
${}^{18}\epsilon_{resp}$	‰	global terrestrial respiration isotopic fractionation	17.83	17.80
$\delta^{18}O_{p\_amount}$	‰	global precipitation water isotope delta	−6.689	−6.781
$\delta^{18}O_{p}$	‰	global photosynthesis precipitation water isotope delta	−5.530	−5.289
$\delta^{18}O_{vap\_amount}$	‰	global water vapor isotope delta	−12.648	−12.653
$\delta^{18}O_{vap}$	‰	global photosynthesis water vapor isotope delta	−12.483	−12.295
$\delta^{18}O_{leafwater}$	‰	global leaf water isotope delta	5.164 ± 1[e]	5.301 ± 1[e]
$\delta^{18}O_{terr}$	‰	global terrestrial tropospheric isotope delta	23.407 ± 1	23.516 ± 1
$\delta^{18}O_{mar}$	‰	global marine tropospheric isotope delta	25.3 ± 2[f]	25.3 ± 2[f]
$\delta^{18}O_{atm}$	‰	global tropospheric isotope delta	23.88 ± 2	23.95 ± 2

[a] Schlesinger and Andrews, 2000. Note that this estimation is for present-day and here, we assume it was similar during the last glacial period.
[b] Badger et al., 2000.
[c] Landais et al., 2007a.
[d] Helman et al., 2005.
[e] Gillon and Yakir, 2001.
[f] Note that the increase of 1 ‰ compared to Luz et al. (2014) value accounts for the 1 ‰ enrichment of the glacial ocean (Waelbroeck et al., 2002).

Table 3. Comparison of isotopic proxy records (speleothem's calcite $\delta^{18}O$) with annual average modeled amount weighted $\delta^{18}O_p$. Note that anomalies from Pausata et al. (2011) are calculated from H1 and YD, while anomalies from Lewis et al. (2010) arise from all identifiable $\delta^{18}O_c$ excursions.

Core	ID	Region	Latitude	Longitude	Data $\Delta\delta^{18}O$	Model $\Delta\delta^{18}O$	Reference
Hulu Cave	XI	China	32.5	119.2	1.4	1.1	Pausata et al. (2011); Lewis et al. (2010)
Songjia Cave	XII	China	~~31.7~~ 32.3	~~110.5~~ 107.2	1.4	1.1	Pausata et al. (2011); Lewis et al. (2010)
Dongge Cave	IX	China	25.3	108.8	1	0.8	Pausata et al. (2011)
Timta Cave	XIII	India	29.8	80.0	3	−3.7	Pausata et al. (2011)
Sanbao Cave	X	China	31.7	110.5	1.2	1.1	Lewis et al. (2010)
Borneo	~~VI~~ VII	Indonesia	4.0	114.0	0.8	0.6	Lewis et al. (2010)
Moomi Cave	VIII	Yemen	12.5	54.3	0.9	0.6	Lewis et al. (2010)
Soreq Cave	VI	Israel	31.5	35.0	0.5	0.5	Lewis et al. (2010)
Rio Grande do Norte	II	northeastern Brazil	−5.7	−37.7	−1.6	−0.1	Lewis et al. (2010)
Santana Cave	V	southern Brazil	−24.5	−48.7	−0.8	−0.9	Lewis et al. (2010)
Botuvera Cave	IV	southern Brazil	−27.2	−49.2	−1.1	−1.1	Lewis et al. (2010)
Cave of the Bells	III	North America	31.7	−110.8	−0.8	0.8	Lewis et al. (2010)
Poleva Cave	I	Europe	44.7	21.8	−2	−1.0	Lewis et al. (2010)

Table 4. Comparison of mega-biomes during Heinrich Stadials between pollen reconstructions (references are included in the table) and simulated vegetations (compiled from HS_exp using ORCHIDEE vegetation model). Note that simulated C3 and C4 grasses are merged into 1 mega-biome because pollen-based biome reconstructions do not allow us to distinguish between the two PFTs.

Core	ID	Region	Latitude	Longitude	resolution[a] (yr/sample)	which HS?	Mega Biome distribution			Agreement	Reference
							pollen data		model results		
							flora	biome(s) assignation	dominant, subdominant biome		
Kashiru Bog	1	equatorial Africa	−3.47	29.57	410	HS1	grassland and dry shrubland, savannah and xerophytic scrubland	grasses	tropical forest, grasses	fair	Hessler et al. (2010); Handiani et al. (2012)
Lake Tanganyika	2	equatorial Africa	−8.5	30.85	610	HS1	warm temperate mixed forest, savannah and xerophytic scrubland	temperate forest, grasses	grasses, tropical forest	fair	Hessler et al. (2010); Handiani et al. (2012)
Lake Masoko	3	equatorial Africa	−9.33	33.75	550	HS1	warm temperate mixed forest, savannah and xerophytic scrubland	temperate forest, grasses	grasses, tropical forest	fair	Hessler et al. (2010); Handiani et al. (2012)
Lake Malawi	4	equatorial Africa	−11.29	34.44	200	HS1	savannah and xerophytic scrubland, tropical forest	grasses, tropical forest	grasses	good	Hessler et al. (2010); Handiani et al. (2012)
Barombi Mbo	5	equatorial Africa	4.51	9.4	590	HS1	savannah and xerophytic scrubland, tropical forest	grasses, tropical forest	grasses, tropical forest	good	Hessler et al. (2010); Handiani et al. (2012)
KS 84-063	6	equatorial Africa	4.4	−4.18	450	HS1	tropical forest, warm temperate mixed forest	tropical forest, temperate forest	tropical forest, grasses	good	Hessler et al. (2010); Handiani et al. (2012)
ODP 1078-C	7	equatorial Africa	−11.92	13.4	140	HS1	warm temperate mixed forest, temperate montane forest	temperate forest, boreal forest	bare soil, tropical forest	bad[b] (soil $>90\,\%$)	Hessler et al. (2010); Handiani et al. (2012)
GEOB 1023 – Cunene River Mouth	8	equatorial Africa	−17.15	11.02	185	HS1	savannah and xerophytic scrubland, grassland and dry shurbland	grasses	none	none	Hessler et al. (2010); Handiani et al. (2012)
Lake Caco	9	South America	−2.97	−43.42	80	HS1	warm temperate mixed forest, tropical forest	temperate forest, tropical forest	bare soil, tropical forest	moderate	Hessler et al. (2010); Handiani et al. (2012)
Colonia	10	South America	−23.87	−46.71	710	HS1	savannah and xerophytic scrubland, grassland and dry shurbland	grasses	grasses, temperate forest	good	Hessler et al. (2010); Handiani et al. (2012)
La Laguna, Bogota	11	South America	4.92	−74.03	670	HS1	savannah and xerophytic scrubland, grassland and dry shurbland	grasses	bare soil	bad (soil $=100\,\%$)	Hessler et al. (2010); Handiani et al. (2012)

Table 4. Continued.

Core	ID	Region	Latitude	Longitude	resolution[a] (yr/sample)	which HS?	Mega Biome distribution			Agreement	Reference
							pollen data		model results		
							flora	biome(s) assignation	dominant, subdominant biome		
Fuquene	12	South America	4.92	−74.03	520	HS1	savannah and xerophytic scrubland, temperate montane forests	grasses, temperate forest	bare soil	bad (soil = 100 %)	Hessler et al. (2010); Handiani et al. (2012)
GEOB 3104	13	South America	−3.67	−37.72	670	HS1	temperate montane forest, warm temperate mixed forest	temperate forest	tropical forest, bare soil	bad[b]	Hessler et al. (2010); Handiani et al. (2012)
GEOB 3910-2	14	South America	−4.15	−36.21	125	HS1	savannah and xerophytic scrubland, warm temperate mixed forests	grasses, temperate forest	tropical forest, bare soil	bad[b]	Hessler et al. (2010); Handiani et al. (2012)
MD03-2622	15	South America	10.71	−65.17	420	HS3, HS4, HS5	montane forest, semi-deciduous forest, savannah (except HS4)	temperate forest, grasses	none	none	Hessler et al. (2010); Handiani et al. (2012)
17 962	16	Australasia	7.18	112.08	370	HS4	tropical forest	tropical forest	tropical forest, grasses	good	Harrison and Sanchez-Goni (2010)
18 300	17	Australasia	4.35	108.65	526	HS4	tropical forest	tropical forest	tropical forest, grasses	good	Harrison and Sanchez-Goni (2010)
18 323	18	Australasia	2.78	107.88	420	HS4	tropical forest	tropical forest	tropical forest, grasses	good	Harrison and Sanchez-Goni (2010)
Lake Wangroom	19	Australasia	−38.35	142.6	362	HS4	herbaceous and shrublands	grasses	temperate forest, tropical forest	bad	Harrison and Sanchez-Goni (2010)
Tyrendarra Swamp	20	Australasia	−38.2	141.76	337	HS4	herbaceous and shrublands	grasses	temperate forest, tropical forest	bad	Harrison and Sanchez-Goni (2010)
Lake Surprise	21	Australasia	−38.06	141.92	345	HS4	herbaceous and shrublands	grasses	temperate forest, tropical forest	bad	Harrison and Sanchez-Goni (2010)
Kohuora	22	Australasia	−36.57	174.52	375	HS4	herbaceous and shrublands	grasses	temperate forest, tropical forest	bad	Harrison and Sanchez-Goni (2010)
Native Companion Lagoon	23	Australasia	−27.68	153.41	655	HS4	tropical forest and open forest, woodland	tropical forest, temperate forest	bare soil, temperate forest	moderate	Harrison and Sanchez-Goni (2010)
Ioannina 284	24	Europe	39.75	20.85	325	HS4	grassland and dry shrubland	grasses	boreal forest, grasses	fair	Fletscher et al. (2010)
Megali Limni	25	Europe	39.1	26.32	150	HS4	grassland and dry shrubland with 40 % xerophytic steppe elements	grasses	grasses, boreal forest	good	Fletscher et al. (2010)
Lago Grande di Monticchio	26	Europe	40.93	15.62	210	HS4	grassland and dry shrubland with 40 % xerophytic steppe elements	grasses	boreal forest, grasses	fair	Fletscher et al. (2010)
MD04-2845	27	Europe	45.35	−5.22	540	HS3	grassland and dry shrubland	grasses	none	none	Fletscher et al. (2010)
MD99-2331	28	Europe	41.15	−9.68	390	HS4	grassland and dry shrubland	grasses	none	none	Fletscher et al. (2010)

Table 4. Continued.

Core	ID	Region	Latitude	Longitude	resolution[a] (yr/sample)	which HS?	Mega Biome distribution: pollen data flora	Mega Biome distribution: pollen data biome(s) assignation	Mega Biome distribution: model results dominant, subdominant biome	Agreement	Reference
MD95-2039	29	Europe	40.58	−10.35	300	HS4	grassland and dry shrubland	grasses	none	none	Fletscher et al. (2010)
MD95-2042	30	Europe	37.8	−10.17	360	HS4	grassland and dry shrubland with 40 % xerophytic steppe elements	grasses	none	none	Fletscher et al. (2010)
ODP site 976	31	Europe	36.2	−4.3	240	HS4	grassland and dry shrubland with 40 % xerophytic steppe elements	grasses	bare soil, boreal forest	bad (soil > 90 %)	Fletscher et al. (2010)
MD95-2043	32	Europe	36.13	−2.62	260	HS4	grassland and dry shrubland with 40 % xerophytic steppe elements	grasses	bare soil, boreal forest	bad (soil > 90 %)	Fletscher et al. (2010)
Khoe	33	Japan	51.34	142.14	750	HS4	cold deciduous and evergreen conifer forest	boreal forest	boreal forest, grasses	good	Takahara et al. (2010)
Kenbuchi	34	Japan	44.05	142.38	250	HS1, HS2	cold deciduous forest	boreal forest	boreal forest, grasses	good	Takahara et al. (2010)
MD01-2421	35	Japan	36.02	141.77	150	HS4	cold evergreen conifer forest	boreal forest	boreal forest, temperate forest	good	Takahara et al. (2010)
Lake Nojiri	36	Japan	36.83	138.22	100	HS4	increase of cold evergreen conifer forest within cool conifer forest	temperate forest, boreal forest	none	none	Takahara et al. (2010)
Lake Biwa	37	Japan	35.22	136	300	HS4	increase of cool conifer forest within temperate conifer forest	temperate forest	boreal forest, temperate forest	fair	Takahara et al. (2010)
Kamiyoshi Basin	38	Japan	35.1	135.59	800	HS4	increase of cool conifer within temperate conifer forest, and deciduous broadleaf forest	temperate forest	boreal forest, temperate forest	fair	Takahara et al. (2010)
Toushe Basin	39	Japan	23.82	120.88	300	HS4	temperate deciduous or warm temperate evergreen forest	temperate forest	boreal forest, temperate forest	good	Takahara et al. (2010)
Fargher Lake	40	North-America	45.88	−122.58	270	HS4	boreal forest	boreal forest	none	none	Jimenez-Moreno et al. (2010)
Carp Lake	41	North-America	45.91	−120.88	630	HS4	open temperate and pine forest	temperate forest	none	none	Jimenez-Moreno et al. (2010)
Little Lake	42	North-America	44.16	−123.58	260	HS4	boreal-temperate forest	boreal forest, temperate forest	none	none	Jimenez-Moreno et al. (2010)
W8709A-13PC	43	North-America	42.25	−127.66	430	HS4	boreal forest with decrease in heterophyla	boreal forest	none	none	Jimenez-Moreno et al. (2010)
EW-9504-17PC	44	North-America	42.23	−125.81	460	HS1, HS2, HS3	warm temperate	temperate forest, tropical forest	none	none	Jimenez-Moreno et al. (2010)
ODP 893A	45	North-America	34.28	−120.03	220	HS4	open temperate forest	temperate forest	temperate forest, bare soil	good	Jimenez-Moreno et al. (2010)

Table 4. Continued.

Core	ID	Region	Latitude	Longitude	resolution[a] (yr/sample)	which HS?	Mega Biome distribution			Agreement	Reference
							pollen data		model results		
							flora	biome(s) assignation	dominant, subdominant biome		
Bear Lake	46	North-America	41.95	−111.3	680	HS4	xerophytic shrubland	grasses	grasses	good	Jimenez-Moreno et al. (2010)
Camel Lake	47	North-America	30.26	−85.01	300	HS4	temperate forest with increase in southeastern pine forest	temperate forest	boreal forest, temperate forest	fair	Jimenez-Moreno et al. (2010)
Lake Tulane	48	North-America	27.58	−81.5	480	HS4	southeastern pine forest, florida scrub	grasses, temperate forest	bare soil, temperate forest	moderate	Jimenez-Moreno et al. (2010)

[a] Sampling resolutions of the MIS where vegetation changes occur. Mean sampling resolution is 393 yrs.
[b] Similar to Handiani et al. (2012) model results.

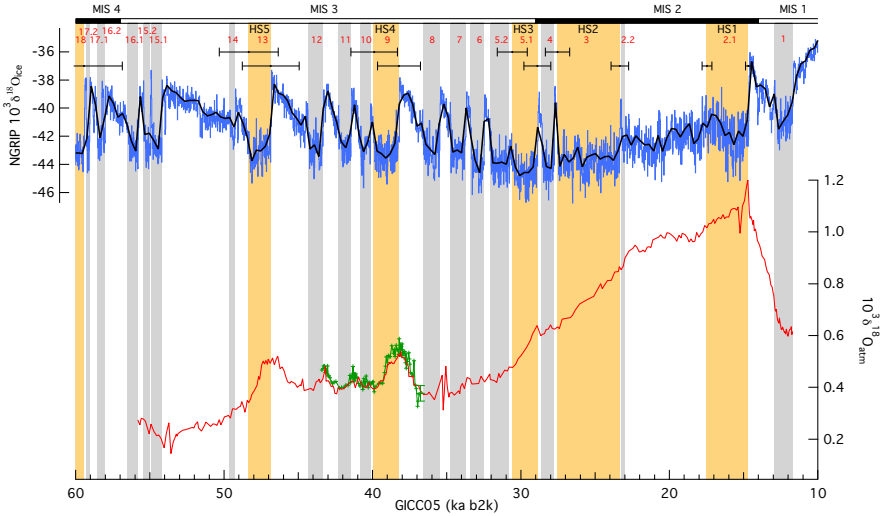

Fig. 1. Greenland Stadials (GS) and Heinrich Stadials (HS) during the last glacial period. Red numbers indicate GS and black labels HSs. **(a)** Black line: NGRIP δ^{18}O, ‰, on the GICC05 timescale back to 60 ka b2k. **(b)** Red line: Siple Dome atmospheric δ^{18}O (Severinghaus et al., 2009) on GICC05 timescale. The transfer of Siple Dome atmospheric δ^{18}O on the GICC05 chronology is achieved by using the Siple Dome gas age scale compatible with the GICC05 chronology (Guillevic, 2013), based on match points between Siple Dome methane variations (Brook et al., 2005; Ahn et al., 2012) (depth point) and NEEM methane variations (Chappellaz et al., 2013) (GICC05 gas age point). A linear interpolation is then performed between match points to calculate the Siple Dome gas age. Green line: NEEM atmospheric δ^{18}O, ‰ (± 0.03 ‰) (Guillevic et al., 2014). Colored areas: GSs. Grey: GS with no major Heinrich event. Orange: HS1, HS2, HS3, HS4, HS5 and end of HS6: GSs with a major Heinrich event. Black error bars indicate HS onset and end uncertainty (2σ), based on Rasmussen et al. (2013) Maximum Counting Error (MCE). Top (right to left): black and white vertical bar indicate Marine Isotope Stage 1 to 4.

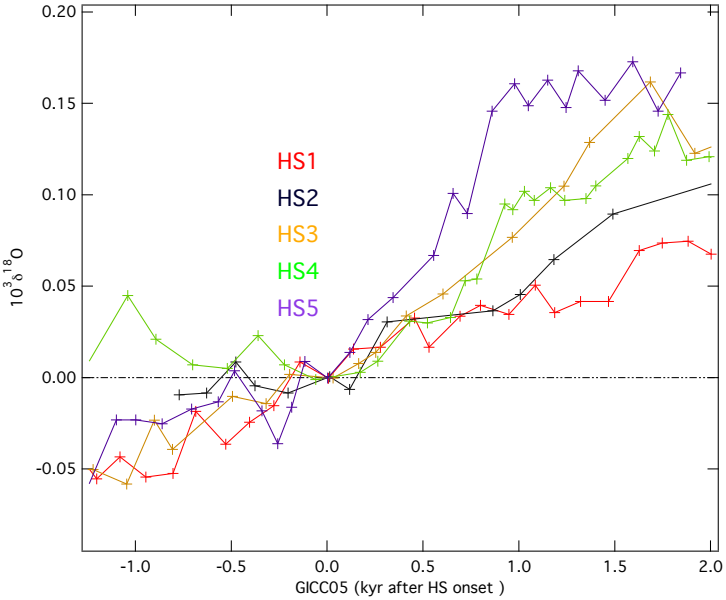

Fig. 2. Evolution of Siple Dome atmospheric oxygen δ^{18}O (Severinghaus et al., 2009) during Heinrich Stadial on the GICC05 timescale.

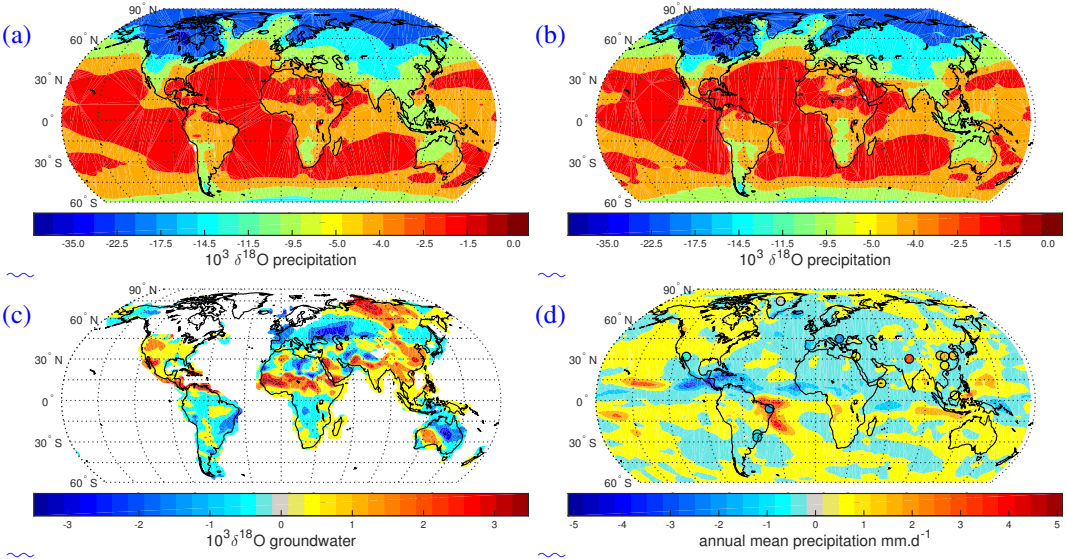

Fig. 3. Amount weighted annual-mean δ^{18}O of precipitation for **(a)** LGM_ctrl and **(b)** HS_exp experiments obtained with LMDZ-iso. Note that the anomaly can be seen in Fig. 4a. **(c)** HS_exp–LGM_ctrl annual mean anomaly of groundwater δ^{18}O. Groundwater δ^{18}O represents the isotopic value of the substrate water for photosynthesis (see text for details). **(d)** HS_exp–LGM_ctrl annual mean anomaly of rainfall amount.

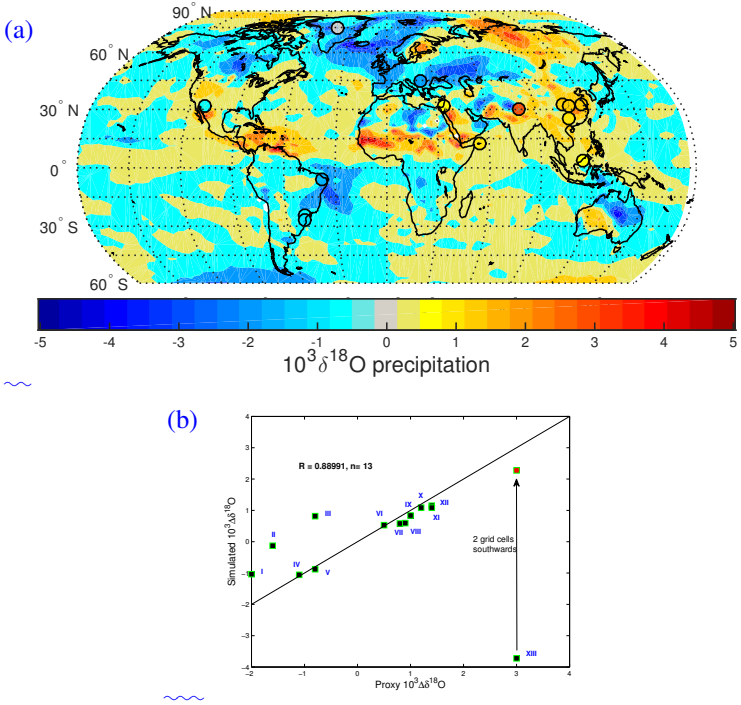

Fig. 4. (a) Model–data comparison of $\underset{\sim}{\delta}^{18}$O precipitation anomaly during HS compared to LGM. Data represent speleothem's calcite δ^{18}O from various locations (see Table 3 for details). **(b)** Comparison of reconstructed HS precipitation anomaly $\Delta\delta^{18}$O from selected proxies shown in a and simulated $\Delta\delta^{18}O_p$ anomaly ($R = 0.89$, $n = 13$). Note that the correlation is done with point XIII corrected, as we assume a bias in the model. Refer to Table 3 for details on reconstructed precipitation. Points falling on the line depict the same anomaly in the reconstruction and the simulation. Note that Timta and Dongge (Wang et al., 2005) cave $\delta^{18}O_c$ were estimated from the YD excursion, sometimes called H0 and characterized by a large freshwater input in the NA (Pausata et al., 2011).

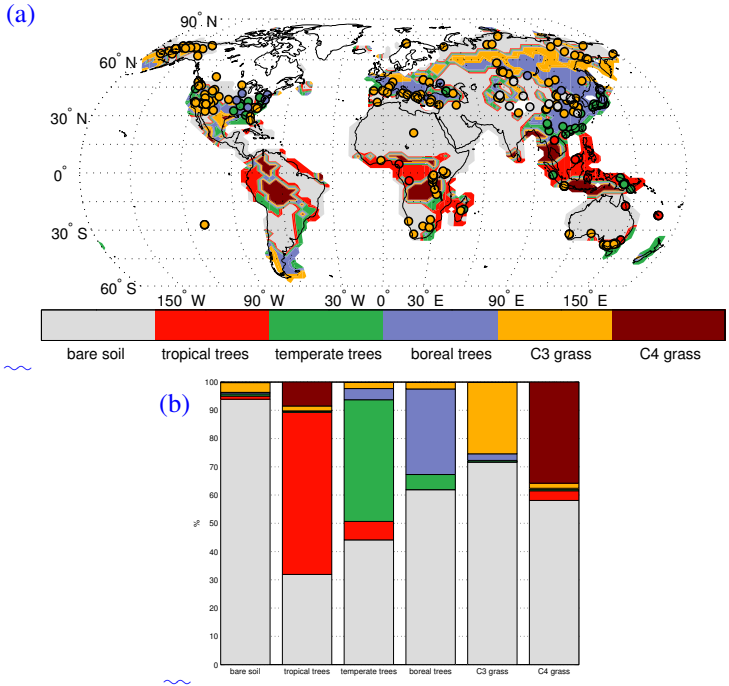

Fig. 5. (a) Model–data comparison of mega-biome distribution for LGM_ctrl based on dominant PFT type simulated by ORCHIDEE. For each grid-cell, the fraction of bare soil, tropical forests, temperate forests, boreal forests, C3 and C4 grasses is considered. The type covering the greatest cell fraction is the dominant type. Note that dominant bare soil fraction denotes more than 80 %. Circles denote LGM mega-biomes inferred from pollen and plant macrofossil records compiled by the BIOME6000 project. Refer to Table 4 to see how PFT's simulated by ORCHIDEE have been assigned to the mega-biomes mapped in this figure. **(b)** Detail of the averaged vegetation composition in grid cells occupied by a dominant mega-biome for LGM_ctrl.

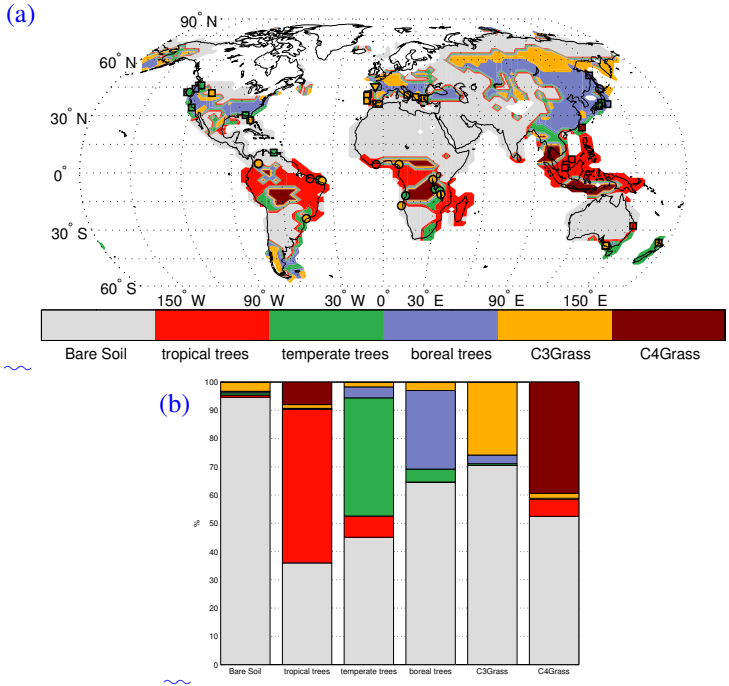

Fig. 6. **(a)** Model–data comparison of mega-biome distribution for HS_exp based on dominant PFT type simulated by ORCHIDEE. For each grid-cell, the fraction of bare soil, tropical forests, temperate forests, boreal forests, C3 and C4 grasses is considered. The type covering the greatest cell fraction is the dominant type. Note that dominant bare soil fraction denotes more than 80 %. Circles denote HS_exp mega-biomes inferred from pollen and plant macrofossil records compilation. Refer to Table 4 to see how PFT's simulated by ORCHIDEE and reconstructed vegetation have been assigned to the mega-biomes mapped in this figure. **(b)** Detail of the averaged vegetation composition in grid cells occupied by a dominant mega-biome for HS_exp.

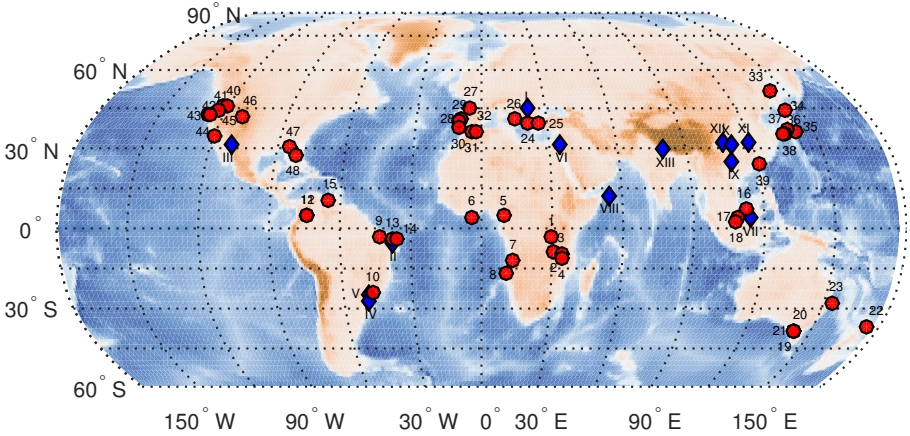

Fig. 7. Location of marine and terrestrial paleoarchives sites included in the model–data comparison. Blue diamonds denote speleothem's calcite δ^{18}O and red circles denote pollen records. Arabic and roman numbers displayed in the map identify the location of the paleoarchives listed in Tables 3 (hydrology) and 4 (vegetation) for site names, references and further details.

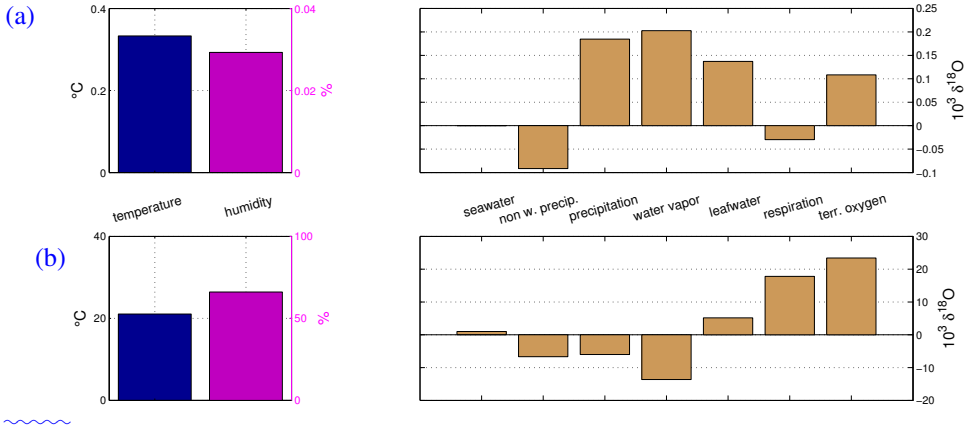

Fig. 8. Evolution of the main simulated factors controlling atmospheric δ^{18}O. Note that all variables are oxygen production weighted, i.e. integrated over vegetated areas, if not stated with "non w.". **(a)** Left panel: HS_exp – LGM_ctrl anomalies of temperature and relative humidity. Right panel: (left to right) HS_exp – LGM_ctrl anomalies of seawater δ^{18}O, amount weighted precipitation δ^{18}O, precipitation δ^{18}O ($\delta^{18}O_p$), water vapor δ^{18}O, leaf water δ^{18}O ($\delta^{18}O_{lw}$), respiratory isotope fractionation ($-^{18}\epsilon_{resp}$) and terrestrial contribution to atmospheric δ^{18}O ($\delta^{18}O_{terr}$). **(b)** LGM_ctrl values of same relevant factors as in **(a)** in $\delta^{18}O_{terr}$ budget.

Note that plotted respiratory isotope fractionation anomaly is inverted as respiration is an oxygen uptake process.

$\delta^{18}O_{lw}$ is controlled by $\delta^{18}O_p$, temperature and relative humidity as described by Eq. (4). Combined with $^{18}\epsilon_{resp}$ as described in Eq. (3), one obtain $\delta^{18}O_{terr}$.

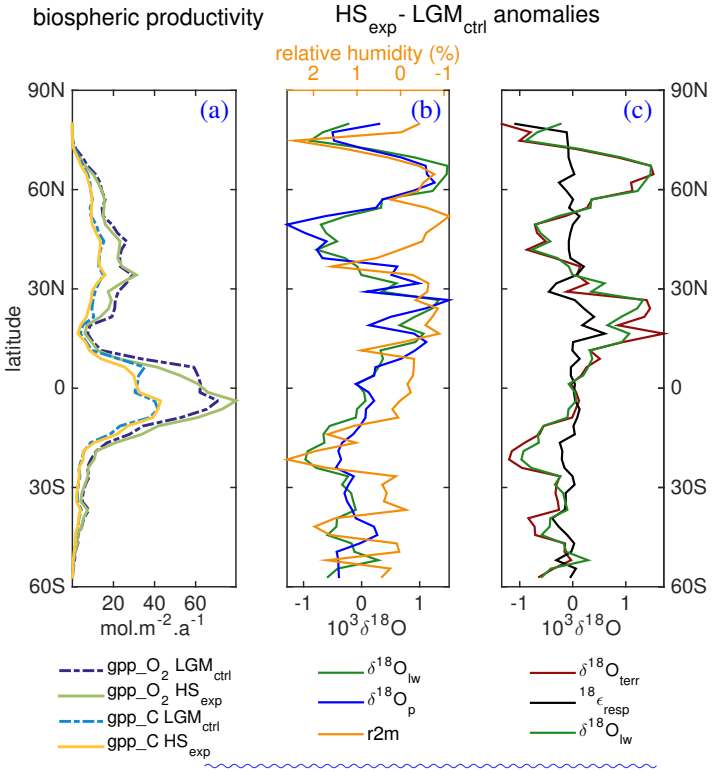

Fig. 9. **(a)** Zonal annual mean of gross primary productivity expressed in terms of carbon (GPP_C) and oxygen (GPP_O_2) annual molar fluxes for LGM_ctrl and HS_exp, resp. **(b)** Zonal annual mean anomalies of $\delta^{18}O_{lw}$, $\delta^{18}O_p$ and relative humidity (be aware of its inverted x axis). **(c)** Zonal annual mean anomalies for $-^{18}\epsilon_{resp}$, $\delta^{18}O_{lw}$ and $\delta^{18}O_{terr}$. Note that all variables of panels **(b)** and **(c)** are oxygen production (GPP_O_2) weighted.

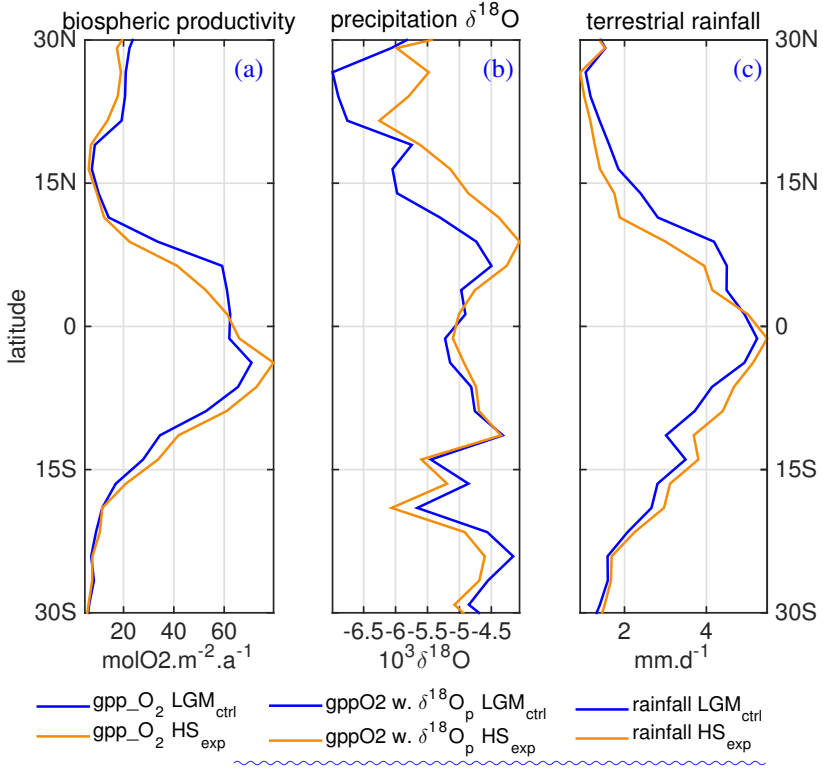

Fig. 10. Intertropical profiles of **(a)** Zonal annual mean of gross primary productivity expressed in terms of oxygen (GPP_O_2) annual molar fluxes for LGM_ctrl and HS_exp. **(b)** Zonal annual mean of oxygen production weighted $\delta^{18}O_p$ for LGM_ctrl and HS_exp. **(c)** Zonal annual mean of rainfall amount for LGM_ctrl and HS_exp.

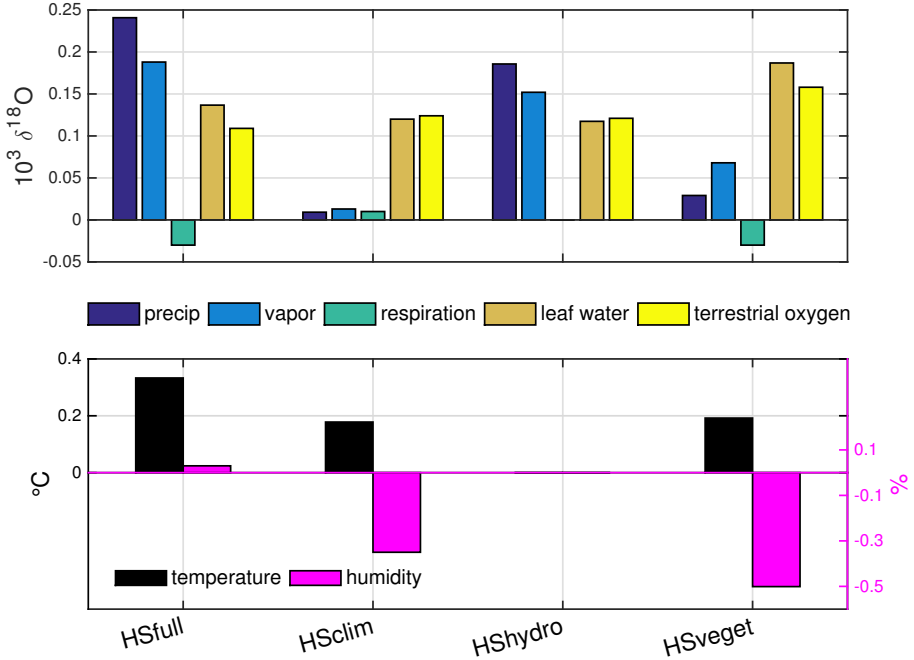

Fig. 11. Summary of sensitivity study experiments. HSfull uses same settings as HS_exp, while HSclim, HShydro and HSveget experiments are identical to LGM_ctrl, except for meteoric waters isotopic composition, climatic conditions or vegetation production and distribution, respectively, originating from HS_exp. For each of the experiments are presented annual mean anomaly (experiment – LGM_ctrl) of oxygen production weighted temperature, relative humidity, $\delta^{18}O_p$, water vapor $\delta^{18}O$, $\delta^{18}O_{lw}$, ${}^{18}\epsilon_{resp}$ and $\delta^{18}O_{terr}$.